UC San Diego
UC San Diego Previously Published Works

Title
Design and synthesis of novel methoxypyridine-derived gamma-secretase modulators

Permalink
https://escholarship.org/uc/item/4ps6s92t

Journal
Bioorganic & Medicinal Chemistry, 28(22)

ISSN
0968-0896

Authors
Rynearson, Kevin D
Buckle, Ronald N
Herr, R Jason
et al.

Publication Date
2020-11-01

DOI
10.1016/j.bmc.2020.115734

Peer reviewed

Design and synthesis of novel methoxypyridine-derived gamma-secretase modulators

Kevin D. Rynearson[a,*], Ronald N. Buckle[b], R. Jason Herr[b], Nicholas J. Mayhew[b], Xinchao Chen[b], William D. Paquette[b], Samuel A. Sakwa[b], Jinhai Yang[b], Keith D. Barnes[b], Phuong Nguyen[a], William C. Mobley[a], Graham Johnson[c], Juinn H. Lin[d], Rudolph E. Tanzi[e], Steven L. Wagner[a,f,*]

[a]Department of Neurosciences, University of California, San Diego, La Jolla, California 92093-0624, United States

[b]Department of Medicinal Chemistry, AMRI, East Campus, 3 University Place, Rensselaer, New York 12144, United States

[c]NuPharmAdvise, 3 Lakeside Drive, Sanbornton, New Hampshire 03269, United States

[d]Biopharm Consulting Partners, 2 Willet Drive, Ambler, Pennsylvania 19002, United States

[e]Genetics and Aging Research Unit, Department of Neurology, Massachusetts General Hospital, Charlestown, Massachusetts 02129, United States

[f]Veterans Administrative San Diego Healthcare System, La Jolla, California 92161, United States

Abstract

The evolution of gamma-secretase modulators (GSMs) through the introduction of novel heterocycles with the goal of aligning activity for reducing the levels of Aβ42 and properties consistent with a drug-like molecule are described. The insertion of a methoxypyridine motif within the tetracyclic scaffold provided compounds with improved activity for arresting Aβ42 production as well as improved properties, including solubility. *In vivo* pharmacokinetic analysis demonstrated that several compounds within the novel series were capable of crossing the BBB and accessing the therapeutic target. Treatment with methoxypyridine-derived compound **64** reduced Aβ42 levels in the plasma of J20 mice, in addition to reducing Aβ42 levels in the plasma and brain of Tg2576 mice.

[*]**Co-corresponding Authors:** Kevin D. Rynearson, Ph.D., University of California, San Diego, Department of Neurosciences, School of Medicine, Medical Teaching F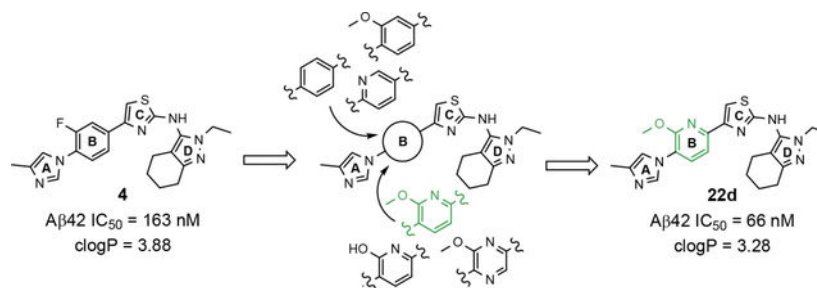acility Room 152, 9500 Gilman Drive, La Jolla, CA 92093-0624, Steven L. Wagner, Ph.D., University of California, San Diego, Department of Neurosciences, School of Medicine, Medical Teaching Facility Room 150, 9500 Gilman Drive, La Jolla, CA 92093-0624.

Graphical Abstract

Aβ42 IC$_{50}$ = 163 nM
clogP = 3.88

4

22d

Aβ42 IC$_{50}$ = 66 nM
clogP = 3.28

Keywords

Gamma secretase modulator; Alzheimer's disease; amyloid beta; Aβ42 reduction; structure activity relationship; methoxypyridines

1 Introduction

The population of Americans affected by Alzheimer's disease (AD) is currently estimated to be 5.8 million, and as individuals of the large baby boomer generation are progressing beyond the age of 65, the population of those with AD is expected to nearly triple over the next 35 years.[1] As a result, AD healthcare spending is projected to cost in excess of $1 trillion by 2050.[1] Despite massive research efforts, no disease modifying treatments currently exist for AD, and consequentially, the disease is reaching epidemic proportions and remains a major unmet clinical need.

AD is a devastating neurological condition which insidiously affects regions of the brain critical for cognition. Originally described by Alois Alzheimer, the eponymous disease predominantly affects the elderly and is characterized by senile plaques composed of aggregated amyloid beta (Aβ) peptides and neurofibrillary tangles, paired helical filaments of the hyper-phosphorylated microtubule-associated protein tau.[2–4] Although disease symptoms largely appear late in life, a large body of evidence indicates that the disease begins with extracellular deposition of Aβ peptides in regions of the brain that are vital for cognition decades prior. Many years after the initial deposition of Aβ peptides, neurofibrillary tangles appear, which closely correlate with the extent of cognitive decline associated with disease progression.[5, 6] The time period between the initial deposition of senile plaques resulting from aberrant biological processes and prior to the manifestation of clinical symptoms, offers the most promising window for therapeutic intervention.

The hallmark neuritic plaques diagnostic for AD form as a result of an imbalance of amyloid peptide variants, which increases the relative levels of Aβ42, a poorly soluble peptide that readily forms aggregates.[7, 8] Genetic evidence implicates subtle shifts in Aβ peptide production biased toward the formation of Aβ42 as playing a causative role in the disease.[9] The production of amyloid peptides, including Aβ42, is the result of sequential processing of the amyloid precursor protein (APP) by two aspartyl proteases.[10–12] The so-called amyloidogenic pathway commences with the cleavage of APP by β-amyloid precursor

protein cleaving enzyme 1 (BACE-1), resulting in the APP-carboxy-terminal fragment (CTF) known as C99. Subsequent cleavages of the membrane bound C99 by γ-secretase provide the APP-intracellular domain (AICD) and the extracellular Aβ peptides, which range from 37 to 43 amino acids in length.[13, 14] As a result of their role in amyloid production, BACE-1 and γ-secretase have garnered intense interest as potential therapeutic targets for the development of disease modifying AD therapeutics.[15–17]

Initially, drug discovery and development efforts focused on γ-secretase inhibitors (GSIs), which suppress the formation of all Aβ peptides including Aβ42.[18] While GSIs were shown to be capable of reducing Aβ peptides in plasma and to some extent cerebrospinal fluid (CSF) during clinical trials, counter-efficacy and off-target effects were also observed. The adverse effects were attributed to the inhibition of the processing of the numerous other γ-secretase substrates, which include the Notch 1 receptor, causing the accumulation of CTFs, which resulted in the discontinuation of GSI development.[19, 20] As an alternative to inhibiting γ-secretase, allosteric modulation alters the substrate cleavage pattern of the enzyme, suppressing the formation of the longer, fibrillogenic Aβ42 peptide in favor of shorter non-fibrillogenic isoforms, Aβ37 and Aβ38.[21–23] Importantly, compounds with this mode of action do not preclude the proteolysis of the numerous critical substrates of γ-secretase and consequentially avoid the inhibition-related side effects associated with GSIs.[24]

Various classes of γ-secretase modulators (GSMs) have been discovered previously; however, the tetracyclic methyl imidazole-derived GSM scaffold has been intensely pursued by both academic and industry laboratories as a potential disease modifying therapeutic for AD (Figure 1).[25–28] γ-Secretase is an intermembrane aspartyl protease complex composed four subunits: presenilin (PS1 or PS2), presenilin enhancer 2 (PEN-2), anterior pharynx defective-1 (Aph-1), and nicastrin.[29, 30] Photoaffinity labeling studies of the enzyme complex using a variety of related methyl imidazole-derived GSMs have revealed that these compounds bind to an allosteric site located on the PS1 subunit's N-terminal fragment (PS1-NTF) distinct from both the binding site of the GSIs as well as the active site of the enzyme and, as a result, do not interfere with the catalytic activity or the processing of the numerous putative substrates.[31, 32]

Despite the therapeutic promise that is associated with methyl imidazole-derived GSMs, the discovery of compounds which align potent activity with favorable ADMET (absorption, distribution, metabolism, excretion, and toxicity) has proved challenging. Previously, our lab utilized compound **3** (NGP-555) as a lead in order to discover novel GSMs, which preserve the activity of the parent molecule while simultaneously improving other properties including solubility, through the preparation of novel heterocyclic D-ring analogs (Scheme 1).[33] While these analogs exhibited improved properties, the activity of these compounds was greatly diminished as demonstrated by tetrahydroindazole **4**. Herein, we describe our ongoing efforts toward the development of a second-generation of GSM compounds through preparation of novel B-ring analogs of our aminothiazole-derived modulators.

2   Design and Synthesis

2.1   Design of B-ring GSM analogs

A focused series of aminothiazole B-ring derivatives were designed with the aim of simultaneously improving both the activity for inhibiting the production of Aβ42, as well as refining crucial physicochemical parameters, including aqueous solubility. Previously, the incorporation of heteroatoms within the D-ring of the aminothiazole-based GSMs led to ligands that demonstrated moderately improved chemical properties and good pharmacokinetic behavior.[33] However, compounds within this novel series did not maintain the modulator activity associated with the parent aminothiazole **3**. Based on literature analysis of methyl imidazole-derived GSMs, various modifications to the B-ring have been reported that favorably influence Aβ activity while also providing ligands with desirable ADMET properties.[31, 34, 35] Leveraging our prior efforts toward identifying a potent GSM with improved physical properties, ligand design focused on reducing lipophilicity through the identification of an optimal heterocyclic B-ring alternative within the 2-aminothiazole scaffold.

Based on the moderately active tetrahydroindazole D-ring analog **4**, a focused series of corresponding B-ring derivatives were conceived in order to assess the functional tolerance of the adjacent chemical environment within the γ-secretase enzyme aimed at simultaneously enhancing modulator activity and improving other problematic properties associated with the ligand through the incorporation of novel bioisosteric functionalities.[33] Compound design prioritized scaffolds containing heterocycles for synthesis, since the prior use of this strategy was demonstrated to be generally successful at addressing poor compound solubility as well as other property-related issues. Derivatives containing phenyl, methoxyphenyl, pyridyl, hydroxypyridyl, methoxypyridyl, and methoxypyrazinyl B-rings were subsequently synthesized.

2.2   Synthesis

The preparation of compounds that explore the consequences of modifying the B-ring of the GSM scaffold was based on a convergent synthetic route in which the coupling of two fragments would provide the desired analog (Scheme 2). Synthesis of the western portion of the scaffold containing phenyl and pyridyl B-rings was initiated by the nucleophilic substitution of acetophenones **6a-c** using 4-methylimdazole to provide ethanones **7a-c**.[36] Subsequent acid catalyzed bromination of **7a,c** furnished the first desired coupling partners, bromoethanones **8a,c**. The construction of the related methoxyphenyl B-ring precursor utilized a similar reaction sequence. Fluoroacetophenone **7b** was subjected to a second nucleophilic substitution using sodium methoxide to provide methoxyphenylethanone **9**. Bromination furnished the desired methoxyphenyl coupling partner **10** in high yield.

While the synthesis of the phenyl-, methoxyphenyl-, and pyridyl B-ring-containing analogs was straightforward, the introduction of the methoxypyridine and methoxypyrazine B-rings required longer reaction sequences for the assembly of the desired coupling intermediates (Scheme 3). The preparation of the western portion of the methoxypyridine B-ring analog was initiated through the nucleophilic aromatic substitution of 2,6-dibromo-3-aminopyridine

by sodium methoxide providing 6-bromo-2-methoxy-3-aminopyridine **12a**.[37] N-formylation of intermediate **12a** was accomplished through the *in situ* generation of formic anhydride allowing straightforward access to formamide **13a**.[38, 39] Conversion to the corresponding ketoformamide was accomplished via nucleophilic substitution of chloropropanone by intermediate **13a**. The construction of the A-ring of the tetracyclic was completed through the cyclization of ketoformamide **14a** using ammonium acetate.[36] Palladium-mediated Heck coupling of bromopyridine **15a** and *n*-butylvinylether followed by acidic hydrolysis allowed the isolation of pyridylethanone **16a**. Finally, acid-catalyzed bromination of intermediate **16a** provided access to the desired coupling fragment, bromoacetophenone **17a** in good yield. While trace amounts of demethylation were observed for the initial transformations from **16** to **17**, this was greatly minimized by conducting the reaction at room temperature and under diluted conditions. Similarly, the construction of methoxypyrazine B-ring coupling fragment utilized the same three-step reaction sequence to construct the methyl imidazole A-ring starting from bromomethoxypyrazamine **12b**. Stille coupling of bromopyrazine intermediate **15b** with tributyl(1-ethoxyvinyl) tin provided pyrazinylethanone **16b**, that upon bromination using tailored conditions, provided the desired methoxypyrazine intermediate **17b**.

The shared eastern portion of the analogs was synthesized from commercially available racemic 2-oxocyclohexane-1-carbonitrile **18** (Scheme 4).[33, 36] Condensation of the starting material with ethylhydrazine, furnished 3-aminocyclohexapyrazole **19** in good yield. Benzoyl thiourea **20** was then isolated following the reaction of benzoyl isothiocyanate with intermediate **19**. Base-mediated removal of the benzoyl group permitted straightforward isolation of the common coupling partner **21**. The desired B-ring analogs were then prepared following Hantzsch condensation of the appropriate bromoketone with thiourea **21,** permitting the formation of the thiazole C-ring (Scheme 5).[40] In addition, a pyridinol B-ring analog **23**, was prepared following demethylation of methoxypyridine **22d** using HBr (Scheme 6). The implementation of a convergent synthetic strategy provided access to a variety novel GSM compounds containing focused B-ring alterations.

3.0   Results and Discussion

3.1   Activity of novel B-ring GSM analogs

Following preparation, the novel analogs' ability to suppress the formation of Aβ42 was determined using an enzyme-linked immunosorbent assay (ELISA). The simplification of the B-ring scaffold through the synthesis of desfluoro analog **22a** resulted in a greater than 4-fold loss in activity, suggesting that the presence of a substituent may be critical to maintaining and improving potency (Table 1). Replacement of the 3-fluoro substituent within the scaffold was well tolerated as demonstrated by methoxyphenyl analog **22c,** which displayed commensurate activity to parent tetrahydroindazole **4**. Alternatively, pyridyl derivative **22b** revealed that the addition of a heteroatom in place of the substituent within the B-ring was deleterious to γ-secretase activity. 3-Methoxypyridine **22d** and 3-hydroxypyridine **23** were then synthesized in order to ascertain if the introduction of substituents within a pyridine derivative was capable of restoring activity. The 3-hydroxypyridine **23** exhibited a modest recovery of potency, whereas the 3-methoxypyridine

22d showed a nearly 3-fold improvement in activity over the parent compound with an IC_{50} value of 60 nM. Varying the heterocyclic B-ring component of methoxypyridine **22d** providing methoxypyrazine **22e** was well tolerated and resulted in a minor decrease in ligand activity for attenuating the production of Aβ42 with an IC_{50} value of 89 nM.

The preparation of novel B-ring analogs of GSM **4** led to the discovery of methoxypyridine **22d** and methoxypyrazine **22e**, which demonstrated improved activity for inhibiting the formation of Aβ42. The general reduction in the overall clogP associated with the integration of heteroatoms within the B-ring was anticipated to lead to increased aqueous solubility. Methoxypyridine **22d** displayed fair kinetic aqueous solubility, whereas methoxypyrazine **22e** remained insoluble despite the observed decrease in clogP (Table 1). The solubility of methoxyphenyl **22c** was also evaluated, since GSMs containing this scaffold have been previously developed and demonstrated good activity as well as ideal ADMET properties. Similar to methoxypyridine **22d**, methoxyphenyl analog **22c** exhibited fair aqueous solubility, which indicates that the character of the aromatic B-ring can influence the solubility of ligands containing a 3-methoxy substituent.

3.2 Expanded SAR of B-ring GSM analogs

Identification of the methoxypyridine **22d**, which exhibited robust activity for attenuating the production of Aβ42 in addition to good aqueous solubility, led us to broaden our exploratory set of B-ring analogs to include additional related scaffolds from our modestly active D-ring GSM series in order to foster a better understanding of the role of the B-ring as it pertains to both activity and physical properties. Tetrahydroindazole **24**, as well as 3-tert-butylpyrazoles **25** and **26** were selected from two distinct families of GSMs for focused chemical B-ring modification (Figure 2).[41] Novel analogs of the selected compounds containing phenyl, pyridyl, methoxyphenyl or methoxypyridyl B-rings were synthesized and evaluated for Aβ42 activity.

The synthesis of the initial focused B-ring analog series provided access to the western portion of the desired analogs (Schemes 2 and 3). The preparation of the eastern coupling partner was achieved using previously establish reaction conditions. Briefly, the thiourea intermediate necessary to furnish the additional tetrahydroindazole compounds commenced through the condensation of 2-oxocyclohexane-1-carbonitrile with methylhydrazine and subsequently followed the same reaction sequence as described in Scheme 4.[33, 36] Similarly, the thiourea coupling component required to synthesize the substituted *tert*-butylpyrazoles began with the addition of the appropriate alkylhydrazine to pivaloylacetonitrile (Scheme 7). The 3-aminopyrazole product, **28,** was then exposed to benzoyl isothiocyanate, providing intermediate **29**, which upon cleavage of the benzoyl group allowed access to the desired thiourea **30**. Finally, the additional B-ring modified aminothiazoles were isolated following Hantzsch condensation of the appropriate western and eastern portions of the molecule (Scheme 8).[40]

The broadened series of compounds were then screened for the ability to suppress the Aβ42 levels. Similar to the initially prepared tetrahydroindazole B-ring analogs, the integration of a phenyl B-ring within the expanded compound series led to a greater than 2-fold loss in

potency for tetrahydroindazole **31a** and N-ethylpyrazole **33a** for suppressing the formation of Aβ42, whereas N-methylpyrazole **32a** showed similar activity to the parent (Table 2). The corresponding 3-pyridyl B-ring analogs **31b**, **32b**, and **33b** also displayed substantial losses in activity. The general trend toward significantly reduced affinity within the phenyl and pyridyl analog series reinforced the assertion that the 3-postion B-ring substituent engages in favorable interactions with the target enzyme. Alternatively, 3-methoxyphenyl derivatives **31c** and **32c**, exhibited a modest improvement in efficacy when compared to the corresponding fluorophenyl compounds. However, the 3-methoxy substituent did not lead to increased affinity for N-ethylpyrazole **33c**, which exhibited a slight reduction in potency. This pattern of activity was also observed for the methoxypyridyl B-ring derivatives; a greater than 2-fold improvement in activity was observed for N-methylpyrazole **32d** and tetrahydroindazole **31d**, whereas N-ethylpyrazole **33d** was less active than the corresponding parent ligand. Although the introduction of either the methoxyphenyl or methoxypyridyl B-ring generally led to improved activity for inhibiting the production of Aβ42, a greater magnitude as well as absolute effect upon the peptide was associated with the presence of the methoxypyridyl B-ring. Furthermore, the inclusion of this functionality addressed the limited solubility that was associated with the previously developed compounds, as shown by methoxypyridyl analogs **31d** and **33d**.

3.3 In vitro ADMET and mouse in vivo pharmacokinetics of GSM 22d

The preparation of a focused series of B-ring analogs identified the methoxypyridine-containing scaffold as a promising replacement for the fluorophenyl moiety within the original GSMs based on the criterion of activity as well as solubility. Since the incorporation of this novel B-ring significantly altered architecture of the scaffold, the most active analog, tetrahydroindazole **22d**, was selected for comprehensive *in vitro* ADMET analysis in order to examine the effect of the methoxypyridyl B-ring upon additional critical parameters. These studies showed that tetrahydroindazole **22d** displayed an adequate cytochrome P450 inhibition profile (Table 3), as well as acceptable hERG ion channel inhibition potential (all IC_{50} values > 1 μM). However, the limited metabolic stability with respect to humans is a potential concern for tetrahydroindazole **22d** despite the good stability observed in the presence of rodent liver microsomes. In addition, similar to the previously developed fluorophenyl GSM series, analog **22d** displayed high plasma protein binding which may limit *in vivo* exposure due to drug sequestration.

Although the ADMET screening of tetrahydroindazole **22d** identified potential limitations that may impede compound development, pharmacokinetic evaluation was undertaken in order to assess the impact of the structural changes associated with the novel methoxypyridyl B-ring upon compound behavior in an *in vivo* setting. Following intravenous administration (iv) of compound **22d** (1 mg/kg), high clearance (Cl = 2,159 mL/hr/kg) in male CD-1 mice was observed (Table 4), which represented approximately 40% of mouse hepatic blood flow (90 mL/min/kg) and was associated with a short plasma half-life (0.5 hr). After oral administration (po), compound **22d** (5 mg/kg) was rapidly absorbed, reaching C_{max} after 0.25 hr. Based on the exposure data for each route of dosing, the bioavailability (F) was estimated to be 53.7%. Given the high clearance of compound **22d**, a significant first-pass effect is expected following oral administration. Assuming that

the liver is responsible for drug elimination, approximately 40% of the absorbed dose will be metabolized during the first-pass, leaving only 60% of the compound capable of reaching systemic circulation. Since 53.7% of analog **22d** is bioavailable, nearly 90% of the oral dose is absorbed from the lumen of the small intestine. The comparison between brain and plasma drug levels of analog **22d** shows a ratio of 0.4 following both oral and iv administration, demonstrating that the compound can readily penetrate the blood-brain barrier (BBB) and reach the site of intended action. Although the brain to plasma ratio is indicative of good CNS penetrance, the metric cannot be used as a predictor of *in vivo* efficacy, since drug action is contingent upon unbound drug rather than absolute levels. Collectively, the pharmacokinetic data demonstrates that despite high clearance in mice, tetrahydroindazole **22d** is readily absorbed and is capable of passing the BBB.

3.4   In vitro biomarker assessment of modulator activity of GSM 22d

Since γ-secretase is critical to the processing of numerous substrates, including the Notch 1 receptor, inhibition of the enzyme is known to lead to adverse effects.[19, 20] Consequently, compound **22d** was subjected to additional scrutiny in order to ensure that the structural modifications did not affect the mode of action. In order to ascertain the preservation function of γ-secretase associated with treatment, vehicle, compound **22d**, and a GSI (DAPT) were incubated with H4 human neuroglioma cells over-expressing human APP751 transfected with the Myc-tagged Notch (N E) construct.[42] Incubation with the GSI led to accumulation of the Notch substrate (NδED) due to inhibition of γ-secretase function (Figure 3), whereas vehicle and compound **22d** did not impair enzyme function, as indicated by the presence of the processed Notch intracellular domain (NICD) and the absence of increased substrate. To further assess the modulator activity of compound **22d**, the Aβ peptide profile elicited by treatment was determined following incubation with SHSY5Y-APP cells. In concordance with γ-secretase modulation, the levels of Aβ42 and Aβ40 were suppressed while levels of Aβ38 were potentiated (Figure 4). Since the activity of the enzyme was preserved, no change in the total levels of Aβ were observed. In addition, the IC_{50} value for Aβ42 in the Meso Scale Multiplex assay was consistent with that of the primary activity screen.

3.5   SAR of D-ring GSM analogs

The simultaneous improvement in activity of suppressing Aβ42 formation and solubility that accompanied the incorporation of a methoxypyridine B-ring led us to pursue additional D-ring analogs. The 2-fold or greater increase in potency observed for tetrahydroindazoles **22d** and **31d** as well as the good solubility exhibited by both compounds supported the examination of previously synthesized and marginally active D-ring tetrahydroindazole compounds in order to examine the broader effect of this B-ring substitution upon ligand activity and physical properties within a more diverse series of analogs aimed at identifying a compound with good drug-like potential.[33]

Amalgamated tetrahydroindazole analogs **34–52** were prepared through the use of the aforementioned Hantzsch condensation of the appropriate substrates, and the impact of the compounds upon Aβ42 production was determined. The N-alkyl derivatives **34** and **35** displayed a greater than 3-fold increase in efficacy over the corresponding fluorophenyl

parent but continued to show the limited aqueous solubility observed within the original series (Table 5). N-tertbutyl tetrahydroindazole **36** similarly exhibited 3-fold increase in activity in addition to ideal solubility despite the added hydrophobic bulk. As observed with the N-alkyl analogs, the N-cycloalkyl tetrahydroindazoles, **37–39**, demonstrated improved potency for attenuating the production of Aβ42. Moreover, a direct correlation between the size of the N-cycloalkyl substituent and solubility was observed in which successive ring expansion rapidly diminished aqueous solubility. Heteroatom insertion within the N-cycloalkyl substituent was likewise better tolerated within methoxypyridyl B-ring compounds. N-tetrahydrofuran **40** and N-tetrahydropyran **41** were 2-fold and 7-fold more potent than the analogous fluorophenyl B-ring compounds, respectively, whereas N-methylpiperidine **42** remained inactive. Similar gains in activity and ideal solubility were also observed for tethered N-heterocyclic analogs in which an ethyl or propyl linker was inserted into the substituent. However, despite the significantly improved efficacy, the more flexible N-substituent of analogs **43–45** do not achieve the levels of activity associated with direct N-substitution of the tetrahydroindazole scaffold. Increased efficacy and good solubility were also achieved by both N-fluoroethyl analog **46** and N-trifluoroethyl analog **47**, which exhibited a greater than 2-fold improvement in potency when compared to the analogous fluorophenyl with IC_{50} values of 47 nM and 57 nM, respectively. The same overall trend of augmented activity and ideal solubility associated with the incorporation of the methoxypyridyl B-ring was also observed for 2-methoxyethane **48**, 2-hydroxyethane **49**, 2-hydroxypropane **50** and 2-hydroxy-2-methylpropane **51**; however, analogs **50** and **51** demonstrated superior activity with IC_{50} values of 50 nM and 38 nM, respectively. Finally, the altered B-ring was even capable of imparting marginal activity to the methylamino-linked tetrahydroindazole **52**. Collectively, the introduction of the methoxypyridyl B-ring was largely able to address the solubility of the tetrahydroindazole series while enhancing biochemical activity and supporting the overall rationale of the design.

The novel series of methoxypyridine-derived tetrahydroindazoles also demonstrated distinct structure-activity relationship (SAR) when compared to the parent fluorophenyl series. The methoxypyridine analogs revealed broad tolerance for N-alkyl substitution within the D-ring of the scaffold as demonstrated by the various linear, branched, and cyclic alkyl functionalities that retain good activity for reducing Aβ42 levels as evidenced by analogs **34–39**. The heterocyclic substituted analogs, unfortunately, were not as active as their alkyl counterparts and suffered from poor metabolic stability (Table 5). Taken together, these results suggest the presence of a rather large hydrophobic region near the N-substituent of the D-ring. The haloalkyl derivatives, such as N-fluoroethane **46** and N-trifluoroethane **47**, also exhibited good modulator activity, indicating that analogs containing smaller N-substituents retain the favorable interactions with γ-secretase of their larger cycloalkyl counterparts. Since variations in the size and connectivity of the N-alkyl substituent result in a modest disparity between the analog activities, the larger N-substituents are likely near a region of open space rather than actively engaging in beneficial interactions with the target enzyme. In addition, 2-hydroxypropane **50** also shows good activity, while 2-hydroxy-2-methylpropane **51** is the most potent analog within the methoxypyridine-derived tetrahydroindazole family with an IC_{50} value of 38 nM. The tolerance exhibited by these compounds for the introduction of a polar substituent is hypothesized to be the result of an

intramolecular hydrogen bond between the hydroxyalkyl moiety and one of the proximal nitrogen atoms within the scaffold which serves to rigidify the D-ring and preserve favorable hydrophobic contacts with the γ-secretase enzyme. Collectively, the significant improvement in activity observed within the tetrahydroindazole series indicates that the methoxypyridyl B-ring engages in beneficial interactions with γ-secretase as well as influences the binding conformation, resulting in access to additional favorable contacts for distal portions of the scaffold.

Although not all of the analogs within this set of derivatives exhibited improved activity for attenuating the production of Aβ42, the broad trend of increased efficacy and solubility demonstrated by the tetrahydroindazole compounds led us to expand the scope of the analogs to include methoxypyridyl B-ring derivatives of other GSMs previously synthesized. Increasing the structural diversity of the methoxypyridine B-ring analogs to include active derivatives of the marginally soluble fluorophenyl 3-tert-butylpyrazole family of compounds as well as the poorly soluble fluorophenyl cyclopentapyrazoles was conducted to explore the impact of this substitution upon physicochemical properties with the overarching aim of identifying a modulator that aligns potent activity with good drug-like behavior.

Through the incorporation of the novel methoxypyridine B-ring, additional D-ring analogs **53–74** were constructed and subsequently evaluated by ELISA for the ability to suppress Aβ42 peptide levels. N-propyl 3-tert-butylpyrazole **53** exhibited a modest loss in activity similar to N-ethylpyrazole **33d** from the pilot B-ring screening series, whereas branched N-alkyl derivatives **54** and **55** showed improved potency with IC_{50} values of 64 nM and 40 nM, respectively (Table 6). However, the hydrophobicity of the N-substituent had a sizable impact on aqueous solubility as evidenced by N-isopropyl analog **54,** which displays ideal solubility, while the N-tert-butyl analog **55** remained poorly soluble. The activity of N-trifluoroethyl analog **57** was largely unaffected by the methoxypyridyl B-ring and exhibited only slightly better potency than the corresponding parent compound. Based on these results, the 3-tert-butylpyrazoles support the presence of a hydrophobic pocket near the 3-substituent; however, distinct from the tetrahydroindazole family of compounds, the 3-tert-butylpyrazoles series favors branched N-alkyl substituents. Alterations to the 3-postion substituent of the pyrazole also led to compounds with 2-fold better activity when juxtaposed to the equivalent fluorophenyl ligand as shown by 3-isopropylpyrazole **58** and 3-methylcyclopropylpyrazole **59**. However, reducing the hydrophobicity of the 3-substituent was deleterious to the overall activity as demonstrated by 3-isopropylpyrazole **58**, whereas the subtle architectural modification of 3-methylcyclopropyl analog **59** led to the most potent derivative of the series with an IC_{50} value of 32 nM. The trend of improved activity was also observed for derivatives characterized by the presence of a 3-trifluoromethyl substituent as shown by N-ethyl analog **60** and N-trifluoroethyl analog **62** despite the reduction in overall hydrophobicity. In addition, the disparate potency of analogs **60** and **62** belies their remarkable structural similarity and is hypothesized to be the result of electronic effects linked to the presence of multiple electron withdrawing functionalities on the pyrazole ring. The incorporation of the novel methoxypyridyl B-ring generally provided 3-tert-butylpyrazole ligands with improved activity for suppressing the formation of Aβ42;

however, increases in aqueous solubility were reserved for compounds with reduced D-ring hydrophobic character.

In a similar fashion, methoxypyridyl B-ring derivatives of the cyclopentapyrazole compounds were also synthesized and evaluated for modulator activity. N-methyl analog **63** exhibited remarkable activity considering that the parent fluorophenyl compound was unable to affect Aβ42 levels (Table 6). The potency of N-ethyl compound **64**, on the other hand, was not influenced by the methoxypyridyl B-ring; however, the increased size of the N-alkyl substituent led to a greater than 2-fold increase in activity within the series (**63** vs. **64**) with an IC_{50} value of 33 nM. Further increase in N-alkyl substituent size in the presence of the methoxypyridyl B-ring was associated with a loss of activity for N-isopropyl analog **65**, whereas N-tert-butyl compound **66** exhibited a nearly 3-fold increase in potency. However, neither of the larger N-alkyl branched analogs was able to surpass the activity of N-ethyl derivative **64**, indicating that the added bulk is likely perturbing subtle enzyme-ligand interactions by influencing the compound's binding conformation. The greater than 3-fold improvement in the activity of N-cyclobutyl analog **67** further suggests that the N-substituent of the D-ring plays a significant role in determining access to ligand conformations that facilitate favorable interactions with γ-secretase, since there is no direct correlation between substituent size or hydrophobic content and activity within the alkyl substituted methoxypyridyl B-ring derivatives. In addition to good activity, N-alkyl analogs **63–67** displayed improved solubility when compared to the equivalent fluorophenyl compounds; however, increasing the size of the N-alkyl D-ring substituent led to a localized accumulation of hydrophobicity and a reduction in aqueous solubility. The novel methoxypyridyl B-ring was also responsible for the nearly 3-fold improvement in potency observed for N-trifluoroethyl analog **69**, which exhibited an IC_{50} value of 36 nM as well as imparting good modulator activity to N-hydroxyethyl analog **70**. Moreover, these analogs demonstrate that the addition of heteroatoms within the N-substituent is well tolerated and results in compounds that exhibit ideal aqueous solubility. Conversely, analogs **71** and **72,** which contain additional methyl substituents upon the fused system, displayed a modest reduction in activity associated with the introduction of the methoxypyridyl moiety, indicating that B-ring is capable of influencing the distal binding conformation, which results in a modest reduction in affinity for the enzyme target. The larger cycloheptapyrazole **73** displayed a greater than 3-fold increase in modulator activity with an IC_{50} value of 32 nM, thus reinforcing the presence of a broad yet narrow pocket which accommodates the D-ring. In addition, despite the increased alkyl functionalization and increased clogP values, derivatives **71–73** exhibit good aqueous solubility. Finally, reducing the size of the D-ring scaffold was deleterious to activity as evidenced by N-ethyl pyrazole analog **74**, indicating the presence of critical hydrophobic interactions between the carbocycle and γ-secretase, which facilitate modulator activity. Overall the previously identified trend of superior activity as well as substantially improved aqueous solubility associated with the methoxypyridyl B-ring was observed for the cyclopentapyrazole series of compounds and paralleled that of the closely related tetrahydroindazole family of analogs. The identification of the methoxypyridyl B-ring proved to be a fortuitous discovery that addressed the primary shortcomings of the initial fluorophenyl aminothiazole series.

3.6   In vitro ADMET of methoxypyridine-derived analogs

The prepared B-ring derivatives significantly broadened our collection of compounds with good activity for suppressing the formation Aβ42 and ideal aqueous solubility. Utilizing these two metrics, compounds were stratified for additional in vitro ADMET studies in order identify other potential property-related liabilities within this novel family of compounds. A tiered ADMET screening paradigm was implemented to allow early triage of molecules with undesirable characteristics. The metabolic stability of methoxypyridyl B-ring analogs was initially evaluated for compounds with fair activity (IC$_{50}$ values   100 nM) and good aqueous solubility (solubility   5 μM). Analogs that exhibited acceptable stability were then evaluated for Cyp inhibition potential and hERG inhibition potential, followed by the evaluation of cell permeability by MDR1-MDCK assay.

ADMET screening of the tetrahydroindazoles showed that N-alkyl and N-cycloalkyl substitution upon the tetrahydroindazole scaffold for the prepared methoxypyridyl B-ring analogs generally show poor metabolic stability as demonstrated by compounds **36** and **37** (Table 5). Since the closely related N-ethyl tetrahydroindazole **22d** exhibited better stability, the modestly soluble N-isopropyl analog **35** was also evaluated, but unfortunately also displayed weak stability, suggesting that increasing the size of the alkyl N-substituent facilitates metabolism of the compound. Poor metabolic stability persisted through the N-heterocyclic substituted compounds as demonstrated by N-tetrahydrofuran **40**. Methylpiperidine **42** and tethered morpholino analogs **44** and **45** were screened to further explore this trend and demonstrated that poor stability is associated with the N-heterocyclic containing compounds and is exacerbated by the insertion of a linker motif. Alternatively, terminally functionalized N-fluoroethane **46** demonstrated robust metabolic stability, while closely related N-trifluoroethane **47** shared the metabolic instability observed for nearly all the compounds within tetrahydroindazole series. Modestly improved stability was also observed for N-hydroxyethyl analog **49** and N-2-methylpropan-2-ol analog **51**. The incongruence with respect to stability across this series of compounds suggests that the novel methoxypyridyl B-ring is not the source of instability.

Guided by the metabolic stability data, N-fluoroethyl analog **46** and N-2-methylpropan-2-ol analog **51** were subjected to further *in vitro* ADMET analysis. Both analogs exhibited acceptable cytochrome p450 inhibition potential, displayed good brain penetration properties, and lacked potent binding to the hERG ion channel (Table 5). However, based on the totality of the *in vitro* data for both compounds, N-fluoroethane **46** exhibited superior ADMET characteristics and was selected for further study. Although two compounds with good drug-like properties were identified, the methoxypyridyl-derived tetrahydroindazole family of compounds by and large suffered from impaired metabolic stability, and future design efforts will focus on incorporation of features which aim to address this parameter.

Methoxypyridyl B-ring analogs of 3-tert-butylpyrazole family of compounds that met the development criterion were also subject to ADMET screening to establish drug-like potential. Consistent with the N-alkyl tetrahydroindazoles, N-ethyl analog **33d** exhibited fair stability, whereas N-isopropyl derivative **54** was significantly metabolized, indicating that the size of the N-alkyl functionality persistently influenced metabolic stability across related

D-ring scaffolds. Conversely, N-fluoroalkyl functionalized analogs, **56** and **57**, displayed improved metabolic stability upon incubation with rodent liver microsomes; however, stability in human liver microsomes, while better, remains limited. Altering the connectivity of the 3-tert-butyl moiety providing methylcyclopropyl analog **59** led to a good overall stability profile. Similarly, modifying the scaffold to include a 3-trifluoromethyl substituent (**60**) resulted in ideal metabolic stability, indicating that both substituents on the pyrazole are capable of moderating metabolism. Collectively, the pyrazole analogs further demonstrate that the introduction of the methoxypyridyl B-ring does impact the physical properties and activities of the ligands; however, it is not the source affecting compound stability. Additional analysis of pyrazoles **59** and **60** established that both compounds possess good Cyp inhibition profiles as well as ideal hERG inhibition potential. These analogs also display moderate permeability and limited efflux, which is consistent with compounds that display high brain penetration. Although most of the 3-tert-butylpyrazoles are readily metabolized, 3-methylcyclopropyl analog **59** and 3-trifluoromethyl analog **60** exhibit acceptable overall ADME profiles, including good stability, which supports the continued investigation of both compounds.

Analysis of the active cyclopentapyrazole compounds reinforced many of the trends observed for the 3-tert-butylpyrazoles and tetrahydroindazoles. Similar to both prior pyrazole-derived D-ring series, good metabolic stability was associated with cyclopentapyrazoles characterized by smaller N-alkyl substituents as demonstrated by analogs **63**-**66** (Table 6). Moreover, compound **65** shows that N-cycloalkyl substitution serves to exacerbate this trend. The cyclopentapyrazole analogs also illustrate that reducing the size of the fused alkyl functionality of the D-ring is not sufficient to improve metabolic stability. Paralleling the related D-ring analogs, increasing the polarity with the N-ethyl substituent provided compounds with improved metabolic stability. N-trifluoroethane **69** and N-hydroxyethane **70** displayed good microsomal stability in two of the three species tested, whereas N-fluoroethane **68** displayed increased stability across all species evaluated. Conversely, analogs **71** and **72** indicate that reducing the polarity of the D-ring through the introduction of methyl substituents upon the cyclopentane ring is deleterious to metabolic stability. Likewise, poor stability was also associated with increasing the size of the fused ring system as illustrated by cycloheptylpyrazole **73**.

The shorter N-alkyl substituted compounds, **63** and **64**, as well as polar functionalized cyclopentapyrazoles that showed comparative stability (**68**, **69**, and **70**) were subjected to additional screening. The close structural relationship of N-methyl **63** and N-ethyl **64** led to similar overall ADMET profiles; both compounds exhibited weak cytochrome p450 inhibitory potential, good brain penetration potential, and modest hERG inhibition. Alternatively, the profiles of N-fluoroethyl **68**, N-trifluoroethyl **69** and N-hydroxyethyl **70** display more variability. Cytochrome p450 inhibition profiles of N-fluoroethane **68** and trifluoroethane **69** were ideal and acceptable, respectively. However, N-hydroxyethane **70** was a potent 3A4 inhibitor, and screening for hERG inhibition potential revealed a potential liability for analog **69**. Although ADMET properties precluded the development of many of the cyclopentapyrazoles, N-alkyl substituted compounds **63**, **64**, and N-fluoroethane **68** generally demonstrated acceptable profiles.

3.7 Pharmacokinetics of GSM analogs

Pharmacokinetic study of selected methoxypyridine-derived analogs was undertaken to assess the effect of the related structural modifications upon in vivo parameters. Following intravenous administration to male CD-1 mice, compound clearance was generally high with the exception of 3-methylcyclopropyl analog **59** and cyclopentapyrazole **63** (Table 7). The clearance observed for compounds **59** and **63** were approximately 13% and 24% of mouse hepatic blood flow (~90 mL/min/kg), whereas the clearance ranged from 30% to 64% of mouse hepatic blood flow for the other dosed analogs. The elevated clearance levels of pyrazole **60** and cyclopentapyrazole **64** were consistent with the measured in vitro metabolic activity; conversely, despite being very metabolically stable, tetrahydroindazole **46** exhibited high clearance (Table 5 and 6). Significant first-pass metabolism is expected for compounds **46**, **60**, and **64** based on the high rate of clearance. In contrast, less variability was observed with respect to volume of distribution (V_{ss}) of the dosed analogs. A relatively large V_{ss} was measured for all of the compounds; volumes 2 to 5-fold higher than body water in mice (0.65 L/kg), which indicates that the binding of these compounds is biased toward tissue proteins rather than plasma proteins. In addition, compound half-life ($t_{1/2}$) was generally short and ranged from 0.65 to 3.84 hrs in mice following intravenous administration. The truncated $t_{1/2}$ is primarily due to the high Cl and, to a lesser extent, the difference in V_{ss}. Brain to plasma ratios for all of the compounds were also measured and, although variable, showed brain penetration that is sufficient for accessing the therapeutic target.

Following oral administration, all of the selected derivatives showed high oral bioavailability in mice. Tetrahydroindazole **46** exhibited the lowest bioavailability (46.4%) within the series; however, accounting for the approximately 60% of compound that is expected to be metabolized during the first-pass through the liver, the oral absorption is nearly complete in mice. Similarly, the fraction of dose absorbed is greater than 80% for analogs **60**, **63**, and **64** when accounting for first-pass effects. The period to reach maximum drug concentration (T_{max}) following oral administration was relatively short, ranging from 0.25 to 1.0 hr, with the exception of 3-methylcyclopropyl analog **59**. The time period to achieve the T_{max} is in the range of rodent gastric emptying, which suggests that the rate of intestinal absorption is quite rapid for these compounds. In addition, the longer period to achieving T_{max} for compound **59** is likely the result of a slower rate of dissolution resulting from its limited solubility (Table 6).

3.8 Pharmacodynamics of compounds 46 and 64

Although the more active GSMs considered for continued development display similar ADMET parameters and pharmacokinetic profiles, tetrahydroindazole **46** and cyclopentapyrazole **64** were selected for pharmacodynamic study using transgenic J20 mice that over-express human APP.[43] Following a 3-day treatment with either vehicle or test article, a dose-dependent reduction in plasma Aβ42 and Aβ40 was observed for compound **64** (Figure 5). Although the dose escalation of tetrahydroindazole **46** led to a greater suppression of Aβ42 and Aβ40 in plasma, the effect seems to plateau between 50 and 100 mg/kg. This effect was also reflected in the exposure data, which shows reduced plasma and brain drug levels at the top dose, suggesting that higher dosing may lead to prolonged absorption while the high clearance identified in the pharmacokinetic study remains

unchanged (Table 8). As a result of the shift in the absorption pattern at the high dose, the measured concentration of compound **46** is lower, but likely sustained over a longer period of time resulting the observed pharmacodynamic effect. Consequentially, cyclopentapyrazole **64** exhibited superior activity, suppressing Aβ42 by 76% at a dose of 100 mg/kg. In addition, both compounds also reduced Aβ38 levels. Based on the mode of action, the inhibition of Aβ38 was not expected and was inconsistent with the in vitro data showing potentiation of Aβ38 following GSM treatment (Figure 6).

Based on the superior pharmacodynamic effect of cyclopentapyrazole **64** in J20 transgenic mice, an additional efficacy study was conducted using Tg2576 transgenic mice that overexpress human APP containing the Swedish (K,M to N,L) double mutation to further ascertain the impact on the various Aβ peptides.[44] Female Tg2576 mice were orally dosed daily with either vehicle or 50 mg/kg of compound **64** for 14 days and the drug levels in plasma and brain were determined in addition to Aβ levels. Consistent with the mode of action, treatment with cyclopentapyrazole **64** decreased the levels of Aβ42 and Aβ40 while potentiating the levels of Aβ38 in plasma (Figure 7). In addition, brain Aβ42 levels were reduced by 23%, demonstrating that the compound is capable of crossing the blood brain barrier and reaching the desired site of pharmacodynamic action in brain. Furthermore, consistent with the in vitro permeability data, the brain to plasma drug levels demonstrated adequate penetration to account for observed effect in brain (Table 9).

4.0 Summary and conclusion

A focused effort to improve the activity and ADMET properties of aminothiazole-derived GSMs through the modification of the B-ring led to the identification of methoxypyridine as potential replacement for the fluorophenyl moiety. Integration of this novel structural motif within the B-ring of our scaffolds generally led to both improved activities for reducing Aβ42 and increased solubility across three related aminothiazole series. Subsequent ADMET screening of the highly active GSM analogs led to the selection of subset of structurally diverse compounds for pharmacodynamic evaluation. Based on the aggregate of data, tetrahydroindazole **46** and cyclopentapyrazole **64** were tested in transgenic mice to determine in vivo efficacy for attenuating Aβ42. While compound **64** was capable of reducing Aβ42 in the plasma and brain of Tg2576 mice, the dose required for therapeutic efficacy is likely too high to allow for adequate safety margins with respect to hERG inhibition. Although the discovery of the methoxypyridine led to improved GSM analogs, further optimization of the scaffold with respect to activity is likely necessary.

5.0 Experimental

5.1 Cell-based ELISA assay for measuring extracellular Aβ42 levels

Human SHSY5Y neuroblastoma cells stably overexpressing wild-type human APP751 (SHSY5Y-APP) have been described previously. Briefly, SHSY5Y-APP cells were plated on a 96-well plate at 75K per well. Following overnight incubation at 37 °C, wells were treated with various concentrations of compound in order to generate dose response curves. For treatment, a 25 mM stock solution of compound in DMSO was prepared. The DMSO stock solution was then diluted to 10 μM using cell media. The 10-point dose response curve was

generated following treatments that ranged from 0.3 pM – 10 μM for each compound with a 1:3.16 dilution across the plate with a total volume of 125 μL pre well. After being treated for 24 hours, the SHSY5Y-APP cells treated with either vehicle or compound were then inspected for obvious signs of toxicity. The quantity of Aβ42 was then quantified by ELISA.

In order to quantify Aβ42, coating antibody, Aβ35–42 (lot 454.23), was diluted 1:200 in TBS (Tris Buffered Saline, pH 7.4, Sigma T6664). Then, 100 μL of antibody Aβ35–42 was pipetted into each well of the micro plate. The plate was sealed and incubated at 4 °C for 21 hours. The coating antibody was then aspirated, rinsed with 200 μL of TBS, and aspirated again. Then, 200 μL of 1% BSA (bovine serum albumin) in TBS blocking agent was applied to each well followed by a one-hour incubation at room temperature. The wells were then aspirated, and 50 μL of sample from treated cells was added, followed by a two-hour incubation period. Each well of the plate was then washed three times with 200 μL of PBS/0.1%Tween-20. Then, 50 μL of Aβ1–12 mAb 436 (alkaline phosphatase conjugated antibody) diluted to 1:8000 in 1% BSA/TBS/0.1% Tween-20 was added to each well of the plate. The plate was then incubated for another two hours at room temperature and was washed six times with 200 μL of PBS/0.1%Tween-20. Finally, 50 μL of CDP-Star (Sapphire) luminescence substrate was added to each well of the plate and incubated for 15 minutes at room temperature in the dark. Then, the amount of Aβ42 was measured by reading the plate using a GloRunner Pro microplate luminometer by Turner Biosystems. For every plate quantified, a standard Aβ42 curve was generated. The Aβ42 IC_{50} values were determined from the 10-point concentration response curves (in duplicate at each concentration) by a four-parameter fit nonlinear regression analysis using Graphpad Prism software. The assays were required to demonstrate a Z′ score of   0.5 and to have a test-retest reliability with an r^2 of   0.75 for the GSM compounds, which represent a broad range of potencies. In addition, upon its discovery, compound **22d** was utilized as an internal standard for all subsequently prepared analogs on each assay plate and subjected to the same Z′ score and r^2 metrics to ensure the reproducibility and reliability of the data.

5.2   Measurement of extracellular Aβ42, Aβ40, and Aβ38 levels

Samples were tested using the Meso Scale Discovery Aβ triplex immunoassay with 4G8 detection (Catalog # K15141E-1, MSD Rockville, MD) to quantitate levels of Aβ38, Aβ40, and Aβ42. The kit was run according to the manufacturer's instructions. Briefly, 25 μL of SULFO-TAG conjugated 4G8 detection antibody and 25 μL of sample were added to a blocked MSD multiplex plate pre-coated with capture antibodies that were specific for Aβ38, Aβ40 and Aβ42 and incubated for 2 hr with shaking at room temperature. The plate was read on an MSD SECTOR® Imager 6000 after the addition of read buffer. Concentrations of Aβ38, Aβ40, and Aβ42 in samples were back-fitted from the respective standard curves using MSD Workbench software.

5.3   Pharmacokinetic evaluation

Male CD-1 mice (6–8 week-old) were administered a single dose of the test article via tail vein (iv) or by oral gavage (po) dose route. Formulations were prepared using 3% N-methylpyrrolidine (NMP)/45% polyethylene glycol 300 (PEG300)/12% ethanol/40% sterile water for iv administration and 5% NMP/95% PEG300 for oral administration.

Plasma was collected from mice at 0.083, 0.25, 0.5, 1, 2, 4, 8, and 24 hr for iv-dosed animals and at 0.25, 0.5, 1, 2, 4, 8, and 24 hr for orally dosed animals (n=3/timepoint). Brains were collected at 1, 2, 8, and 24 hr regardless of the route of administration (n=3/timepoint). Blood was collected from the retro-orbital sinus of mice under isoflurane anesthesia into tubes containing K_3EDTA, processed to plasma, and then stored frozen at $-70 \pm 10°C$ for subsequent drug levels analysis.

5.4 Drug level bioanalysis

Plasma and brain tissue samples were analyzed for drug levels using a discovery grade HPLC/MS/MS method. Mean plasma drug concentration versus time data were subjected to pharmacokinetic analysis using WinNonlin® (Version 4.1; Pharsight Corp.; Cary, NC). Data were subjected to non-compartmental analysis using WinNonlin® Model 200 (for extravascular administration) or Model 201 (for IV bolus administration); a uniform weighting factor was applied to each data set. T_{max} and C_{max} values were determined directly from the data. AUC_{last} values were calculated using the log/linear trapezoidal (IV dose) or linear up/log down trapezoidal (PO dose). Half-life values were calculated from the first order rate constant associated with the observed terminal portion of the plasma drug concentration versus time curve, as estimated by regression analysis, using a minimum of three non-zero time points after T_{max}. The regression with the largest adjusted R^2 (square of the correlation coefficient) was selected as the best fit. Estimated half-life values with an adjusted R^2 of less than 0.800 were considered to be unreliable and were excluded from inclusion in the tabulation of kinetic parameters. Bioavailability (F) was calculated as follows:

$$F\ (\%) = [(AUC_{0\text{-}INFpo}) \times Dose_{iv} \div (AUC_{0\text{-}INFiv}) \times Dose_{po})] \times 100$$

5.5 Pharmacodynamic study using J20 mice

Female J20 mice (5–6 month-old) were administered vehicle (5% NMP/95% PEG300) or test article at doses of 25, 50, and 100 mg/kg via oral gavage for three consecutive days (n=5/dose). Animals were sacrificed 4 hours post final dose on day 3. Plasma and brain were collected for the analysis of Aβ peptides and drug levels. Plasma and brain Aβ levels were quantified using Meso Scale multiplex kits and MSD SECTOR® Imager 6000. Statistical analysis was performed using Graphpad Prism software, and results were expressed as mean ± SEM. ANOVA was used to detect a significant effect.

5.6 Pharmacodynamic study using Tg2576 mice

Female Tg2576 mice (5–6 month-old) were administered vehicle (5% NMP/95% PEG300) or test article at a dose of 50 mg/kg via oral gavage for 14 consecutive days. Animals were sacrificed 4 hours post final dose on day 14. Plasma and brain were collected for the analysis of Aβ peptides and drug levels. Plasma and brain Aβ levels were quantified using Meso Scale multiplex kits and MSD SECTOR® Imager 6000. Statistical analysis was performed using Graphpad Prism software, and results were expressed as mean ± SEM. ANOVA was used to detect a significant effect.

5.7 Synthetic procedures

All reactions were performed under a dry atmosphere of nitrogen unless otherwise specified. Indicated reaction temperatures refer to the reaction bath, while room temperature (rt) is noted as 25 °C. Commercial grade reagents and anhydrous solvents were used as received from vendors and no attempts were made to purify or dry these components further. Removal of solvents under reduced pressure was accomplished with a Buchi rotary evaporator at approximately 28 mm Hg pressure using a Teflon-linked KNF vacuum pump. Thin layer chromatography was performed using 1" x 3" AnalTech No. 02521 silica gel plates with fluorescent indicator. Visualization of TLC plates was made by observation with either short wave UV light (254 nm lamp), 10% phosphomolybdic acid in ethanol or in iodine vapors. Flash column chromatography was carried out using a Teledyne Isco CombiFlash Companion Unit with RediSep Rf silica gel columns. Proton NMR spectra were obtained either on 300 MHz Bruker Nuclear Magnetic Resonance Spectrometer or 500 MHz Bruker Nuclear Magnetic Resonance Spectrometer and chemical shifts (δ) are reported in parts per million (ppm), and coupling constant (J) values are given in Hz, with the following spectral pattern designations: s, singlet; d, doublet; t, triplet; q, quartet; dd, doublet of doublets; m, multiplet; br, broad; sym, symmetrical. Tetramethylsilane (TMS) was used as an internal reference. Melting points were uncorrected and were obtained using a MEL-TEMP Electrothermal melting point apparatus. Mass spectroscopic analyses were performed either using positive mode electron spray ionization (ESI) on a Varian ProStar LC-MS with a 1200L quadrapole mass spectrometer or using positive mode atmospheric pressure chemical ionization (APCI) on a Shimadzu LC-MS system. High performance liquid chromatography (HPLC) purity analysis was conducted using a Varian Pro Star HPLC system with a binary solvent system A and B using a gradient elution [A, H_2O with either 0.05% or 0.1% trifluoroacetic acid (TFA); B, CH_3CN with either 0.05% or 0.1% TFA] and flow rate = 1 mL/min, with UV detection at 254 nm. All final compounds were purified to 95% purity and these purity levels were measured by a Varian Pro Star HPLC system. The following Varian Pro Star HPLC methods were used to establish compound purity:

A. Phenomenex Luna C18(2) column (4.6×250 mm); mobile phase, A = H_2O with 0.1% TFA and B = CH_3CN with 0.1% TFA; gradient: 10–95% B (0.0–10 min; hold for 6 min); UV detection at 254 nm.

B. SunFire C18 column (4.6×250 mm); mobile phase, A = H_2O with 0.1% TFA and B = CH_3CN with 0.1% TFA; gradient: 10–100% B (0.0–20 min; hold for 5 min); UV detection at 254 nm.

C. SunFire C18 column (4.6×250 mm); mobile phase, A = H_2O with 0.1% TFA and B = CH_3CN with 0.1% TFA; gradient: 0–100% B (0.0–15 min; hold for 5 min)); UV detection at 254 nm.

D. SunFire C18 column (4.6×250 mm); mobile phase, A = H_2O with 0.05% TFA and B = CH_3CN with 0.05% TFA; gradient: 5–95% B (0.0–10 min; hold for 8 min)); UV detection at 254 nm.

E. SunFire C18 column (4.6×250 mm); mobile phase, A = H_2O with 0.05% TFA and B = CH_3CN with 0.05% TFA; gradient: 10–100% B (0.0–20 min; hold for 5 min)); UV detection at 254 nm.
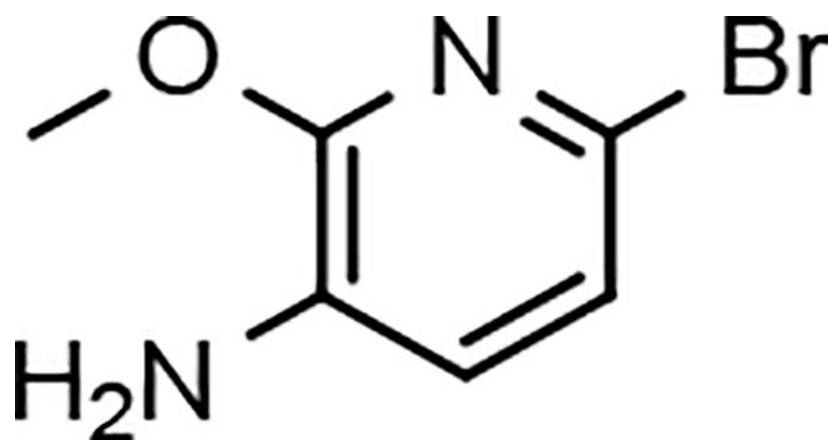
6-bromo-2-methoxypyridin-3-amine (12a)—Sodium methoxide (powder, 600 g, 11.1 mol) was added to a solution of commercially available 2,6-dibromopyridin-3-amine (**11a**, 400 g, 1.59 mol) in 1,4-dioxane (3500 mL) at room temperature under nitrogen. The resulting mixture was heated to 100 °C for 18 h. The reaction mixture was cooled to 0 °C and quenched by the careful addition of aqueous ammonium chloride (600 g in 1500 mL of water). The mixture was stirred for 15 minutes and concentrated in vacuo to remove as much 1,4-dioxane as possible. The residue was diluted with ethyl acetate (3000 mL), filtered through silica gel (500 g), and eluted with ethyl acetate (3000 mL). The aqueous layer was separated. The combined organic layer was washed with brine (2 × 500 mL), dried over sodium sulfate, filtered, and the solvents were removed under reduced pressure to afford 6-bromo-2-methoxypyridin-3-amine (**12a**) as a purple solid (314 g, 98%) that was suitable for use without further purification: Multimode MS (M+H) 203; 1H NMR (500 MHz, CDCl$_3$) δ 6.86 (d, J = 7.5 Hz, 1H), 6.76 (d, J = 7.5 Hz, 1H), 3.98 (s, 3H), 3.74 (br s, 2H).
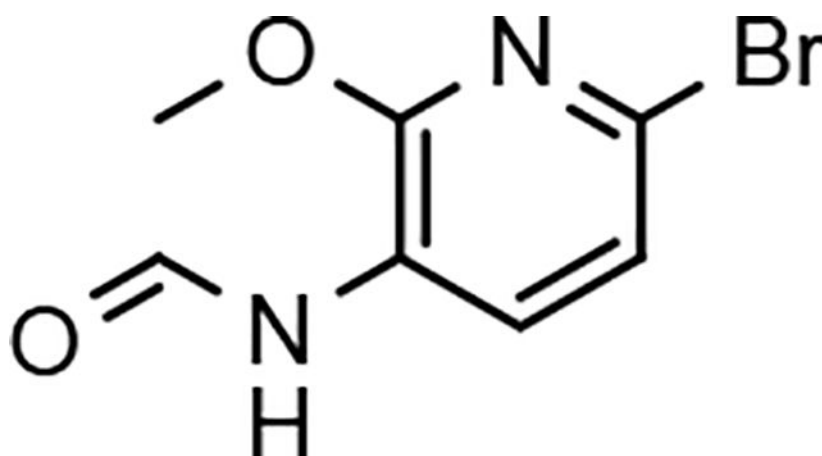
N-(6-bromo-2-methoxypyridin-3-yl)formamide (13a)—Acetic anhydride (522 g, 5.11 mol) was added slowly to formic acid (587 g, 12.8 mol) at 0 °C under nitrogen. The mixture was stirred at 0 °C for 30 min, warmed at room temperature, and stirred for 30 minutes. The mixture was recooled to 0 °C and a solution of 6-bromo-2 methoxypyridin-3-amine (**12a**, 346 g, 1.70 mol) in THF (2200 mL) was slowly added. Following addition, the ice bath was removed, and the reaction was stirred at room temperature for 2 h. The reaction mixture was

poured into 1:1 ice/water (8 L), stirred for 30 minutes, and filtered. The solids were further dried under high vacuum for 18 h to afford *N*-(6-bromo-2-methoxypyridin-3-yl)formamide (**13a**) as a red-brown solid (408 g, >99%), which was suitable for use without further purification: Multimode MS (M+H) 231; 1H NMR (500 MHz, CDCl$_3$) δ 8.49 (d, J = 8.0 Hz, 1H), 8.48 (s, 1H), 7.60 (br s, 1H), 7.07 (d, J = 8.0 Hz, 1H), 4.03 (s, 3H).
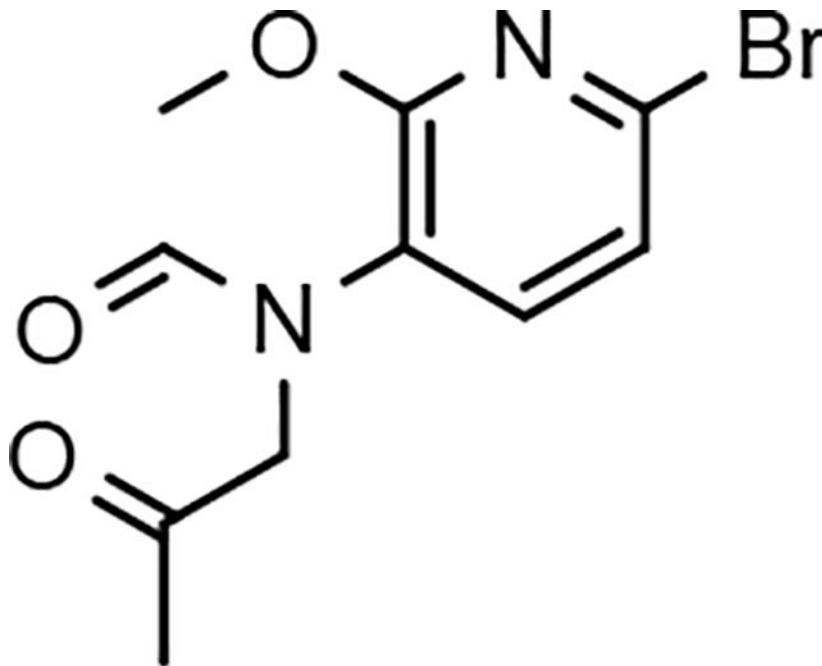
***N*-(6-bromo-2-methoxypyridin-3-yl)-*N*-(2-oxopropyl)formamide** (**14a**)—Potassium carbonate (powder, 325 mesh, Aldrich catalog #: 347825, 855 g, 6.20 mol) and potassium iodide (29.4 g, 0.177 mmol) were added to a solution of *N*-(6-bromo-2-methoxypyridin3-yl)formamide (**13a**, 408 g, 1.77 mol) in *N,N*-dimethylformamide (4000 mL) at room temperature under nitrogen. To the resulting mixture was slowly added 2-chloroacetone (408 g, 4.43 mol). The mixture was stirred at room temperature overnight. The resulting suspension was carefully poured into 1:1 ice/water (12 L) and stirred vigorously for 25 minutes. The resulting solid was collected by filtration and washed with water. The solid was dried for two days under high vacuum (at 60 °C) to afford *N*-(6-bromo-2-methoxypyridin-3-yl)-*N*-(2-oxopropyl)formamide (**14a**) as a brown solid (474 g, 93%) that was suitable for use without further purification: Multimode MS (M+H) 287; 1H NMR (500 MHz, CDCl$_3$) δ 8.22 (s, 1H), 7.48 (d, J = 8.0 Hz, 1H), 7.13 (d, J = 8.0 Hz, 1H), 4.47 (s, 2H), 3.99 (s, 3H), 2.17 (s, 3H).
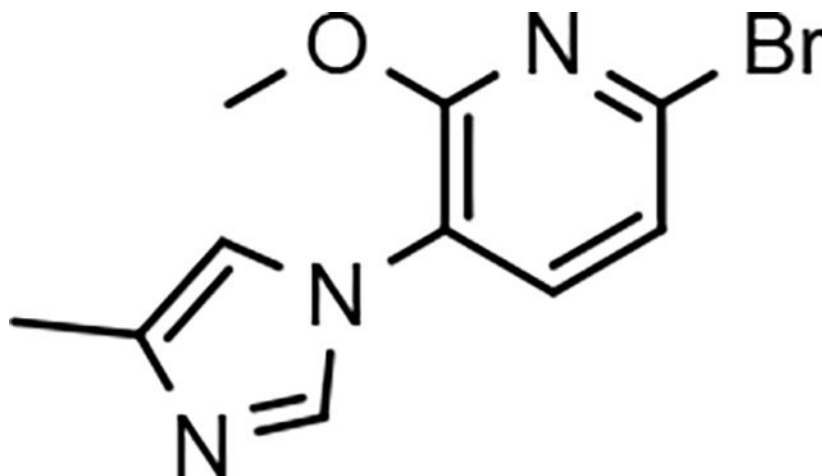
6-bromo-2-methoxy-3-(4-methyl-1H-imidazol-1-yl)pyridine (15a)—Ammonium acetate (636 g, 8.26 mol) was added to a stirred solution of *N*-(6-bromo-2-methoxypyridin-3-yl)-*N*-(2-oxopropyl)formamide (**14a**, 474 g, 1.65 mol) in acetic acid (4000 mL) at room temperature. After addition, the mixture was heated to 120 °C for 10 h. After cooling to room temperature, the mixture was concentrated in vacuo (at 60 °C) to remove the majority of the acetic acid. The resulting residue was diluted with ethyl acetate (4000 mL) and water (4000 mL). With fast stirring at room temperature, solid potassium carbonate was slowly added to the reaction mixture (neutralized to pH 8). The layers were separated, and the aqueous phase was extracted with ethyl acetate (2 × 1000 mL). The combined organic phase was dried over anhydrous sodium sulfate, filtered, and concentrated. The resulting residue was purified by flash column chromatography on silica gel, eluting with heptane/ethyl acetate (gradient of 4:1 to 3:7), to afford 6-bromo-2-methoxy-3-(4-methyl-1*H*-imidazol-1-yl)pyridine (**15a**, 380 g, 85%) as a light brown solid: Multimode MS (M+H) 268; 1H NMR (500 MHz, CDCl$_3$) δ 7.72 (d, J = 1.5 Hz, 1H), 7.39 (d, J = 8.0 Hz, 1H), 7.16 (d, J = 8.0 Hz, 1H), 6.92 (m, 1H), 4.03 (s, 3H), 2.29 (s, 3H).
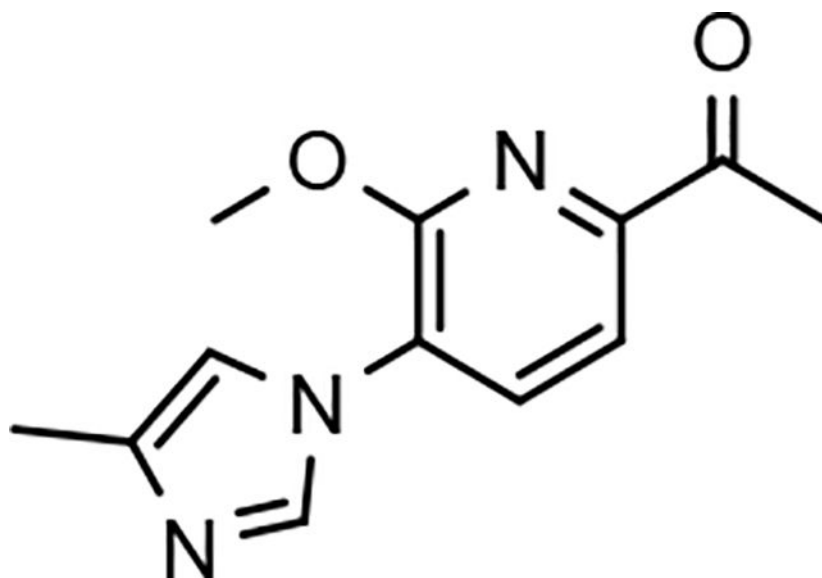
***1-(6-methoxy-5-(4-methyl-1H-imidazol-1-yl)pyridin-2-yl)ethan-1-one* (16a)**—To a
solution of 6-bromo-2-methoxy-3-(4-methyl-1*H*-imidazol-1-yl)pyridine (**15a**, 100 g, 0.373
mol), 1-(vinyloxy)butane (74.6 g, 0.746 mmol), and triethylamine (75.3 g, 0.746 mol) in
ethylene glycol (1000 mL) at room temperature under nitrogen was added dichloro[1,1'-
bis(diphenylphosphino) ferrocene] palladium (II) dichloromethane adduct (8.18 g, 11.2
mmol). The mixture was heated to 100 °C for 4 h (reaction progress was monitored by
LCMS; heating the reaction mixture for too long will result in a lower yield) and then cooled
to room temperature. The mixture was diluted with 2:1 ethyl acetate/water (3 L) and the
resulting layers were separated. The organic layer was washed with brine (2 × 500 mL),
dried with sodium sulfate, filtered, and concentrated. The resulting reaction residue was
purified by flash column chromatography on silica gel, eluting with heptane/ethyl acetate
(gradient of 4:1 to 1:1) to afford 6-(1-butoxyvinyl)-2-methoxy-3-(4-methyl-1*H*-imidazol-1-
yl)pyridine as a yellow solid (78.4 g, 73%) that was suitable for use without further
purification. Then aqueous hydrochloric acid (2 N, 550 mL) was added to a solution of 6-(1-
butoxyvinyl)-2-methoxy-3-(4-methyl-1H-imidazol-1-yl)pyridine (A6, 78.4 g, 0.273 mol) in
acetone (2200 mL) at room temperature. After stirring the reaction mixture for 30 minutes,
the organic solvent was removed under reduced pressure, and the mixture was diluted with
water (1000 mL) and extracted with ethyl acetate (2000 mL). The organic layer was washed
with water (~500 mL), and the ethyl acetate layer was discarded. With fast stirring,
potassium carbonate was slowly added (neutralized to pH 8) to the combined aqueous
layers. The resulting mixture was extracted with ethyl acetate (2 × 2000 mL). The combined
organic layer was washed with brine (2 × 500 mL) and dried over anhydrous sodium sulfate,
filtered, and concentrated to afford 1-(6-methoxy-5-(4-methyl-1*H*-imidazol-1-yl)pyridin-2-
yl)ethanone (**16a**) as a light yellow solid (60.6 g, 96%) that was suitable for use without
further purification: LCMS (M+H) 232; 1H NMR (300 MHz, CDCl$_3$) δ 7.91 (d, J = 1.5 Hz,
1H), 7.76 (d, J = 8.0 Hz, 1H), 7.67 (d, J = 8.0 Hz, 1H), 7.04 (m, 1H), 4.18 (s, 3H), 2.71 (s,
3H), 2.31 (d, J = 0.9 Hz, 3H).
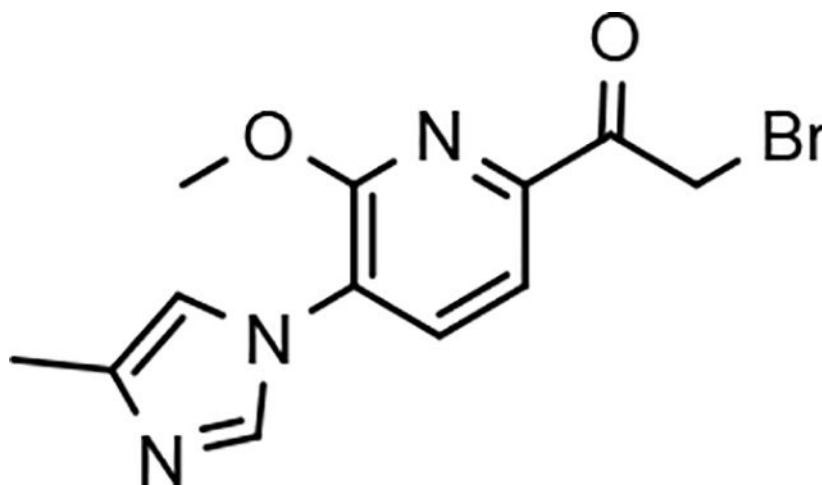
**2-bromo-1-(6-methoxy-5-(4-methyl-1H-imidazol-1-yl)pyridin-2-yl)ethan-1-one
(17a)**—Hydrogen bromide (2 mL, 33% solution in acetic acid) was added to a solution of
1-(6-methoxy-5-(4-methyl-1*H*-imidazol-1-yl)pyridin-2-yl)ethanone (**16a**, 2.07 g, 8.95
mmol) in chloroform (90 mL) and ethyl acetate (90 mL). To this mixture was added bromine
[412 μL, 8.05 mmol, in chloroform (10 mL) and ethyl acetate (10 mL)] drop-wise over ~2 h
at room temperature. After complete addition of the bromine, the reaction was stirred a
further 2 h at room temperature. The solvents were removed under reduced pressure and the
solids taken back up in chloroform (30 mL) and ethyl acetate (30 mL). The solvents were
removed again under reduced pressure. Ethyl acetate (30 mL) was then added and the
reaction again concentrated under reduced pressure and dried under high vacuum for 18 h to
afford 2-bromo-1-(6-methoxy-5-(4-methyl-1*H*-imidazol-1-yl)pyridin-2-yl)ethanone
hydrobromide (**17a**) as a tan solid (3.84 g, 92%) that was suitable for use without further
purification: APCI MS (M+H) 310.
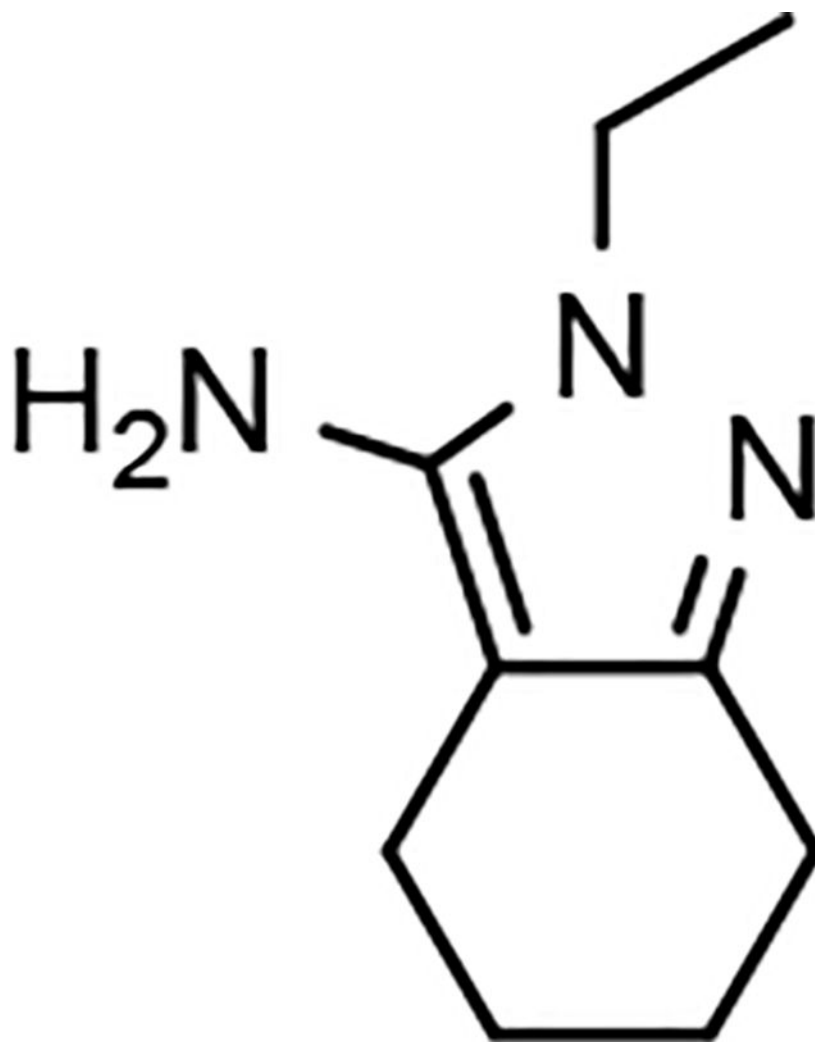
2-Ethyl-4,5,6,7-tetrahydro-2H-indazol-3-amine (19)—A solution of 2-oxocyclohexanecarbonitrile (**18**, 2.57 g, 20.9 mmol) and ethyl hydrazine oxalate (4.70 g, 31.3 mmol) in ethanol (40 mL) was stirred at reflux for 18 h, cooled to room temperature and the solvent removed under reduced pressure. The residue was diluted with methylene chloride (150 mL) and saturated aqueous sodium bicarbonate (100 mL) was added. The organic layer was separated and the aqueous layer was further extracted with methylene chloride (2×100 mL). The combined organic layers were washed with brine (50 mL), dried (MgSO$_4$), filtered and concentrated under reduced pressure. The resulting residue was further purified by flash column chromatography on silica gel, eluting with methanol/methylene chloride (gradient of 2:98 to 4:96) to afford 2-ethyl-4,5,6,7-tetrahydro-2*H*-indazol-3-amine (**19**) as a while solid (2.73 g, 79%): ^{1}H NMR (300 MHz, CDCl$_3$) δ 3.95 (q, $J = 7.2$ Hz, 2H), 3.24 (br s, 2H), 2.61–2.55 (m, 2H), 2.34–2.28 (m, 2H), 1.83–1.68 (sym m, 4H), 1.38 (t, $J = 7.2$ Hz, 3H).
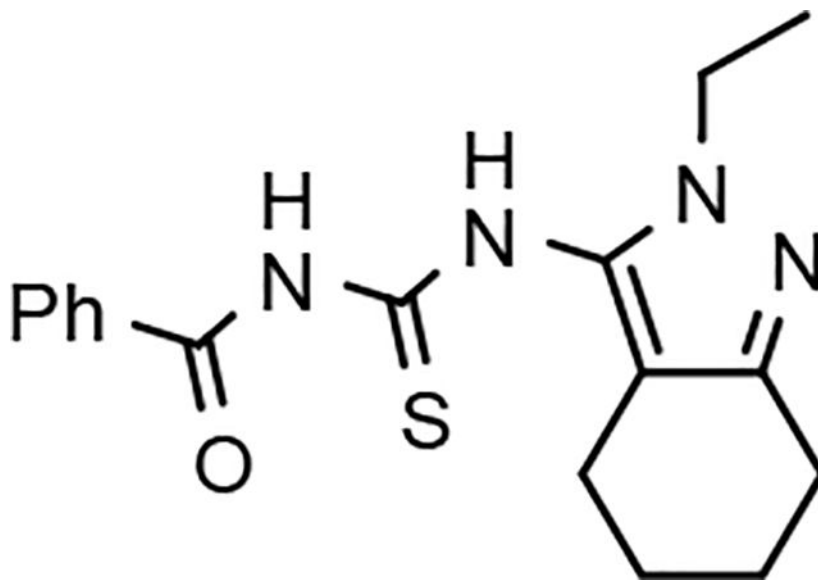
N-((2-Ethyl-4,5,6,7-tetrahydro-2H-indazol-3-yl)carbamothioyl)benzamide (20)—
A solution of 2-ethyl-4,5,6,7-tetrahydro-2*H*-indazol-3-amine (**19**, 800 mg, 4.84 mmol) and benzoyl isothiocyanate (869 mg, 5.32 mmol) in acetone (35 mL) was stirred at 60 °C for 18 h, cooled to room temperature and the solvent removed under reduced pressure. The resulting residue was purified by flash column chromatography on silica gel, eluting with ethyl acetate/hexanes (gradient of 1:9 to 1:1 over 40 minutes), to afford *N*-((2-ethyl-4,5,6,7-tetrahydro-2*H*-indazol-3-yl)carbamothioyl)benzamide (**20**) as an off-white solid (1.41 g, 89%): ESI MS (M+H) 329; ^{1}H NMR (300 MHz, CDCl₃) δ 11.81 (s, 1H), 9.28 (s, 1H), 7.93–7.88 (m, 2H), 7.72–7.65 (m, 1H), 7.60–7.53 (m, 2H), 4.06 (q, *J* = 7.2 Hz, 2H), 2.71–2.65 (m, 2H), 2.49–2.41 (m, 2H), 1.88–1.70 (m, 4H), 1.45 (t, *J* = 7.2 Hz, 3H).
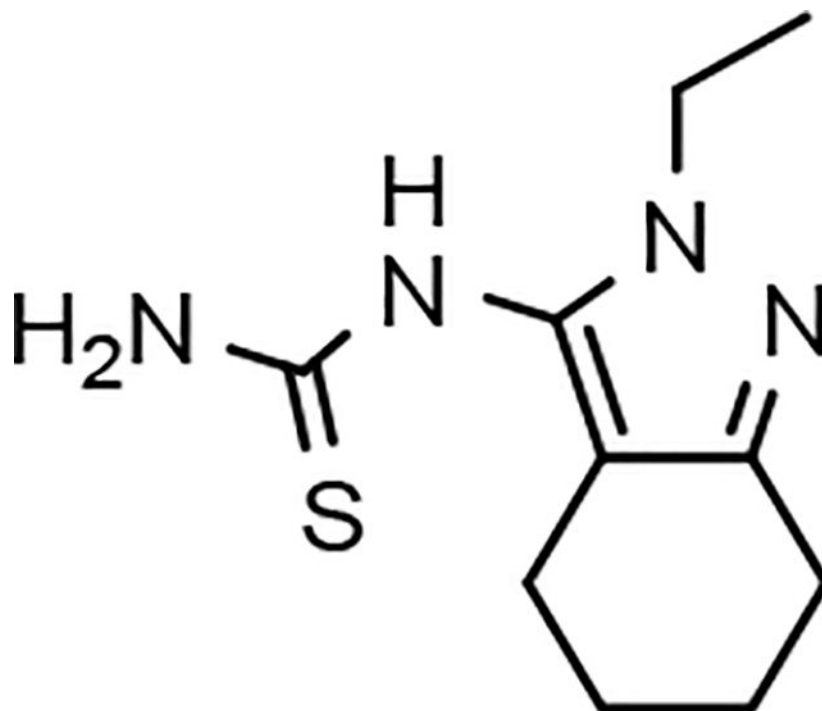
1-(2-Ethyl-4,5,6,7-tetrahydro-2H-indazol-3-yl)thiourea (21)—A mixture of *N*-((2-ethyl-4,5,6,7-tetrahydro-2*H*-indazol-3-yl)carbamothioyl)benzamide (**20**, 1.41 g, 4.29 mmol) and potassium carbonate (1.13 g, 8.16 mmol) in methanol (43 mL) was stirred at room temperature for 18 h, and concentrated directly onto silica gel, then purified by flash column chromatography on silica gel, eluting with methanol/methylene chloride (gradient of 0:100 to 1:19 over 40 minutes), to afford 1-(2-ethyl-4,5,6,7-tetrahydro-2*H*-indazol-3-yl)thiourea (**21**) as an off-white solid (904 mg, 94%): ESI MS (M+H) 225; ^{1}H NMR (300 MHz, DMSO-d_6) δ 9.23 (br s, 1H), 8.04 (br s, 1H), 7.06 (br s, 1H), 3.81 (q, *J* = 7.2 Hz, 2H), 2.54–2.45 (m, 2H), 2.29–2.22 (m, 2H), 1.77–1.56 (m, 4H), 1.24 (t, *J* = 7.2 Hz, 3H).
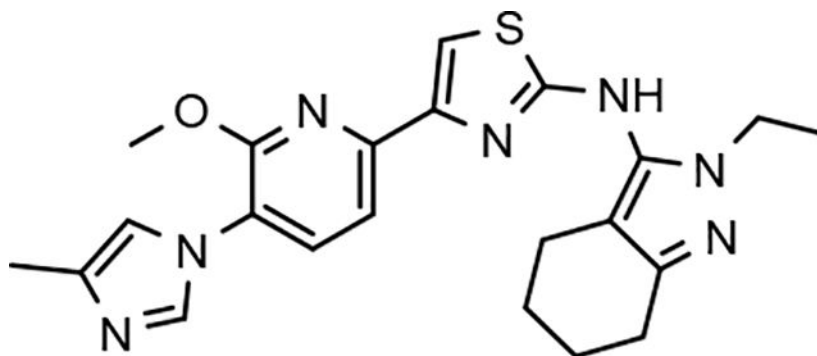
N-(2-ethyl-4,5,6,7-tetrahydro-2H-indazol-3-yl)-4-(6-methoxy-5-(4-methyl-1H-imidazol-1-yl)pyridin-2-yl)thiazol-2-amine (22d)—White solid; mp 198–201 °C; ESI MS (M+H) 436; ^{1}H NMR (500 MHz, DMSO-d_6) δ 9.70 (s, 1H), 7.90 (d, *J* = 1.0 Hz, 1H), 7.87 (d, *J* = 7.5 Hz, 1H), 7.51 (s, 1H), 7.50 (d, *J* = 7.5 Hz, 1H), 7.24 (s, 1H), 4.00 (s, 3H),

3.94 (q, J = 7.0 Hz, 2H), 2.55–2.50 (m, 2H), 2.38–2.32 (m, 2H), 2.16 (s, 3H), 1.77–1.60 (m, 4H), 1.27 (t, J = 7.0 Hz, 3H); HPLC >99% (AUC), (Method C), t_R = 9.4 min.
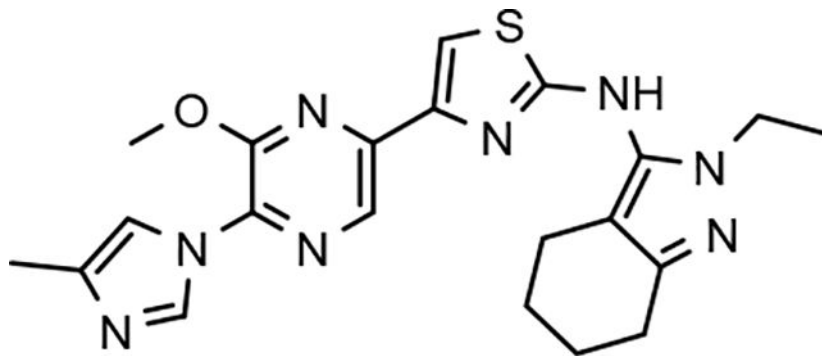
N-(2-ethyl-4,5,6,7-tetrahydro-2H-indazol-3-yl)-4-(6-methoxy-5-(4-methyl-1H-imidazol-1-yl)pyrazin-2-yl)thiazol-2-amine (22e)—Light yellow solid; mp 236–240 °C; APCI MS (M+H) 437; ^{1}H NMR 300 MHz, (DMSO-d_6) δ 9.85 (s, 1H), 8.43 (s, 1H), 8.37 (d, J = 1.2 Hz, 1H), 7.63 (s, 1H), 7.56 (s, 1H), 4.12 (s, 3H), 3.94 (q, J = 7.2 Hz, 2H), 2.54 (t, J = 5.7 Hz, 2H), 2.33 (t, J = 5.7 Hz, 2H), 2.18 (s, 3H), 1.80–1.59 (m, 4H), 1.26 (t, J = 7.2 Hz, 3H); HPLC 97.8% (AUC), (Method D), t_R = 8.4 min.
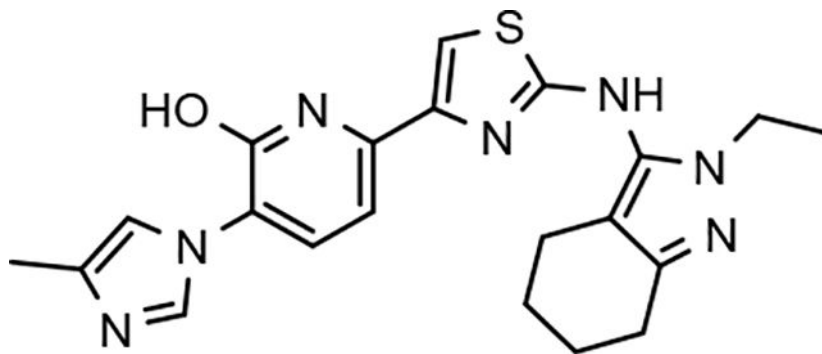
6-(2-((2-ethyl-4,5,6,7-tetrahydro-2H-indazol-3-yl)amino)thiazol-4-yl)-3-(4-methyl-1H-imidazol-1-yl)pyridin-2-ol (23)—Light brown solid; mp >300 °C dec; ESI MS (M+H) 422; ^{1}H NMR (500 MHz, DMSO-d_6) δ 12.1 (s, 1H), 9.78 (s, 1H), 8.14 (s, 1H), 7.75 (s, 1H), 7.72 (d, J = 8.0 Hz, 1H), 7.34 (s, 1H), 6.80 (br s, 1H), 3.92 (q, J = 7.0 Hz, 2H), 2.54–2.49 (m, 2H), 2.33–2.29 (m, 2H), 2.14 (s, 3H), 1.76–1.60 (m, 4H), 1.25 (t, J = 7.0 Hz, 3H); HPLC >99% (AUC), (Method B), t_R = 8.4 min.
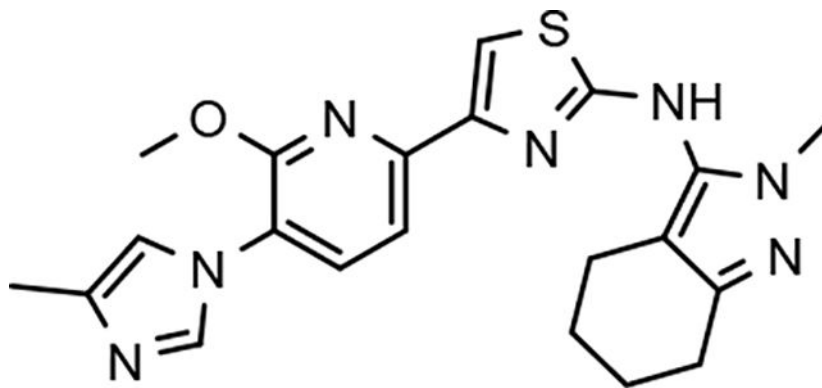
***4-(6-methoxy-5-(4-methyl-1H-imidazol-1-yl)pyridin-2-yl)-N-(2-methyl-4,5,6,7-
tetrahydro-2H-indazol-3-yl)thiazol-2-amine* (31d)—**Light brown solid; mp 177–181
°C; ESI MS (M+H) 422; ^{1}H NMR (500 MHz, DMSO-d_6) δ 9.75 (s, 1H), 7.90 (d, *J* = 1.0 Hz,
1H), 7.86 (d, *J* = 8.0 Hz, 1H), 7.51 (s, 1H), 7.50 (d, *J* = 8.0 Hz, 1H), 7.24 (s, 1H), 4.00 (s,
3H), 3.61 (s, 3H), 2.55–2.50 (m, 2H), 2.38–2.31 (m, 2H), 2.16 (s, 3H), 1.77–1.60 (m, 4H);
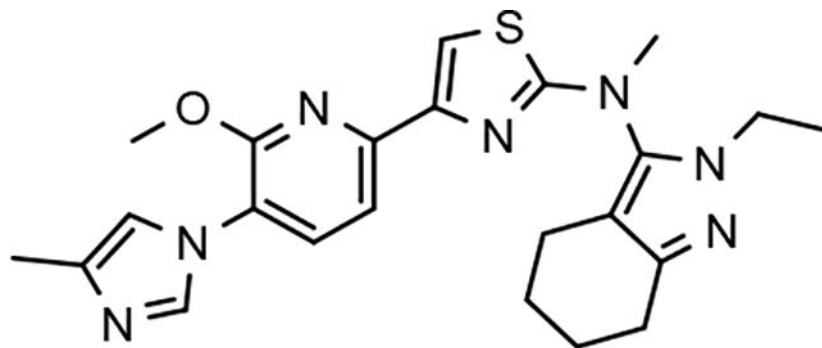HPLC 96.9% (AUC), (Method B), t_R = 9.1 min.
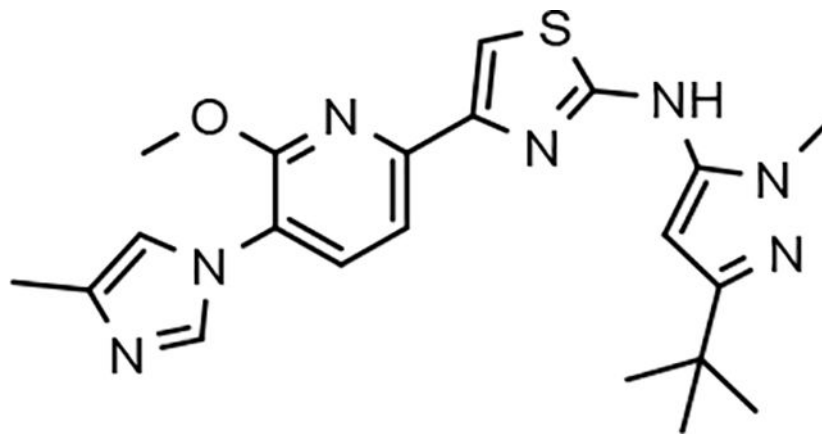
***N-(3-(tert-Butyl)-1-methyl-1H-pyrazol-5-yl)-4-(6-methoxy-5-(4-methyl-1H-
imidazol-1-yl)pyridin-2-yl)thiazol-2-amine* (32d)—**Off-white solid; APCI MS (M+H)
424; ^{1}H NMR (500 MHz, DMSO-d_6) δ 10.18 (s, 1H), 7.95 (s, 1H), 7.92 (d, *J* = 8.0 Hz, 1H),
7.58 (s, 1H), 7.57 (d, *J* = 8.0 Hz, 1H), 7.26 (s, 1H), 6.33 (s, 1H), 4.02 (s, 3H), 3.67 (s, 3H),
2.16 (s, 3H), 1.24 (s, 9H); HPLC >99% (AUC), (Method B), t_R = 9.5 min.
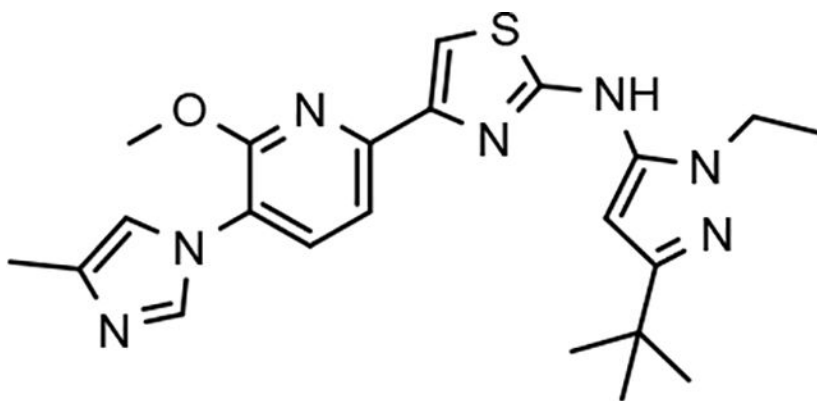
N-(3-(tert-Butyl)-1-ethyl-1H-pyrazol-5-yl)-4-(6-methoxy-5-(4-methyl-1H-imidazol-1-yl)pyridin-2-yl)thiazol-2-amine (33d)—Off-white solid; mp 164–169 °C; APCI MS (M+H) 438; ^{1}H NMR (300 MHz, DMSO-d_6) δ 10.11 (s, 1H), 7.91 (dd, J = 3.3, 3.6 Hz, 2H), 7.58 (s, 1H), 7.56 (d, J = 3.6 Hz, 1H), 7.25 (s, 1H), 6.33 (s, 1H), 4.03 (q, J = 6.9 Hz, 2H), 4.02 (s, 3H), 2.16 (s, 3H), 1.27 (t, J = 7.2 Hz, 3H), 1.25 (s, 9H); HPLC 97.0% (AUC), (Method B), t_R = 11.0 min.
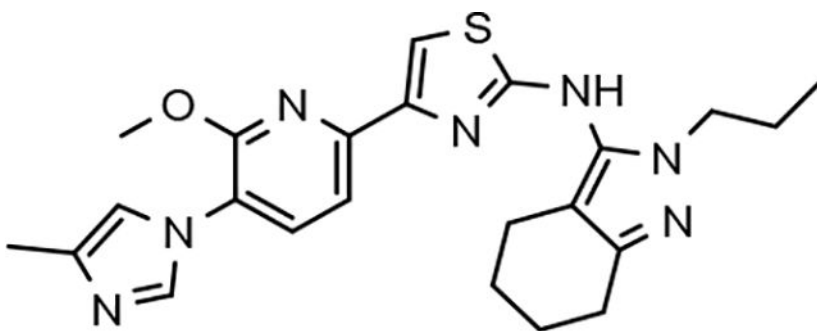
4-(6-methoxy-5-(4-methyl-1H-imidazol-1-yl)pyridin-2-yl)-N-(2-propyl-4,5,6,7-tetrahydro-2H-indazol-3-yl)thiazol-2-amine (34)—Off-white solid; mp 204–208 °C; ESI MS (M+H) 450; ^{1}H NMR (500 MHz, DMSO-d_6) δ 9.70 (s, 1H), 7.90 (d, J = 1.0 Hz, 1H), 7.87 (d, J = 7.5 Hz, 1H), 7.50 (d, J = 7.5 Hz, 1H), 7.49 (s, 1H), 7.24 (m, 1H), 4.00 (s, 3H), 3.86 (t, J = 7.0 Hz, 2H), 2.55–2.50 (m, 2H), 2.34–2.30 (m, 2H), 2.16 (s, 3H), 1.77–1.60 (m, 6H), 0.81 (t, J = 7.5Hz, 3H); HPLC 98.8% (AUC), (Method B), t_R = 11.0 min.
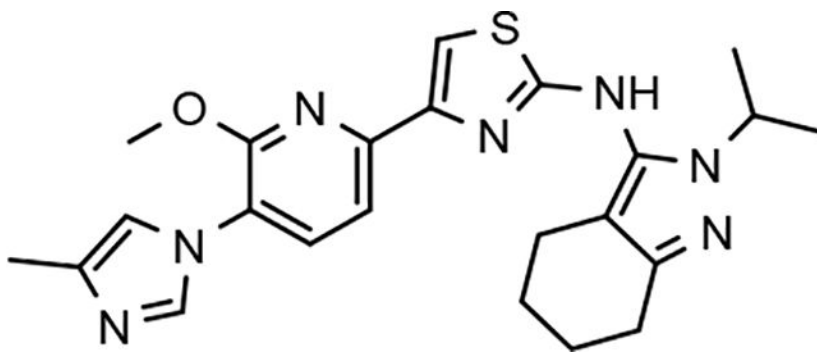
**N-(2-isopropyl-4,5,6,7-tetrahydro-2H-indazol-3-yl)-4-(6-methoxy-5-(4-methyl-1H-imidazol-1-yl)pyridin-2-yl)thiazol-2-amine (35)**—White solid; mp 130–134 °C; APCI MS (M+H) 450; ^{1}H NMR (500 MHz, DMSO-d_6) δ 9.64 (s, 1H), 7.90 (d, J = 0.6 Hz, 1H), 7.86 (d, J = 8.0 Hz, 1H), 7.50 (d, J = 7.5 Hz, 1H), 7.48 (s, 1H), 7.24 (s, 1H), 4.44 (m, J = 6.5 Hz, 1H), 4.00 (s, 3H), 2.55 (m, 2H), 2.32 (m, 2H), 2.16 (s, 3H), 1.73 (m, 2H), 1.65 (m, 2H), 1.32 (d, J = 6.5 Hz, 6H); HPLC 96.1% (AUC), (Method B), t_R = 11.2 min.
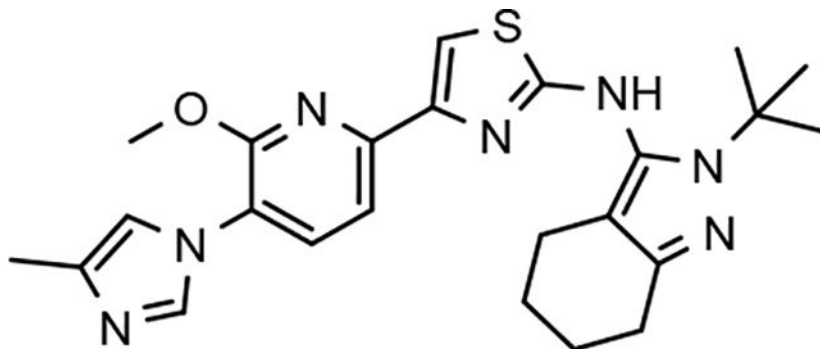
N-(2-(tert-butyl)-4,5,6,7-tetrahydro-2H-indazol-3-yl)-4-(6-methoxy-5-(4-methyl-1H-imidazol-1-yl)pyridin-2-yl)thiazol-2-amine (36)—Off-white solid; mp 207–210 °C; APCI MS (M+H) 464; ^{1}H NMR (300 MHz, DMSO-d_6) δ 9.54 (s, 1H), 7.92 (d, J = 1.2 Hz, 1H), 7.87 (d, J = 8.1 Hz, 1H), 7.52 (d, J = 8.1 Hz, 1H), 7.47 (s, 1H), 7.25 (s, 1H), 3.99 (s, 3H), 2.50 (m, 2H), 2.27 (m, 2H), 2.16 (s, 3H), 1.78–1.58 (m, 4H), 1.53 (s, 9H); HPLC >99% (AUC), (Method B), t_R = 11.8 min.
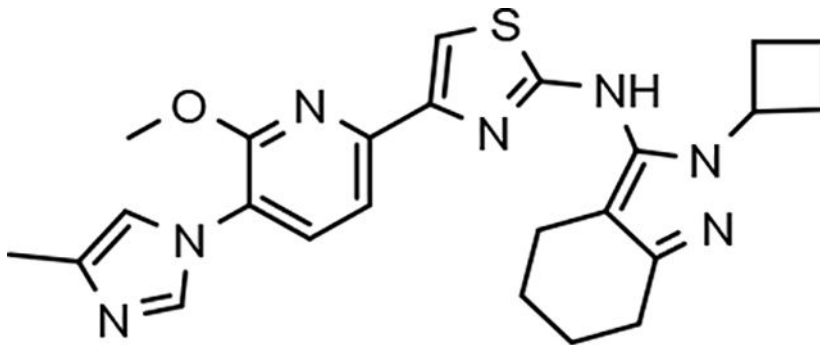
N-(2-cyclobutyl-4,5,6,7-tetrahydro-2H-indazol-3-yl)-4-(6-methoxy-5-(4-methyl-1H-imidazol-1-yl)pyridin-2-yl)thiazol-2-amine (37)—Off-white solid; mp 141–146 °C; APCI MS (M+H) 462; ^{1}H NMR (300 MHz, DMSO-d_6) δ 9.69 (s, 1H), 7.90 (d, J = 1.2 Hz, 1H), 7.87 (d, J = 8.1 Hz, 1H), 7.50 (s, 1H), 7.49 (d, J = 7.8 Hz, 1H), 7.24 (s, 1H), 4.71 (m, 1H), 4.00 (s, 3H), 2.57 (m, 2H), 2.46 (m, 2H), 2.37–2.21 (m, 4H), 2.16 (s, 3H), 1.81–1.58 (m, 6H); HPLC >99% (AUC), (Method B), t_R = 11.7 min.
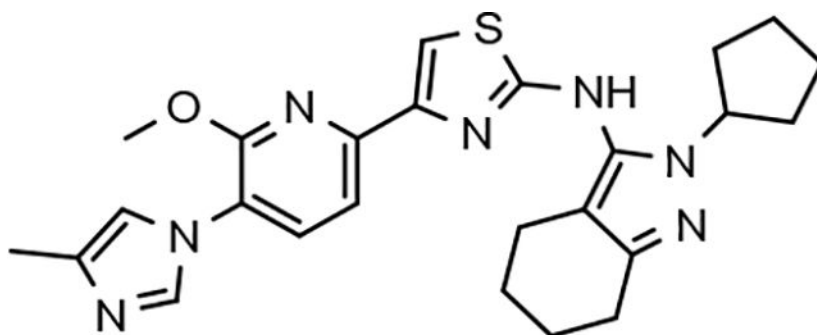
N-(2-cyclopentyl-4,5,6,7-tetrahydro-2H-indazol-3-yl)-4-(6-methoxy-5-(4-methyl-1H-imidazol-1-yl)pyridin-2-yl)thiazol-2-amine (38)—Brown solid; mp 110–120 °C; ESI MS (M+H) 476; ^{1}H NMR (500 MHz, CDCl$_3$) δ 7.87 (s, 1H), 7.58–7.54 (m, 2H), 7.39 (s, 1H), 6.99 (s, 1H), 6.80 (br s, 1H), 4.69–4.59 (m, 1H), 4.07 (s, 3H), 2.69 (t, $J =$ 7.0 Hz, 2H), 2.42 (t, $J =$ 7.0 Hz, 2H), 2.32 (s, 3H), 2.08–1.55 (m, 12H); HPLC >99% (AUC), (Method A), t_R = 9.7 min.
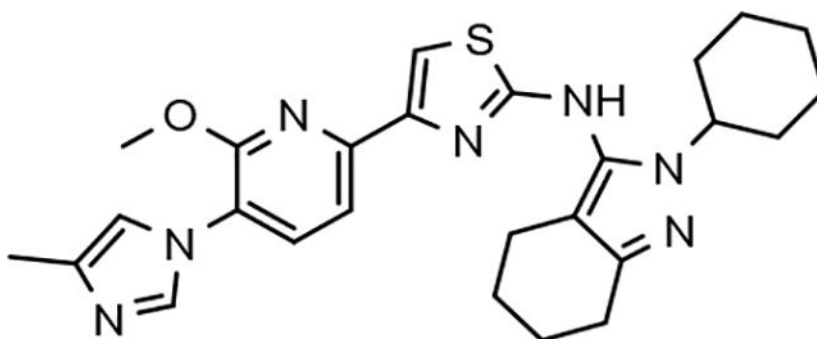
N-(2-cyclohexyl-4,5,6,7-tetrahydro-2H-indazol-3-yl)-4-(6-methoxy-5-(4-methyl-1H-imidazol-1-yl)pyridin-2-yl)thiazol-2-amine (39)—Orange-brown solid; mp 168–174 °C; APCI MS (M+H) 490; ^{1}H NMR (300 MHz, DMSO-d_6) δ 9.68 (s, 1H), 7.93 (s, 1H), 7.88 (d, $J =$ 7.8 Hz, 1H), 7.51 (d, $J =$ 7.8 Hz, 1H), 7.49 (s, 1H), 7.25 (s, 1H), 4.03 (m, 1H), 4.00 (s, 3H), 2.31 (m, 2H), 2.16 (s, 3H), 1.86–1.57 (m, 12H), 1.39–1.08 (m, 4H); HPLC 97.3% (AUC), (Method B), t_R = 12.3 min.
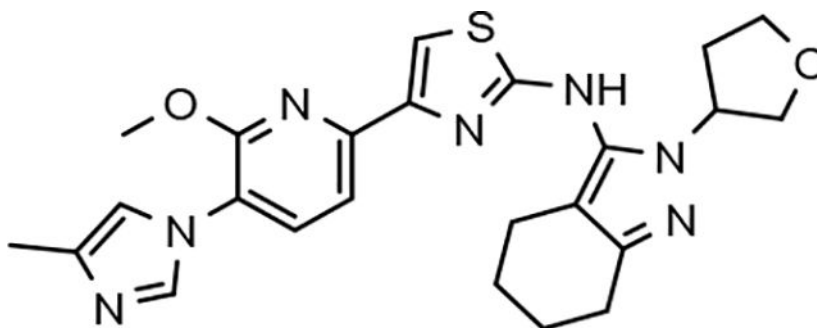
(+/−)-4-(6-methoxy-5-(4-methyl-1H-imidazol-1-yl)pyridin-2-yl)-N-(2-(tetrahydrofuran-3-yl)-4,5,6,7-tetrahydro-2H-indazol-3-yl)thiazol-2-amine (40)—

Off-white solid; mp 154–158 °C; APCI MS (M+H) 478; ^{1}H NMR (300 MHz, DMSO-d_6) δ 9.77 (s, 1H), 7.91 (d, J = 1.5 Hz, 1H), 7.87 (d, J = 8.1 Hz, 1H), 7.52 (s, 1H), 7.49 (d, J = 8.1 Hz, 1H), 7.24 (s, 1H), 4.91 (m, 1H), 4.00 (s, 3H), 3.95 (m, 2H), 3.83–3.71 (m, 2H), 2.55 (m, 2H), 2.32 (m, 2H), 2.20 (m, 2H), 2.15 (s, 3H), 1.80–1.59 (m, 4H); HPLC 97.4% (AUC), (Method B), t_R = 11.1 min.
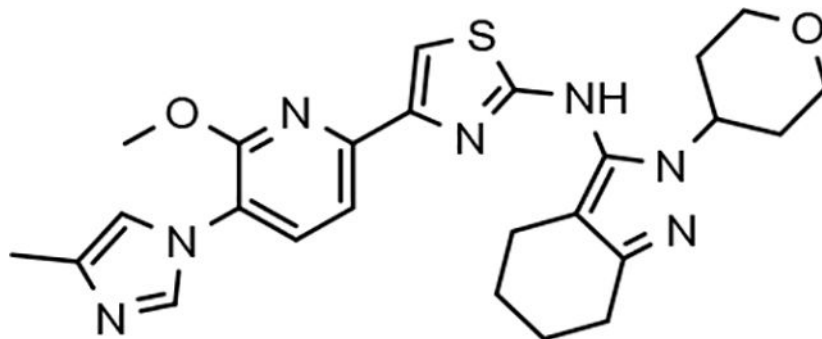
4-(6-methoxy-5-(4-methyl-1H-imidazol-1-yl)pyridin-2-yl)-N-(2-(tetrahydro-2H-pyran-4-yl)-4,5,6,7-tetrahydro-2H-indazol-3-yl)thiazol-2-amine (41)—White solid; mp 186–191 °C; ESI MS (M+H) 492; ^{1}H NMR (300 MHz, DMSO-d_6) δ 9.73 (s, 1H), 7.91 (d, J = 1.2 Hz, 1H), 7.87 (d, J = 8.1 Hz, 1H), 7.50 (t, J = 3.9 Hz, 2H), 7.25 (s, 1H), 4.31 (m, 1H), 4.00 (s, 3H), 3.92 (m, 2H), 3.39 (m, 2H), 2.55 (m, 2H), 2.32 (m, 2H), 2.15 (s, 3H), 2.10–1.90 (m, 2H), 1.80–1.59 (m, 6H); HPLC 97.5% (AUC), (Method B), t_R = 11.1 min.
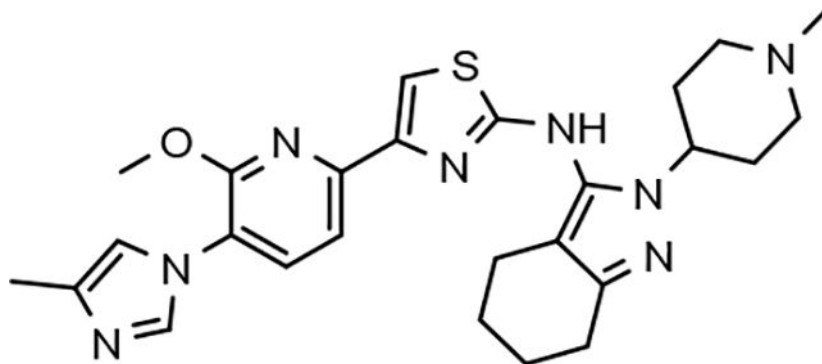
4-(6-methoxy-5-(4-methyl-1H-imidazol-1-yl)pyridin-2-yl)-N-(2-(1-methylpiperidin-4-yl)-4,5,6,7-tetrahydro-2H-indazol-3-yl)thiazol-2-amine (42)—Light brown solid; mp 150–153 °C; APCI MS (M+H) 505; ^{1}H NMR (300 MHz, CDCl$_3$) δ 7.83 (d, J = 1.2 Hz, 1H), 7.61–7.45 (m, 3H), 7.36 (s, 1H), 6.99 (s, 1H), 4.11 (m, 1H), 4.05 (s, 3H), 2.94 (d, J = 11.4 Hz, 2H), 2.67 (t, J = 6.0 Hz, 2H), 2.40 (t, J = 6.0 Hz, 2H), 2.30 (s, 3H), 2.27 (s, 3H), 2.24 (m, 1H), 2.02 (t, J = 11.4 Hz, 3H), 1.89–1.65 (m, 6H); HPLC 96.4% (AUC), (Method B), t_R = 9.3 min.
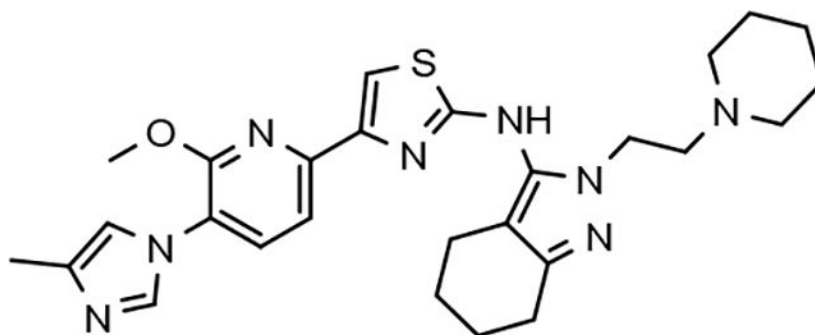
4-(6-methoxy-5-(4-methyl-1H-imidazol-1-yl)pyridin-2-yl)-N-(2-(2-(piperidin-1-yl)ethyl)-4,5,6,7-tetrahydro-2H-indazol-3-yl)thiazol-2-amine (43)—Off-white solid; mp 80–90 °C; ESI MS (M+H) 519; ^{1}H NMR (500 MHz, CDCl$_3$) δ 10.90 (br s, 1H), 7.79 (s, 1H), 7.61 (d, J = 8.0 Hz, 1H), 7.57 (d, J = 8.0 Hz, 1H), 7.39 (s, 1H), 6.99 (s, 1H), 4.29–4.12 (m, 2H), 4.07 (s, 3H), 2.85–2.49 (m, 8H), 2.45 (t, J = 6.0 Hz, 2H), 2.30 (s, 3H), 1.95–1.70 (m, 4H), 1.68–1.50 (m, 6H); HPLC >99% (AUC), (Method A), t_R = 8.4 min.
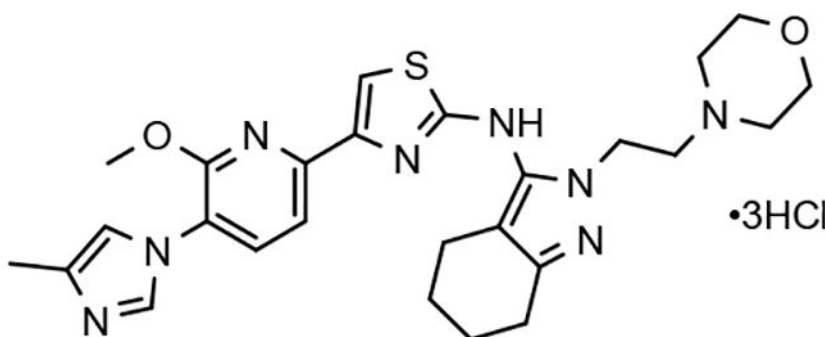
4-(6-methoxy-5-(4-methyl-1H-imidazol-1-yl)pyridin-2-yl)-N-(2-(2-morpholinoethyl)-4,5,6,7-tetrahydro-2H-indazol-3-yl)thiazol-2-amine trihydrochloride (44)—Light brown solid; mp 160–170 °C; ESI MS (M+H) 521; ^{1}H NMR (500 MHz, DMSO-d_6) δ 11.31 (br s, 1H), 10.28 (br s, 1H), 9.45 (s, 1H), 8.11 (d, J = 8.0 Hz, 1H), 7.82 (s, 1H), 7.66 (s, 1H), 7.57 (d, J = 8.0 Hz, 1H), 6.3–5.5 (br s, 2H), 4.47–4.44 (m, 2H), 4.04 (s, 3H), 4.00–3.70 (br s, 4H), 3.59–3.55 (m, 2H), 3.50–3.00 (br s, 4H), 2.57–2.50 (m, 2H), 2.36 (s, 3H), 2.37–2.30 (m, 2H), 1.80–1.60 (m, 4H); HPLC 93.5% (AUC), (Method C), t_R = 8.6 min.
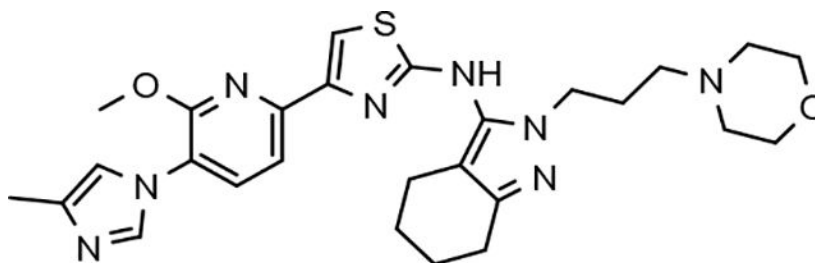
4-(6-methoxy-5-(4-methyl-1H-imidazol-1-yl)pyridin-2-yl)-N-(2-(3-morpholinopropyl)-4,5,6,7-tetrahydro-2H-indazol-3-yl)thiazol-2-amine (45)—

Yellow solid; mp 80–90 °C; ESI MS (M+H) 535; ^{1}H NMR (500 MHz, CDCl$_3$) δ 10.55 (br s, 1H), 7.81 (d, J = 1.0 Hz, 1H), 7.63–7.59 (m, 2H), 7.39 (s, 1H), 6.99 (s, 1H), 4.15–4.05 (m, 6H), 4.07 (s, 3H), 2.68 (t, J = 6.0 Hz, 2H), 2.59–2.49 (m, 4H), 2.44 (t, J = 6.0 Hz, 2H), 2.31 (s, 3H), 2.24–2.23 (m, 2H), 2.08–2.06 (m, 2H), 1.87–1.82 (m, 2H), 1.77–1.65 (m, 2H); HPLC >99% (AUC), (Method A), t_R = 8.5 min.
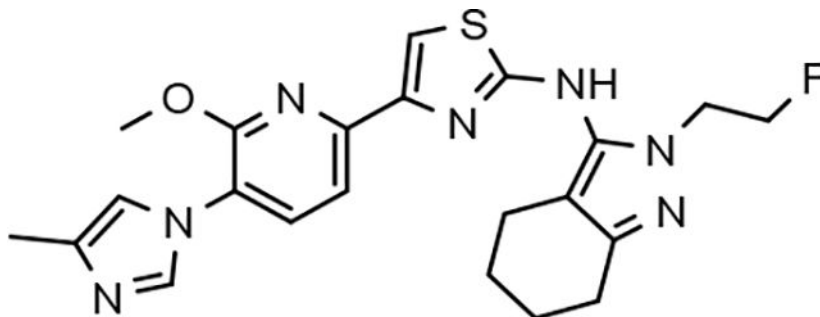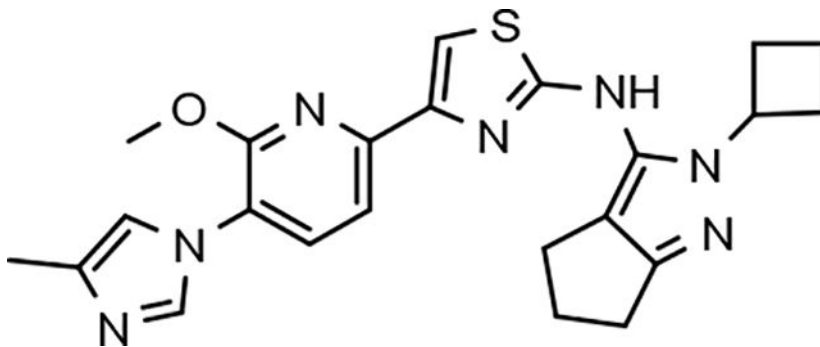

N-(2-(2-fluoroethyl)-4,5,6,7-tetrahydro-2H-indazol-3-yl)-4-(6-methoxy-5-(4-methyl-1H-imidazol-1-yl)pyridin-2-yl)thiazol-2-amine (46)—White solid; mp 190–192 °C; APCI MS (M+H) 454; ^{1}H NMR (300 MHz, DMSO-d_6) δ 9.75 (s, 1H), 7.90 (d, J = 1.1 Hz, 1H), 7.87 (d, J = 8.2 Hz, 1H), 7.52 (s, 1H), 7.50 (d, J = 8.2 Hz, 1H), 7.24 (s, 1H), 4.70 (dt, J = 47.1, 4.9 Hz, 2H), 4.23 (dt, J = 26.1, 4.9 Hz, 2H), 4.00 (s, 3H), 2.53 (m, 2H), 2.34 (m, 2H), 2.16 (s, 3H), 1.73 (m, 4H); HPLC >99% (AUC), (Method D), t_R = 8.6 min.
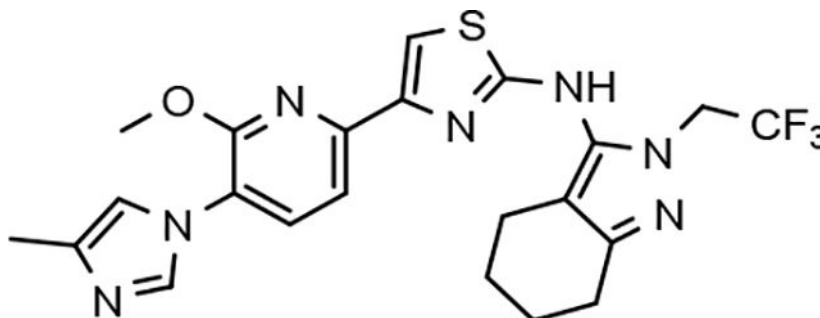
4-(6-methoxy-5-(4-methyl-1H-imidazol-1-yl)pyridin-2-yl)-N-(2-(2,2,2-trifluoroethyl)-4,5,6,7-tetrahydro-2H-indazol-3-yl)thiazol-2-amine (47)—Light yellow solid; mp 122–126 °C; ESI MS (M+H) 490; ^{1}H NMR (300 MHz, DMSO-d_6) δ 9.86 (s, 1H), 7.91 (d, J = 1.2 Hz, 1H), 7.87 (d, J = 7.8 Hz, 1H), 7.55 (s, 1H), 7.50 (d, J = 7.8 Hz, 1H), 7.24 (m, 1H), 4.88 (q, J = 8.7 Hz, 2H), 4.00 (s, 3H), 2.60–2.53 (m, 2H), 2.39–2.31 (m, 2H), 2.16 (s, 3H), 1.80–1.60 (m, 4H); HPLC 98.1% (AUC), (Method A), t_R = 9.6 min.
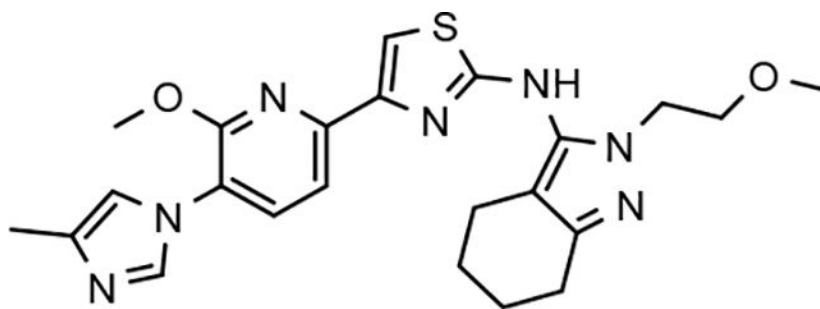
4-(6-methoxy-5-(4-methyl-1H-imidazol-1-yl)pyridin-2-yl)-N-(2-(2-methoxyethyl)-4,5,6,7-tetrahydro-2H-indazol-3-yl)thiazol-2-amine (48)—White solid; mp 78–82 °C; ESI MS (M+H) 466; ^{1}H NMR (500 MHz, CDCl$_3$) δ 7.98 (br s, 1H), 7.69 (br s, 1H), 7.66 (d, J = 8.0 Hz, 1H), 7.60 (d, J = 8.0 Hz, 1H), 7.42 (s, 1H), 7.02 (s, 1H), 4.24 (t, J = 5.0 Hz, 2H), 4.08 (s, 3H), 3.68 (t, J = 5.0 Hz, 2H), 3.40 (s, 3H), 2.68 (t, J = 6.0 Hz, 2H), 2.43 (t, J = 6.0 Hz, 2H), 2.36 (s, 3H), 1.87–1.81 (m, 2H), 1.77–1.72 (m, 2H); HPLC 98.5% (AUC), (Method B), t_R = 9.6 min.
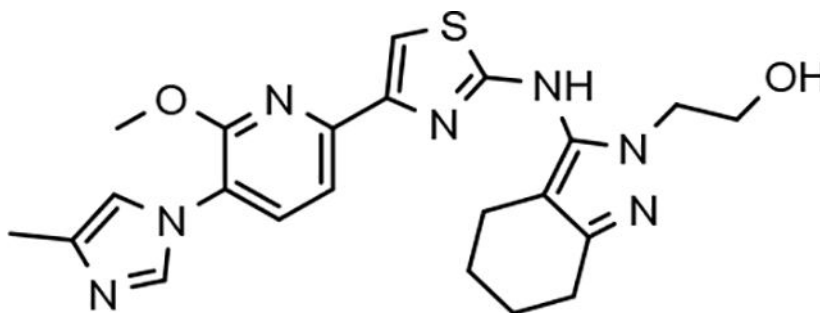
2-(3-((4-(6-methoxy-5-(4-methyl-1H-imidazol-1-yl)pyridin-2-yl)thiazol-2-yl)amino)-4,5,6,7-tetrahydro-2H-indazol-2-yl)ethanol (49)—White solid; mp 132–136 °C; ESI MS (M+H) 452; ^{1}H NMR (300 MHz, DMSO-d_6) δ 9.66 (s, 1H), 7.93 (s, 1H), 7.87 (d, J = 7.8 Hz, 1H), 7.51 (s, 1H), 7.50 (d, J = 7.8 Hz, 1H), 7.26 (m, 1H), 4.85 (t, J = 5.6 Hz, 1H), 4.00 (s, 3H), 4.00–3.94 (m, 2H), 3.70–3.60 (m, 2H), 2.55–2.50 (m, 2H), 2.36–2.30 (m, 2H), 2.16 (s, 3H), 1.78–1.60 (m, 4H); HPLC >99% (AUC), (Method B), t_R = 9.8 min.
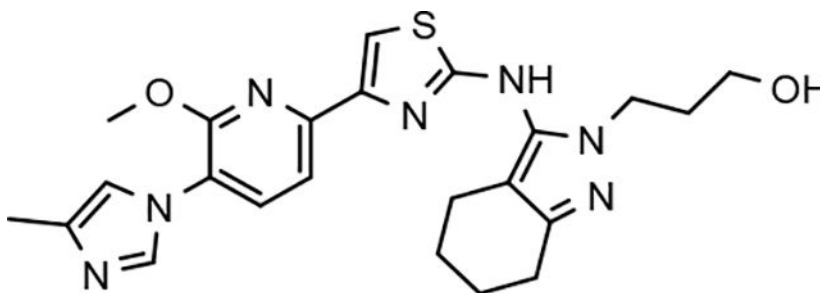
3-(3-((4-(6-methoxy-5-(4-methyl-1H-imidazol-1-yl)pyridin-2-yl)thiazol-2-yl)amino)-4,5,6,7-tetrahydro-2H-indazol-2-yl)propan-1-ol (50)—Light orange solid; mp 178–182 °C; ESI MS (M+H) 466; ^{1}H NMR (300 MHz, DMSO-d_6) δ 9.71 (s, 1H), 7.91

(d, *J* = 1.2 Hz, 1H), 7.87 (d, *J* = 7.8 Hz, 1H), 7.51 (d, *J* = 7.8 Hz, 1H), 7.50 (s, 1H), 7.24 (m, 1H), 4.55 (dd, *J* = 5.1, 5.1 Hz, 1H), 4.03–3.90 (s, 2H), 4.00 (s, 3H), 3.42–3.30 (m, 2H), 2.60–2.47 (m, 2H), 2.37–2.30 (m, 2H), 2.15 (s, 3H), 2.40–2.10 (m, 6H); HPLC >99% (AUC), (Method A), t_R = 8.1 min.
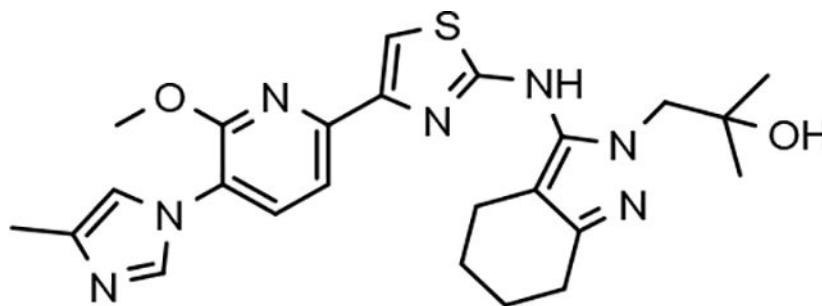
1-(3-((4-(6-methoxy-5-(4-methyl-1H-imidazol-1-yl)pyridin-2-yl)thiazol-2-yl)amino)-4,5,6,7-tetrahydro-2H-indazol-2-yl)-2-methylpropan-2-ol (51)—Yellow solid; mp 90–100 °C; ESI MS (M+H) 480; ¹H NMR (300 MHz, DMSO-*d₆*) δ 9.60 (s, 1H), 7.91 (s, 1H), 7.87 (d, *J* = 8.0 Hz, 1H), 7.52 (s, 1H), 7.51 (d, *J* = 8.0 Hz, 1H), 7.25 (s, 1H), 4.92 (s, 1H), 4.00 (s, 3H), 3.88 (s, 2H), 2.60–2.51 (m, 2H), 2.38–2.29 (m, 2H), 2.16 (s, 3H), 1.80–1.56 (m, 4H), 1.06 (s, 6H); HPLC 96.8% (AUC), (Method A), t_R = 8.4 min.

N-(2-ethyl-4,5,6,7-tetrahydro-2H-indazol-3-yl)-4-(6-methoxy-5-(4-methyl-1H-imidazol-1-yl)pyridin-2-yl)-N-methylthiazol-2-amine (52)—Off-white solid; mp 74–79 °C; APCI MS (M+H) 450; ¹H NMR (300 MHz, DMSO-*d₆*) δ 7.92 (d, *J* = 1.2 Hz, 1H), 7.90 (d, *J* = 8.1 Hz, 1H), 7.63 (d, *J* = 7.8 Hz, 1H), 7.52 (s, 1H), 7.25 (t, *J* = 1.2 Hz, 1H), 4.00 (s, 3H), 3.90 (q, *J* = 7.2 Hz, 2H), 3.43 (s, 3H), 2.56 (m, 2H), 2.33 (m, 2H), 2.16 (d, *J* = 0.9 Hz, 3H), 1.81–1.60 (m, 4H), 1.29 (t, *J* = 7.2 Hz, 3H); HPLC >99% (AUC), (Method B), t_R = 12.5 min.
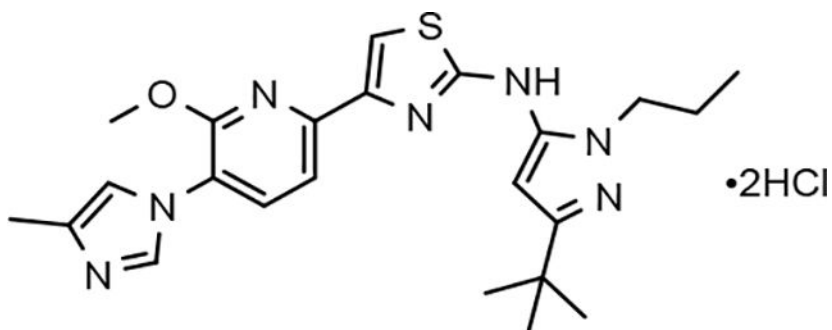
N-(3-(tert-butyl)-1-propyl-1H-pyrazol-5-yl)-4-(6-methoxy-5-(4-methyl-1H-imidazol-1-yl)pyridin-2-yl)thiazol-2-amine dihydrochloride (53)—Brown solid; mp 200–205 °C; APCI MS (M+H) 452; ^{1}H NMR (500 MHz, DMSO-d_6) δ 10.17 (s, 1H), 9.39 (s, 1H), 8.13 (d, J = 8.0 Hz, 1H), 7.81 (s, 1H), 7.69 (s, 1H), 7.66 (d, J = 8.0 Hz, 1H), 6.36 (s, 1H), 4.40–3.80 (br s, 2H), 4.05 (s, 3H), 3.96 (t, J = 7.2 Hz, 2H), 2.35 (s, 3H), 1.71 (m, 2H), 1.25 (s, 9H), 0.83 (t, J = 7.2 Hz, 3H); HPLC 95.7% (AUC), (Method B), t_R = 10.1 min.
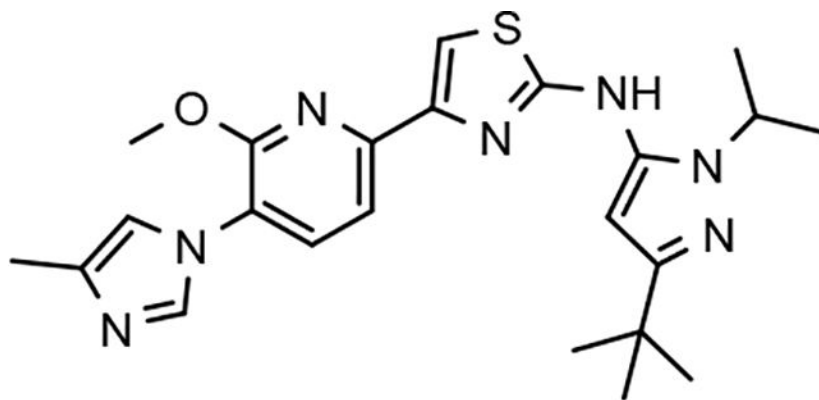
N-(3-(tert-butyl)-1-isopropyl-1H-pyrazol-5-yl)-4-(6-methoxy-5-(4-methyl-1H-imidazol-1-yl)pyridine-2-yl)thiazol-2-amine (54)—White solid; mp 170–174 °C; ESI MS (M–H) 450; ^{1}H NMR (500 MHz, DMSO-d_6) δ 9.98 (s, 1H), 7.91–7.89 (m, 2H), 7.56–7.54 (m, 2H), 7.25 (s, 1H), 6.27 (s, 1H), 4.55–4.50 (m, 1H), 4.02 (s, 3H), 2.16 (s, 3H), 1.34 (d, J = 6.5 Hz, 6H), 1.25 (s, 9H); HPLC >99% (AUC), (Method B), t_R = 10.6 min.
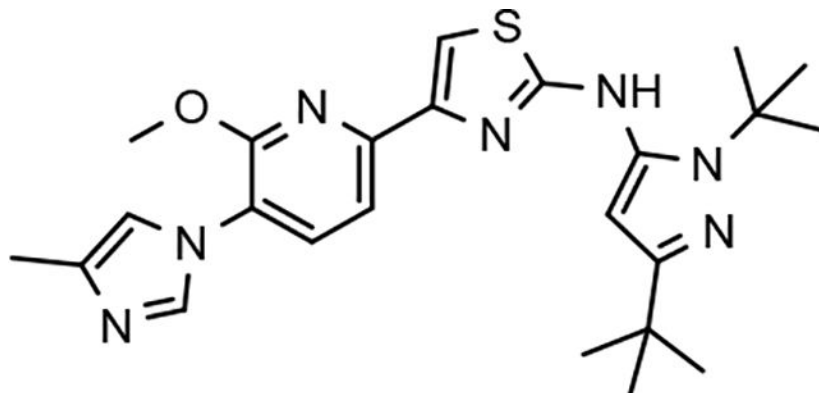
N-(1,3-di-tert-butyl-1H-pyrazol-5-yl)-4-(6-methoxy-5-(4-methyl-1H-imidazol-1-yl)pyridin-2-yl)thiazol-2-amine (55)—Light yellow solid; mp 206–210 °C; ESI MS (M +H) 466; ^{1}H NMR (300 MHz, DMSO-d_6) δ 9.55 (s, 1H), 7.91 (d, J = 1.2 Hz, 1H), 7.87 (d, J = 7.8 Hz, 1H), 7.53 (d, J = 7.8 Hz, 1H), 7.47 (s, 1H), 7.24 (m, 1H), 6.23 (s, 1H), 4.00 (s, 3H), 2.16 (s, 3H), 1.55 (s, 9H), 1.23 (s, 9H); HPLC >99% (AUC), (Method A), t_R = 12.1 min.
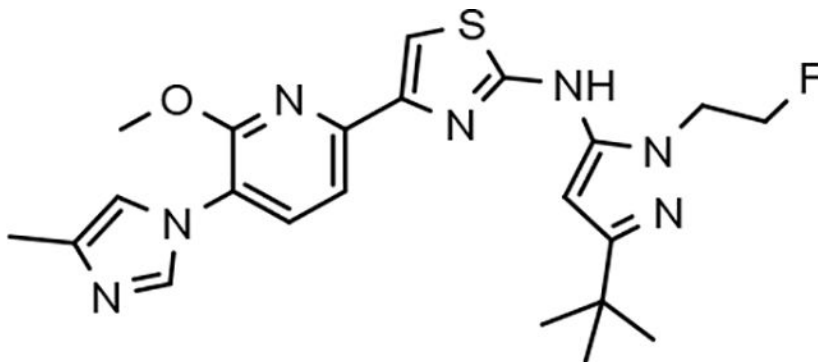
N-(3-(tert-butyl)-1-(2-fluoroethyl)-1H-pyrazol-5-yl)-4-(6-methoxy-5-(4-methyl-1H-imidazol-1-yl)pyridin-2-yl)thiazol-2-amine (56)—White solid; mp 210–214 °C; ESI MS (M+H) 456; ^{1}H NMR (300 MHz, DMSO-d_6) δ 10.2 (s, 1H), 7.94 (s, 1H), 7.93 (d, J = 8.0 Hz, 1H), 7.59–7.57 (m, 2H), 7.26 (s, 1H), 6.42 (s, 1H), 4.79 (t, J = 5 Hz, 1H), 4.64 (t, J = 5 Hz, 1H), 4.39 (t, J = 5 Hz, 1H), 4.31 (t, J = 5 Hz, 1H),), 4.29 (s, 3H), 2.16 (s, 3H), 1.26 (s, 9H); HPLC >99% (AUC), (Method A), t_R = 9.1 min.
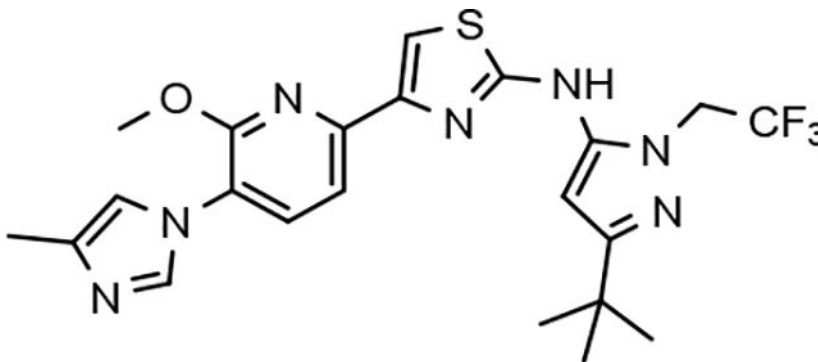
N-(3-(tert-butyl)-1-(2,2,2-trifluoroethyl)-1H-pyrazol-5-yl)-4-(6-methoxy-5-(4-methyl-1H-imidazol-1-yl)pyridin-2-yl)thiazol-2-amine (57)—Off-white solid; mp 220–225 °C; ESI MS (M+H) 492; ^{1}H NMR (300 MHz, CDCl$_3$) δ 7.94 (s, 1H), 7.61–7.50 (m, 2H), 7.33 (s, 1H), 7.00 (s, 1H), 6.24 (s, 1H), 4.76–4.66 (m, 2H), 4.07 (s, 3H), 2.33 (s, 3H), 2.2–1.7 (br s, 1H), 1.27 (s, 9H); HPLC >99% (AUC), (Method A), t_R = 10.1 min.
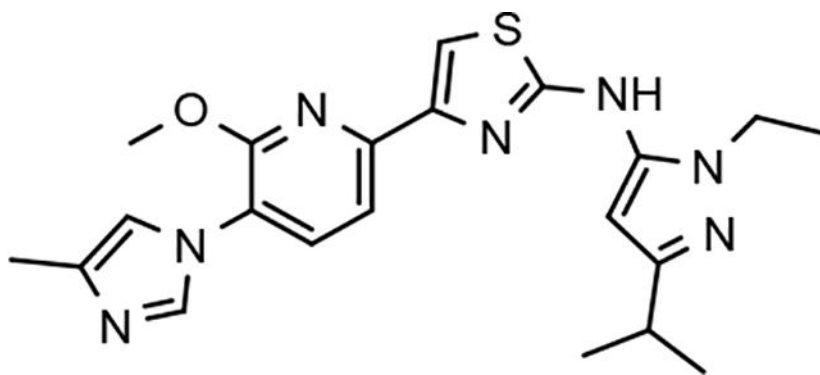
N-(1-ethyl-3-isopropyl-1H-pyrazol-5-yl)-4-(6-methoxy-5-(4-methyl-1H-imidazol-1-yl)pyridin-2-yl)thiazol-2-amine (58)—Light yellow solid; mp 170–174 °C; ESI MS (M+H) 424; ^{1}H NMR (500 MHz, DMSO-d_6) δ 10.14 (s, 1H), 7.91 (d, J = 1.2 Hz, 1H), 7.90 (d, J = 7.8 Hz, 1H), 7.58 (s, 1H), 7.57 (d, J = 7.8 Hz, 1H), 7.25 (s, 1H), 6.30 (s, 1H), 4.04 (q, J = 7.2 Hz, 2H), 4.02 (s, 3H), 2.84 (septet, J = 6.9 Hz, 1H), 2.16 (s, 3H), 1.27 (t, J = 7.2 Hz, 3H), 1.20 (d, J = 6.9 Hz, 6H); HPLC >99% (AUC), (Method B), t_R = 10.5 min.
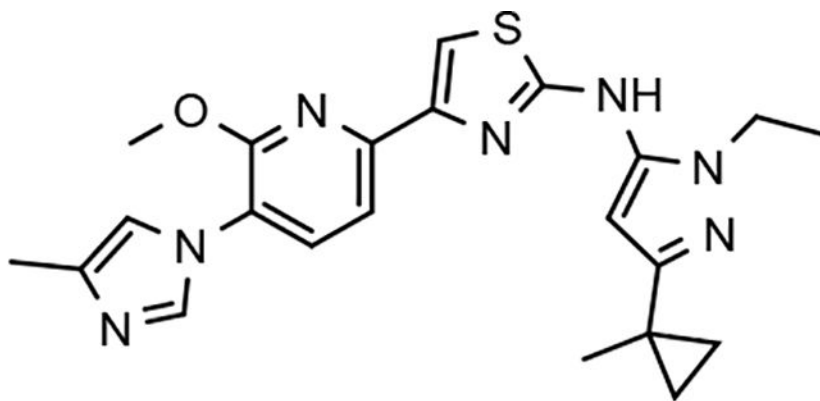
N-(1-ethyl-3-(1-methylcyclopropyl)-1H-pyrazol-5-yl)-4-(6-methoxy-5-(4-methyl-1H-imidazol-1-yl)pyridin-2-yl)thiazol-2-amine (59)—Off-white solid; mp 178–182 °C; ESI MS (M+H) 436; ^{1}H NMR (300 MHz, DMSO-d_6) δ 10.13 (s, 1H), 7.92 (d, J = 1.2 Hz, 1H), 7.91 (d, J = 8.0 Hz, 1H), 7.58 (s, 1H), 7.56 (d, J = 8.0 Hz, 1H), 7.25 (m, 1H), 6.21 (s, 1H), 4.01 (s, 3H), 3.99 (q, J = 7.2 Hz, 2H), 2.16 (s, 3H), 1.38 (s, 3H), 1.25 (t, J = 7.2 Hz, 3H), 0.86 (dd, J = 6.0, 3.6 Hz, 2H), 0.68 (dd, J = 6.0, 3.6 Hz, 2H); HPLC >99% (AUC), (Method A), t_R = 8.6 min.
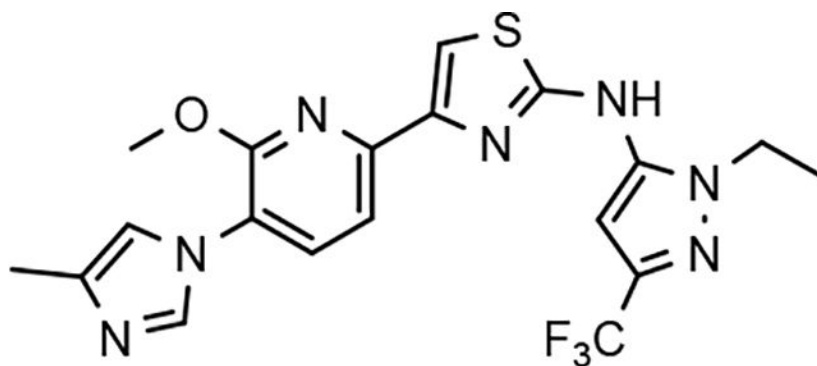
N-(1-ethyl-3-(trifluoromethyl)-1H-pyrazol-5-yl)-4-(6-methoxy-5-(4-methyl-1H-imidazol-1-yl)pyridin-2-yl)thiazol-2-amine (60)—Light brown solid; mp 222–225 °C; APCI MS (M+H) 450; ^{1}H NMR (500 MHz, DMSO-d_6) δ 10.60 (s, 1H), 7.93 (d, J = 8.0 Hz, 1H), 7.91 (d, J = 1.0 Hz, 1H), 7.67 (br s, 1H), 7.59 (d, J = 8.0 Hz, 1H), 7.24 (s, 1H), 7.00 (br s, 1H), 4.21 (q, J = 7.5 Hz, 2H), 4.03 (s, 3H), 2.16 (d, J = 1.0 Hz, 3H), 1.36 (t, J = 7.5 Hz, 3H); HPLC >99% (AUC), (Method D), t_R = 9.1 min.
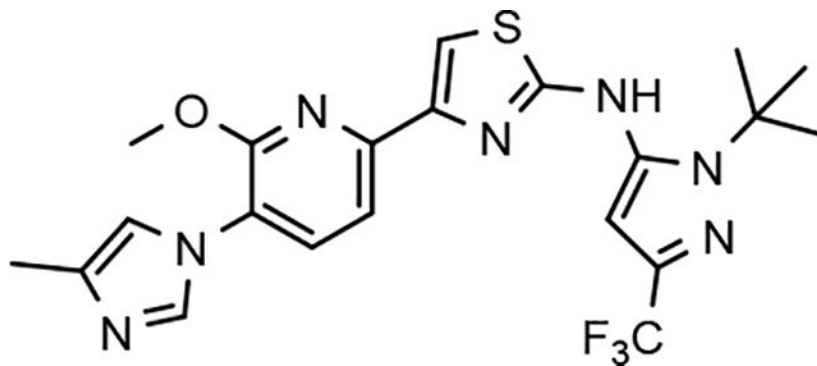
N-(1-(tert-butyl)-3-(trifluoromethyl)-1H-pyrazol-5-yl)-4-(6-methoxy-5-(4-methyl-1H-imidazol-1-yl)pyridin-2-yl)thiazol-2-amine (61)—White solid; mp 197–200 °C; APCI MS (M+H) 478; ^{1}H NMR (300 MHz, DMSO-d_6) δ 9.89 (s, 1H), 7.90 (s, 1H), 7.87 (d, J = 8.7 Hz, 1H), 7.57 (s, 1H), 7.50 (d, J = 8.1 Hz, 1H), 7.24 (s, 1H), 6.98 (s, 1H), 4.01 (s, 3H), 2.16 (s, 3H), 1.62 (s, 9H); HPLC >99% (AUC), (Method B), t_R = 14.0 min.
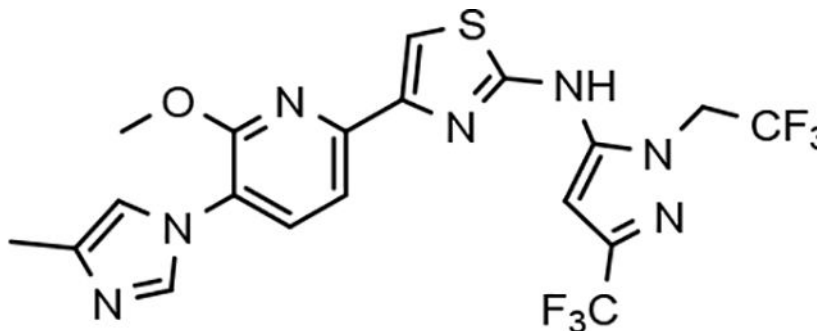
4-(6-methoxy-5-(4-methyl-1H-imidazol-1-yl)pyridin-2-yl)-N-(1-(2,2,2-trifluoroethyl)-3-(trifluoromethyl)-1H-pyrazol-5-yl)thiazol-2-amine (62)—Off-white solid; mp 230–234 °C; APCI MS (M+H) 504; ^{1}H NMR (300 MHz, DMSO-d_6) δ 10.97 (br s, 1H), 7.95 (d, J = 8.1 Hz, 1H), 7.93 (d, J = 1.2 Hz, 1H), 7.70 (br s, 1H), 7.64 (d, J = 8.1 Hz, 1H), 7.26 (s, 1H), 7.08 (br s, 1H), 5.24 (m, 2H), 4.04 (s, 3H), 2.16 (s, 3H); HPLC >99% (AUC), (Method B), t_R = 13.3 min.
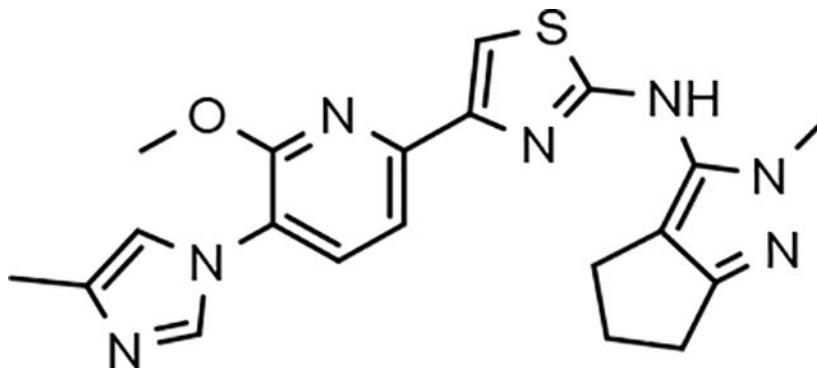
4-(6-methoxy-5-(4-methyl-1H-imidazol-1-yl)pyridin-2-yl)-N-(2-methyl-2,4,5,6-tetrahydrocyclopenta[c]pyrazol-3-yl)thiazol-2-amine (63)—White solid; mp 196–199 °C; ESI MS (M+H) 408; ^{1}H NMR (300 MHz, DMSO-d_6) δ 10.04 (s, 1H), 7.90 (d, J = 1.8 Hz, 1H), 7.88 (d, J = 7.8 Hz, 1H), 7.55 (s, 1H), 7.53 (d, J = 8.1 Hz, 1H), 7.24 (s, 1H), 4.01 (s, 3H), 3.64 (s, 3H), 2.63–2.53 (m, 4H), 2.37–2.23 (m, 2H), 2.16 (m, 3H); HPLC >99% (AUC), (Method D), t_R = 8.1 min.
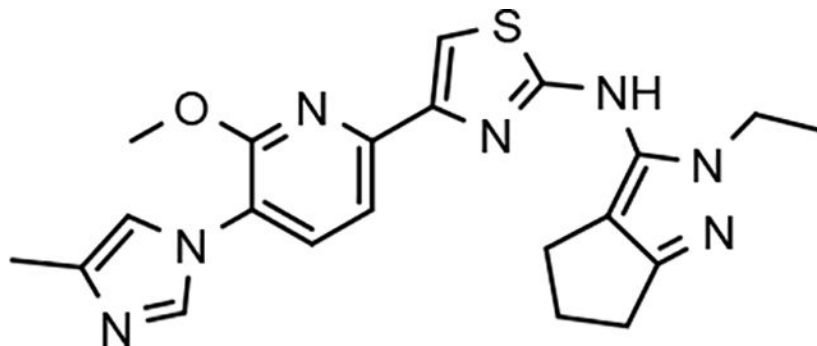
N-(2-ethyl-2,4,5,6-tetrahydrocyclopenta[c]pyrazol-3-yl)-4-(6-methoxy-5-(4-methyl-1H-imidazol-1-yl)pyridin-2-yl)thiazol-2-amine (64)—White solid; mp 228–232 °C dec; ESI MS (M+H) 422; ^{1}H NMR (500 MHz, DMSO-d_6) δ 9.95 (s, 1H), 7.90 (s, 1H), 7.88 (d, J = 8.0 Hz, 1H), 7.54 (s, 1H), 7.53 (d, J = 8.0 Hz, 1H), 7.24 (s, 1H), 4.01 (s, 3H), 3.97 (q, J = 7.0 Hz, 2H), 2.60–2.55 (m, 4H), 2.34–2.28 (m, 2H), 2.16 (s, 3H), 1.27 (t, J = 7.0 Hz, 3H); HPLC >99% (AUC), (Method C), t_R = 9.1 min.
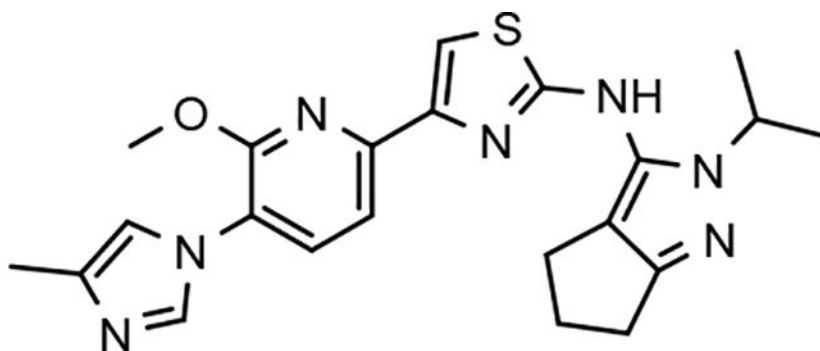
N-(2-isopropyl-2,4,5,6-tetrahydrocyclopenta[c]pyrazol-3-yl)-4-(6-methoxy-5-(4-methyl-1H-imidazol-1-yl)pyridin-2-yl)thiazol-2-amine (65)—Light yellow solid; mp 212–216 °C; ESI MS (M+H) 436; ^{1}H NMR (300 MHz, DMSO-d_6) δ 9.93 (s, 1H), 7.91 (d, J = 1.5 Hz, 1H), 7.88 (d, J = 7.8 Hz, 1H), 7.53 (s, 1H), 7.52 (d, J = 7.8 Hz, 1H), 7.25 (m, 1H), 4.46 (septet, J = 6.6 Hz, 1H), 4.01 (s, 3H), 2.63–2.50 (m, 4H), 2.38–2.25 (m, 2H), 2.16 (s, 3H), 1.33 (d, J = 6.6 Hz, 6H); HPLC >99% (AUC), (Method B), t_R = 10.7 min.
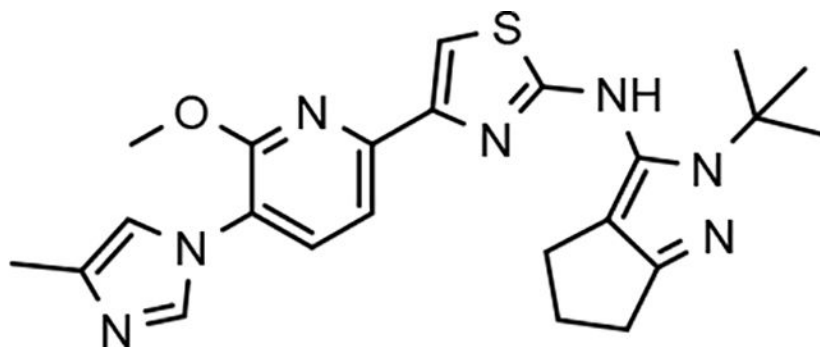
N-(2-(tert-butyl)-2,4,5,6-tetrahydrocyclopenta[c]pyrazol-3-yl)-4-(6-methoxy-5-(4-methyl-1H-imidazol-1-yl)pyridin-2-yl)thiazol-2-amine (66)—Brown solid; mp 95–105 °C; ESI MS (M+H) 450; ^{1}H NMR (300 MHz, CDCl$_3$) δ 7.90 (br s, 1H), 7.59–7.53 (m, 2H), 7.41 (s, 1H), 7.01 (s, 1H), 4.07 (s, 3H), 2.75 (t, J = 6.9 Hz, 2H), 2.56 (t, J = 6.9 Hz, 2H), 2.44–2.37 (m, 3H), 2.33 (s, 3H), 1.65 (s, 9H); HPLC >99% (AUC), (Method A), t_R = 8.9 min.

N-(2-cyclobutyl-2,4,5,6-tetrahydrocyclopenta[c]pyrazol-3-yl)-4-(6-methoxy-5-(4-methyl-1H-imidazol-1-yl)pyridin-2-yl)thiazol-2-amine (67)—White solid; mp 180–183 °C; APCI MS (M+H) 448; ^{1}H NMR (300 MHz, DMSO-d_6) δ 9.93 (s, 1H), 7.94 (s, 1H), 7.88 (d, J = 7.8 Hz, 1H), 7.54 (s, 1H), 7.52 (d, J = 7.8 Hz, 1H), 7.26 (s, 1H), 4.73 (m, 1H), 4.00 (s, 3H), 2.59 (m, 6H), 2.29 (m, 4H), 2.16 (s, 3H), 1.73 (m, 2H); HPLC >99% (AUC), (Method B), t_R = 11.4 min.
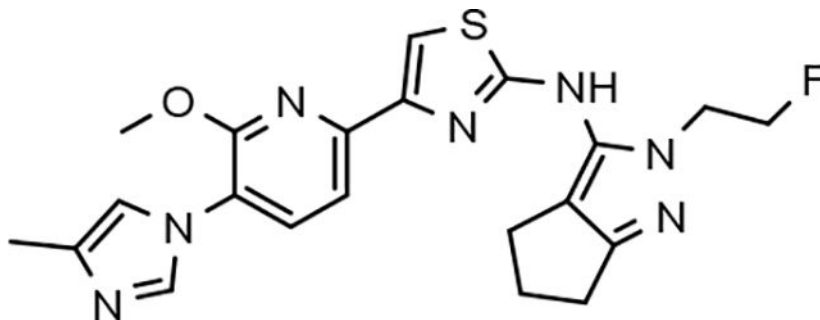
N-(2-(2-fluoroethyl)-2, 4, 5, 6-tetrahydrocyclopenta[c]pyrazol-3-yl)-4-(6-methoxy-5-(4-methyl-1H-imidazol-1-yl) pyridin-2-yl) thiazol-2-amine (68)—White solid; mp 160–163 °C; ESI MS (M+H) 440; ^{1}H NMR (300 MHz, CDCl$_3$) δ 7.91 (s, 1H), 7.64–7.58 (m, 2H), 7.44 (s, 1H), 7.01 (s, 1H), 4.84 (t, J = 5 Hz, 1H), 4.69 (t, J = 5 Hz, 1H), 4.41 (t, J = 5 Hz, 1H), 4.33 (t, J = 5 Hz, 1H), 4.08 (s, 3H), 2.77–2.72 (m, 2H), 2.66–2.61 (m, 2H), 2.60–2.30 (br s, 1H), 2.45–2.40 (m, 2H), 2.34 (s, 3H); HPLC >99% (AUC), (Method A), t_R = 8.6 min.
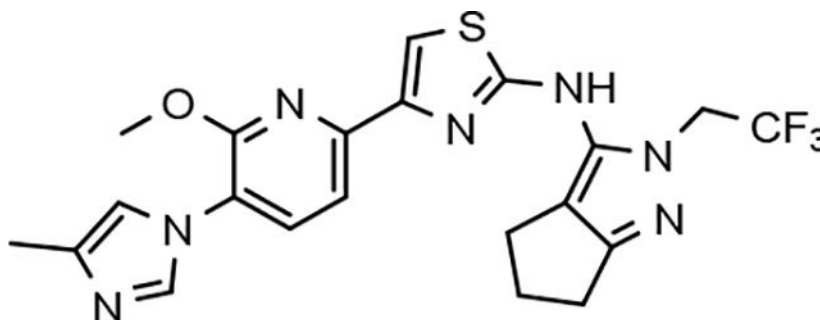
4-(6-methoxy-5-(4-methyl-1H-imidazol-1-yl)pyridin-2-yl)-N-(2-(2,2,2-trifluoroethyl)-2,4,5,6-tetrahydrocyclopenta[c]pyrazol-3-yl)thiazol-2-amine (69)—Brown solid; mp 80–85 °C; ESI MS (M+H) 476; ^{1}H NMR (300 MHz, DMSO-d_6) δ 10.17 (s, 1H), 7.91 (s, 1H), 7.89 (d, J = 8.0 Hz, 1H), 7.60 (s, 1H), 7.54 (d, J = 8.0 Hz, 1H), 7.25 (s, 1H), 5.09–4.85 (m, 2H), 4.02 (s, 3H), 2.67–2.54 (m, 4H), 2.38–2.25 (m, 2H), 2.16 (s, 3H); HPLC 96.9% (AUC), (Method A), t_R = 9.3 min.
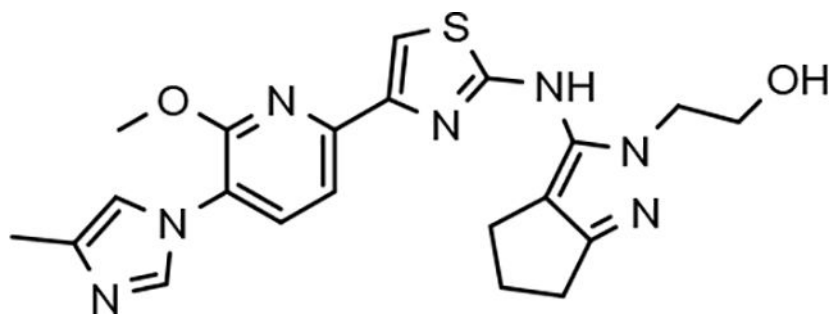
2-(3-((4-(6-methoxy-5-(4-methyl-1H-imidazol-1-yl)pyridin-2-yl)thiazol-2-yl)amino)-5,6-dihydrocyclopenta[c]pyrazol-2(4H)-yl)ethanol (70)—Brown solid; mp 140–145 °C; ESI MS (M+H) 438; ^{1}H NMR (300 MHz, DMSO-d_6) δ 9.92 (s, 1H), 8.21 (s, 1H), 7.93 (d, J = 8.0 Hz, 1H), 7.58 (s, 1H), 7.55 (d, J = 8.0 Hz, 1H), 7.37 (s, 1H), 4.93 (br s, 1H), 4.10–3.95 (m, 5H), 3.71–3.60 (m, 2H), 2.63–2.53 (m, 4H), 2.38–2.29 (m, 2H), 2.19 (s, 3H); HPLC >99% (AUC), (Method A), t_R = 7.8 min.
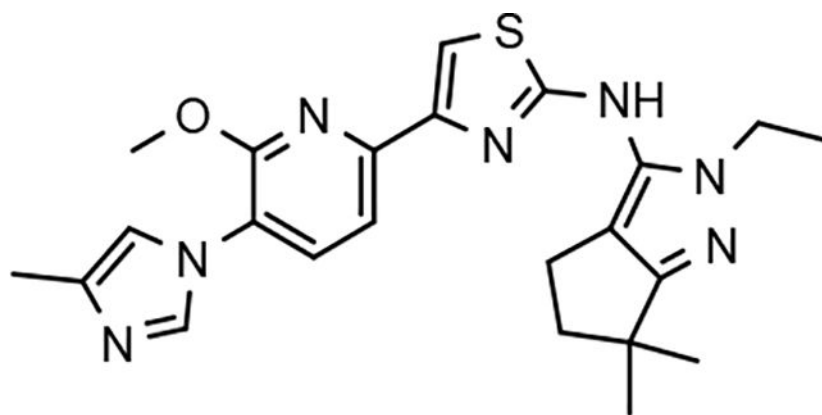
N-(2-ethyl-6,6-dimethyl-2,4,5,6-tetrahydrocyclopenta[c]pyrazol-3-yl)-4-(6-methoxy-5-(4-methyl-1H-imidazol-1-yl)pyridin-2-yl)thiazol-2-amine (71)—White solid; mp 176–180 °C; ESI MS (M+H) 450; ^{1}H NMR (500 MHz, DMSO-d_6) δ 9.93 (s, 1H), 7.90 (d, J = 1.0 Hz, 1H), 7.89 (d, J = 8.0 Hz, 1H), 7.54 (d, J = 8.0 Hz, 1H), 7.53 (s, 1H), 7.24 (m, 1H), 4.01 (s, 3H), 3.97 (q, J = 7.2 Hz, 2H), 2.55 (t, J = 6.7 Hz, 2H), 2.16 (s, 3H), 2.12 (t, J = 6.7 Hz, 2H), 1.27 (t, J = 7.2 Hz, 3H), 1.23 (s, 6H); HPLC >99% (AUC), (Method A), t_R = 8.7 min.
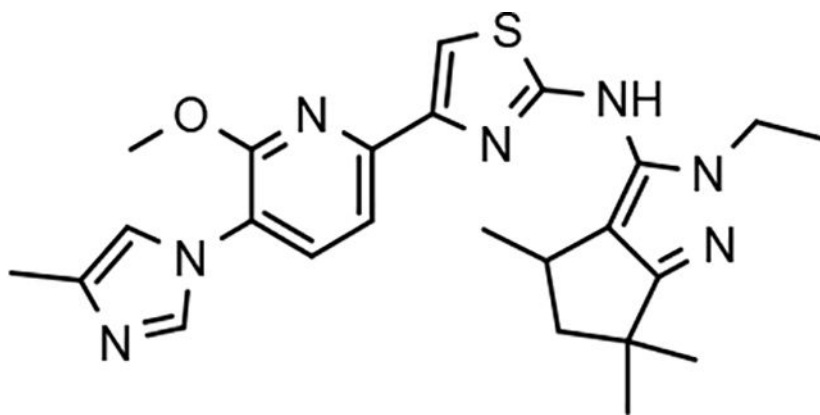
***(+/−)-N-(2-ethyl-4,6,6-trimethyl-2,4,5,6-tetrahydrocyclopenta[c]pyrazol-3-yl)-4-(6-methoxy-5-(4-methyl-1H-imidazol-1-yl)pyridin-2-yl)thiazol-2-amine* (72)** —Light yellow solid; mp 160–164 °C; ESI MS (M+H) 464; ^{1}H NMR (300 MHz, DMSO-d_6) δ 9.90 (s, 1H), 7.91 (d, J = 1.5 Hz, 1H), 7.89 (d, J = 7.8 Hz, 1H), 7.54 (s, 1H), 7.53 (d, J = 7.8 Hz, 1H), 7.25 (m, 1H), 4.02 (s, 3H), 4.03–3.85 (sym m, 2H), 3.10 (q, J = 6.9 Hz, 1H), 2.32 (dd, J = 12.4, 7.0 Hz, 1H), 2.16 (s, 3H), 1.73 (dd, J = 12.4, 8.1 Hz, 1H), 1.32–1.22 (s, 6H), 1.19 (s, 3H), 0.95 (d, J = 6.9 Hz, 3H); HPLC >99% (AUC), (Method A), t_R = 9.2 min.
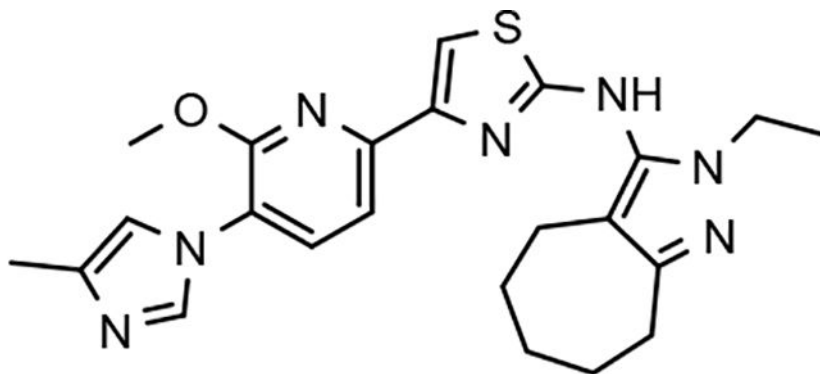
***N-(2-ethyl-2,4,5,6,7,8-hexahydrocyclohepta[c]pyrazol-3-yl)-4-(6-methoxy-5-(4-methyl-1H-imidazol-1-yl)pyridin-2-yl)thiazol-2-amine* (73)**—Yellow solid; mp 217–221 °C; APCI MS (M+H) 450; ^{1}H NMR (300 MHz, DMSO-d_6) δ 9.66 (s, 1H), 7.91 (s, 1H), 7.87 (d, J = 8.1 Hz, 1H), 7.51 (d, J = 8.1 Hz, 1H), 7.48 (s, 1H), 7.24 (s, 1H), 3.99 (s, 3H), 3.89 (q, J = 7.2 Hz, 2H), 2.64 (m, 2H), 2.31 (m, 2H), 2.16 (s, 3H), 1.78 (m, 2H), 1.56 (m, 4H), 1.24 (t, J = 7.2 Hz, 3H); HPLC >99% (AUC), (Method E), t_R = 11.6 min.
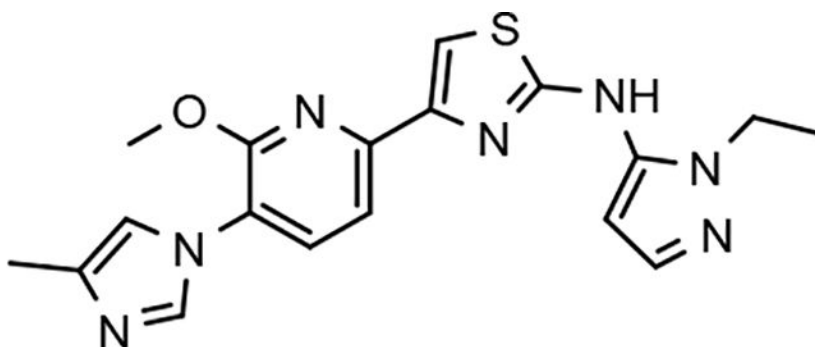
N-(1-ethyl-1H-pyrazol-5-yl)-4-(6-methoxy-5-(4-methyl-1H-imidazol-1-yl)pyridin-2-yl)thiazol-2-amine (74)—Yellow solid; mp 180–187 °C; ESI MS (M+H) 382; ^{1}H NMR (300 MHz, CDCl$_3$) δ 7.90 (s, 1H), 7.59 (s, 2H), 7.55 (s, 1H), 7.41 (s, 1H), 7.00 (s, 1H), 6.31 (s, 1H), 4.20–4.15 (m, 2H), 4.08 (s, 3H), 2.32 (s, 3), 1.90 (br s, 1H), 1.45 (t, J = 7.0 Hz, 3H); HPLC >99% (AUC), (Method A), t_R = 8.1 min.

Supplementary Material

Refer to Web version on PubMed Central for supplementary material.

Acknowledgements

References

1. Association, A. s., Alzheimer's Disease Facts and Figures. Alzheimers Dement 2019, 15 (3), 321–387.

2. Glenner GG; Wong CW, Alzheimer's disease: initial report of the purification and characterization of a novel cerebrovascular amyloid protein. Biochem Biophys Res Commun 1984, 120 (3), 885–90. [PubMed: 6375662]

3. Iwatsubo T; Saido TC; Mann DM; Lee VM; Trojanowski JQ, Full-length amyloid-beta (1–42(43)) and amino-terminally modified and truncated amyloid-beta 42(43) deposit in diffuse plaques. Am J Pathol 1996, 149 (6), 1823–30. [PubMed: 8952519]

4. Dickson DW, The Pathogenesis of Senile Plaques. Journal of Neuropathology & Experimental Neurology 1997, 56 (4), 321–339. [PubMed: 9100663]

5. Rowe CC; Ellis KA; Rimajova M; Bourgeat P; Pike KE; Jones G; Fripp J; Tochon-Danguy H; Morandeau L; O'Keefe G; Price R; Raniga P; Robins P; Acosta O; Lenzo N; Szoeke C; Salvado O; Head R; Martins R; Masters CL; Ames D; Villemagne VL, Amyloid imaging results from the Australian Imaging, Biomarkers and Lifestyle (AIBL) study of aging. Neurobiol Aging 2010, 31 (8), 1275–83. [PubMed: 20472326]

6. Sperling RA; Aisen PS; Beckett LA; Bennett DA; Craft S; Fagan AM; Iwatsubo T; Jack CR Jr.; Kaye J; Montine TJ; Park DC; Reiman EM; Rowe CC; Siemers E; Stern Y; Yaffe K; Carrillo MC; Thies B; Morrison-Bogorad M; Wagster MV; Phelps CH, Toward defining the preclinical stages of Alzheimer's disease: recommendations from the National Institute on Aging-Alzheimer's Association workgroups on diagnostic guidelines for Alzheimer's disease. Alzheimers Dement 2011, 7 (3), 280–92. [PubMed: 21514248]

7. Hardy JA; Higgins GA, Alzheimer's disease: the amyloid cascade hypothesis. Science 1992, 256 (5054), 184–5. [PubMed: 1566067]

8. Hardy J; Selkoe DJ, The amyloid hypothesis of Alzheimer's disease: progress and problems on the road to therapeutics. Science 2002, 297 (5580), 353–6. [PubMed: 12130773]

9. Tanzi RE; Bertram L, Twenty years of the Alzheimer's disease amyloid hypothesis: a genetic perspective. Cell 2005, 120 (4), 545–55. [PubMed: 15734686]

10. Thinakaran G; Koo EH, Amyloid precursor protein trafficking, processing, and function. J Biol Chem 2008, 283 (44), 29615–9. [PubMed: 18650430]

11. De Strooper B; Vassar R; Golde T, The secretases: enzymes with therapeutic potential in Alzheimer disease. Nat Rev Neurol 2010, 6 (2), 99–107. [PubMed: 20139999]

12. Karran E; Mercken M; De Strooper B, The amyloid cascade hypothesis for Alzheimer's disease: an appraisal for the development of therapeutics. Nat Rev Drug Discov 2011, 10 (9), 698–712. [PubMed: 21852788]

13. Oehlrich D; Berthelot DJ; Gijsen HJ, gamma-Secretase modulators as potential disease modifying anti-Alzheimer's drugs. J Med Chem 2011, 54 (3), 669–98. [PubMed: 21141968]

14. Evin G; Barakat A; Masters CL, BACE: Therapeutic target and potential biomarker for Alzheimer's disease. Int J Biochem Cell Biol 2010, 42 (12), 1923–6. [PubMed: 20817005]

15. Durham TB; Shepherd TA, Progress toward the discovery and development of efficacious BACE inhibitors. Curr Opin Drug Discov Devel 2006, 9 (6), 776–91.

16. Stachel SJ, Progress toward the development of a viable BACE-1 inhibitor. Drug Development Research 2009, 70 (2), 101–110.

17. Vassar R; Kandalepas PC, The beta-secretase enzyme BACE1 as a therapeutic target for Alzheimer's disease. Alzheimers Res Ther 2011, 3 (3), 20. [PubMed: 21639952]

18. Bateman RJ; Siemers ER; Mawuenyega KG; Wen G; Browning KR; Sigurdson WC; Yarasheski KE; Friedrich SW; Demattos RB; May PC; Paul SM; Holtzman DM, A gamma-secretase inhibitor decreases amyloid-beta production in the central nervous system. Ann Neurol 2009, 66 (1), 48–54. [PubMed: 19360898]

19. Tomita T, Secretase inhibitors and modulators for Alzheimer's disease treatment. Expert Rev Neurother 2009, 9 (5), 661–79. [PubMed: 19402777]

20. Imbimbo BP; Panza F; Frisardi V; Solfrizzi V; D'Onofrio G; Logroscino G; Seripa D; Pilotto A, Therapeutic intervention for Alzheimer's disease with gamma-secretase inhibitors: still a viable option? Expert Opin Investig Drugs 2011, 20 (3), 325–41.

21. Iwatsubo T; Odaka A; Suzuki N; Mizusawa H; Nukina N; Ihara Y, Visualization of A beta 42(43) and A beta 40 in senile plaques with end-specific A beta monoclonals: evidence that an initially deposited species is A beta 42(43). Neuron 1994, 13 (1), 45–53. [PubMed: 8043280]

22. Weggen S; Eriksen JL; Das P; Sagi SA; Wang R; Pietrzik CU; Findlay KA; Smith TE; Murphy MP; Bulter T; Kang DE; Marquez-Sterling N; Golde TE; Koo EH, A subset of NSAIDs lower amyloidogenic Abeta42 independently of cyclooxygenase activity. Nature 2001, 414 (6860), 212–6. [PubMed: 11700559]

23. Kumar-Singh S; Theuns J; Van Broeck B; Pirici D; Vennekens K; Corsmit E; Cruts M; Dermaut B; Wang R; Van Broeckhoven C, Mean age-of-onset of familial alzheimer disease caused by presenilin mutations correlates with both increased Abeta42 and decreased Abeta40. Hum Mutat 2006, 27 (7), 686–95. [PubMed: 16752394]

24. Rynearson KD; Tanzi RE; Wagner SL, Discovery of Potent Gamma-Secretase Modulators for the Treatment of Alzheimer's Disease. In Translational Neuroscience: Fundamental Approaches for Neurological Disorders, 1st ed.; Tuszynski MH, Ed. Springer Science: New York, 2016; pp 359–368.

25. Portelius E; Van Broeck B; Andreasson U; Gustavsson MK; Mercken M; Zetterberg H; Borghys H; Blennow K, Acute effect on the Abeta isoform pattern in CSF in response to gamma-secretase modulator and inhibitor treatment in dogs. J Alzheimers Dis 2010, 21 (3), 1005–12. [PubMed: 20634579]

26. Borgegard T; Jureus A; Olsson F; Rosqvist S; Sabirsh A; Rotticci D; Paulsen K; Klintenberg R; Yan H; Waldman M; Stromberg K; Nord J; Johansson J; Regner A; Parpal S; Malinowsky D; Radesater AC; Li T; Singh R; Eriksson H; Lundkvist J, First and second generation gamma-

secretase modulators (GSMs) modulate amyloid-beta (Abeta) peptide production through different mechanisms. J Biol Chem 2012, 287 (15), 11810–9. [PubMed: 22334705]

27. Pettersson M; Johnson DS; Humphrey JM; Am Ende CW; Evrard E; Efremov I; Kauffman GW; Stepan AF; Stiff CM; Xie L; Bales KR; Hajos-Korcsok E; Murrey HE; Pustilnik LR; Steyn SJ; Wood KM; Verhoest PR, Discovery of indole-derived pyridopyrazine-1,6-dione gamma-secretase modulators that target presenilin. Bioorg Med Chem Lett 2015, 25 (4), 908–13. [PubMed: 25582600]

28. Pettersson M; Johnson DS; Humphrey JM; Butler TW; Am Ende CW; Fish BA; Green ME; Kauffman GW; Mullins PB; O'Donnell CJ; Stepan AF; Stiff CM; Subramanyam C; Tran TP; Vetelino BC; Yang E; Xie L; Bales KR; Pustilnik LR; Steyn SJ; Wood KM; Verhoest PR, Design of Pyridopyrazine-1,6-dione gamma-Secretase Modulators that Align Potency, MDR Efflux Ratio, and Metabolic Stability. ACS Med Chem Lett 2015, 6 (5), 596–601. [PubMed: 26005540]

29. Takasugi N; Tomita T; Hayashi I; Tsuruoka M; Niimura M; Takahashi Y; Thinakaran G; Iwatsubo T, The role of presenilin cofactors in the gamma-secretase complex. Nature 2003, 422 (6930), 438–41. [PubMed: 12660785]

30. Edbauer D; Winkler E; Regula JT; Pesold B; Steiner H; Haass C, Reconstitution of gamma-secretase activity. Nat Cell Biol 2003, 5 (5), 486–8. [PubMed: 12679784]

31. Crump CJ; Johnson DS; Li YM, Development and mechanism of gamma-secretase modulators for Alzheimer's disease. Biochemistry 2013, 52 (19), 3197–216. [PubMed: 23614767]

32. Pozdnyakov N; Murrey HE; Crump CJ; Pettersson M; Ballard TE; Am Ende CW; Ahn K; Li YM; Bales KR; Johnson DS, gamma-Secretase modulator (GSM) photoaffinity probes reveal distinct allosteric binding sites on presenilin. J Biol Chem 2013, 288 (14), 9710–20. [PubMed: 23396974]

33. Rynearson KD; Buckle RN; Barnes KD; Herr RJ; Mayhew NJ; Paquette WD; Sakwa SA; Nguyen PD; Johnson G; Tanzi RE; Wagner SL, Design and synthesis of aminothiazole modulators of the gamma-secretase enzyme. Bioorg Med Chem Lett 2016, 26 (16), 3928–37. [PubMed: 27426299]

34. Pettersson M; Stepan AF; Kauffman GW; Johnson DS, Novel γ-secretase modulators for the treatment of Alzheimer's disease: a review focusing on patents from 2010 to 2012. Expert Opinion on Therapeutic Patents 2013, 23 (10), 1349–1366. [PubMed: 23875696]

35. Bursavich MG; Harrison BA; Acharya R; Costa DE; Freeman EA; Hodgdon HE; Hrdlicka LA; Jin H; Kapadnis S; Moffit JS; Murphy DA; Nolan S; Patzke H; Tang C; Wen M; Koenig G; Blain JF; Burnett DA, Design, Synthesis, and Evaluation of a Novel Series of Oxadiazine Gamma Secretase Modulators for Familial Alzheimer's Disease. J Med Chem 2017, 60 (6), 2383–2400. [PubMed: 28230986]

36. Wagner SL; Cheng S; Mobley WC; Tanzi RE Compounds and Uses thereof in Modulating Levels of Varoius Amyloid Beta Peptide Alloforms. US 2011/041905, 2011.

37. Parlow JJ; Case BL; Dice TA; Fenton RL; Hayes MJ; Jones DE; Neumann WL; Wood RS; Lachance RM; Girard TJ; Nicholson NS; Clare M; Stegeman RA; Stevens AM; Stallings WC; Kurumbail RG; South MS, Design, parallel synthesis, and crystal structures of pyrazinone antithrombotics as selective inhibitors of the tissue factor VIIa complex. J Med Chem 2003, 46 (19), 4050–62. [PubMed: 12954058]

38. Huffman CW, Formylation of Amines. The Journal of Organic Chemistry 1958, 23 (5), 727–729.

39. Gerack CJ; McElwee-White L, Formylation of amines. Molecules 2014, 19 (6), 7689–713. [PubMed: 24918541]

40. Hantzsch A, Condensationsprodukte aus Aldehydammoniak und ketonartigen Verbindungen. Berichte der deutschen chemischen Gesellschaft 1881, 14 (2), 1637–1638.

41. Raven F; Ward JF; Zoltowska KM; Wan Y; Bylykbashi E; Miller SJ; Shen X; Choi SH; Rynearson KD; Berezovska O; Wagner SL; Tanzi RE; Zhang C, Soluble Gamma-secretase Modulators Attenuate Alzheimer's beta-amyloid Pathology and Induce Conformational Changes in Presenilin 1. EBioMedicine 2017, 24, 93–101. [PubMed: 28919280]

42. Kounnas MZ; Danks AM; Cheng S; Tyree C; Ackerman E; Zhang X; Ahn K; Nguyen P; Comer D; Mao L; Yu C; Pleynet D; Digregorio PJ; Velicelebi G; Stauderman KA; Comer WT; Mobley WC; Li YM; Sisodia SS; Tanzi RE; Wagner SL, Modulation of gamma-secretase reduces beta-amyloid deposition in a transgenic mouse model of Alzheimer's disease. Neuron 2010, 67 (5), 769–80. [PubMed: 20826309]

43. Mucke L; Masliah E; Yu GQ; Mallory M; Rockenstein EM; Tatsuno G; Hu K; Kholodenko D; Johnson-Wood K; McConlogue L, High-level neuronal expression of abeta 1–42 in wild-type human amyloid protein precursor transgenic mice: synaptotoxicity without plaque formation. J Neurosci 2000, 20 (11), 4050–8. [PubMed: 10818140]

44. Hsiao K; Chapman P; Nilsen S; Eckman C; Harigaya Y; Younkin S; Yang F; Cole G, Correlative memory deficits, Abeta elevation, and amyloid plaques in transgenic mice. Science 1996, 274 (5284), 99–102. [PubMed: 8810256]
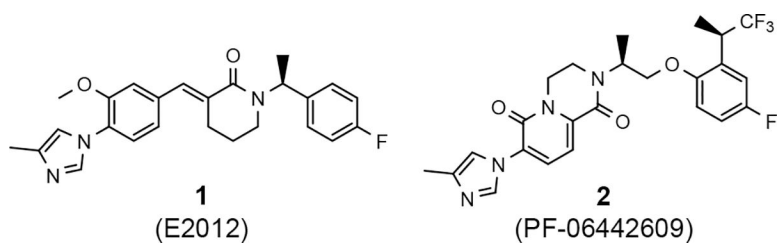
Figure 1.
Representative methyl imidazole-derived GSM scaffolds. E2012 was developed by Eisai. PF-06442609 was developed by Pfizer and illustrates that the general GSM tetracyclic system may be fused.[25–28]
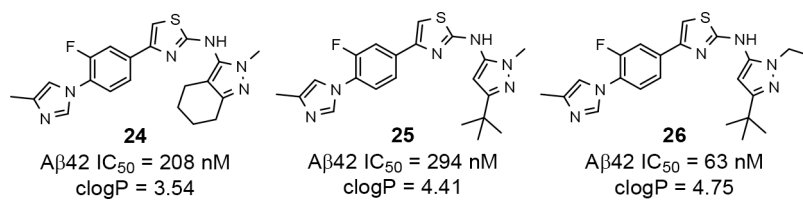
Figure 2.
Fluorophenyl-derived GSMs selected for focused B-ring modification in order to broaden SAR.
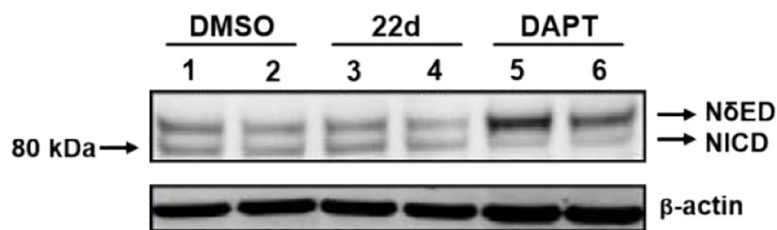
Figure 3.
Stable H4 human neuroglioma cells over-expressing human APP751 (H4-APP751 cells) were transfected with the NΔE construct, and then treated with different concentrations GSM compound **22d** (lane 3 = 10 μM; lane 4 = 1 μM) or GSI (DAPT, lane 5 = 300 nM, lane 6 = 100 nM) for another 24hrs. Vehicle control treatment shown in lanes 1–2. Cells were harvested 48hrs post transfection and applied to Western blotting analysis. Myc antibody was utilized to assess the NΔED and NICD tagged with Myc on their N-termini. β-Actin was utilized as the loading control. Compound **22d** did not inhibit Notching processing; however, DAPT significantly inhibits Notching processing.
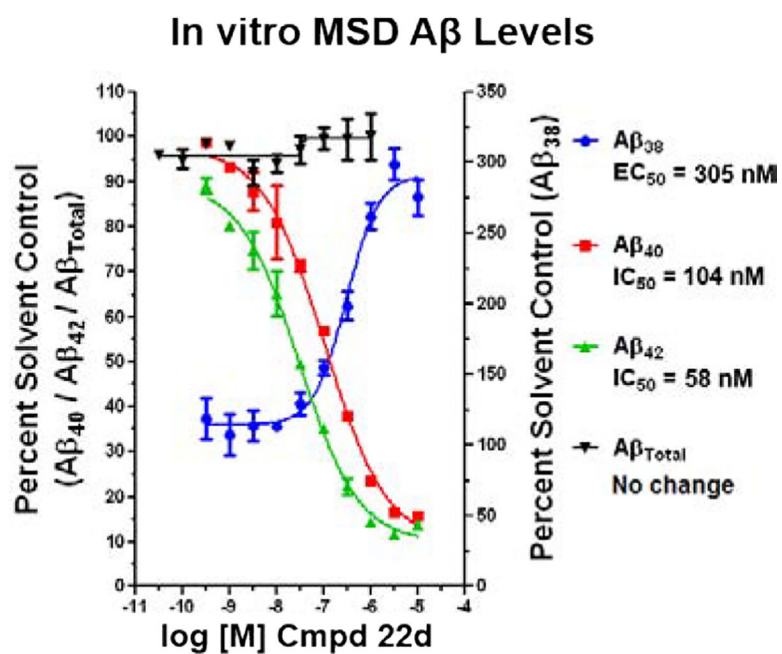
Figure 4.
Concentration response curves of compound **22d** using orthogonal medium throughput
SHSY5Y-APP cell-based screening assays. Aβ38, Aβ40, Aβ42, and total Aβ peptide levels
were determined using Meso Scale Sector 6000 Multiplex assays.
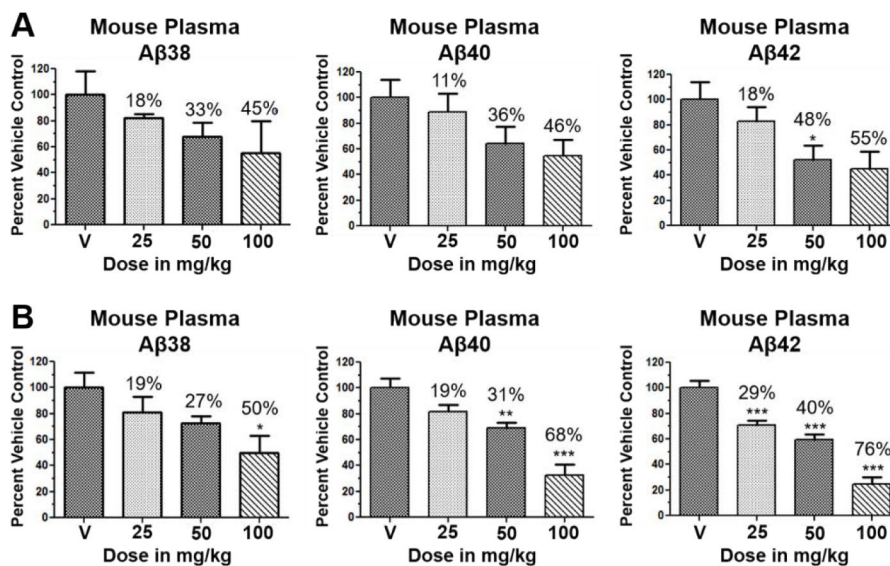
Figure 5.
Levels of Aβ38, Aβ40, and Aβ42 in plasma following daily oral administration of either vehicle, compound **46** (A), or compound **64** (B) to female 5–6 month-old J20 mice ($n = 5$/dose) were measured following a 3-day treatment course. Percent reduction in amyloid is indicated for the study. Aβ38, Aβ40, and Aβ42 peptide levels were determined using Meso Scale Sector 6000 Multiplex assays. Statistical analysis was performed using Graphpad Prism software and results are expressed as mean ± SEM, and Anova was used to detect a significant effect. *: $p < 0.05$. **: $p < 0.005$. ***: $p < 0.0005$.
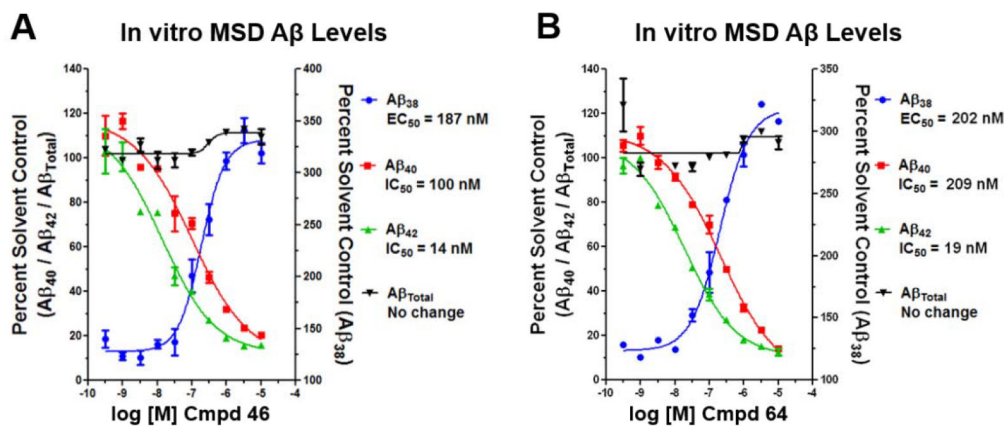
Figure 6.
Concentration response curves of compound **46** (A) and compound **64** (B) using orthogonal medium throughput SHSY5Y-APP cell-based screening assays. Aβ38, Aβ40, Aβ42, and total Aβ peptide levels were determined using Meso Scale Sector 6000 Multiplex assay.
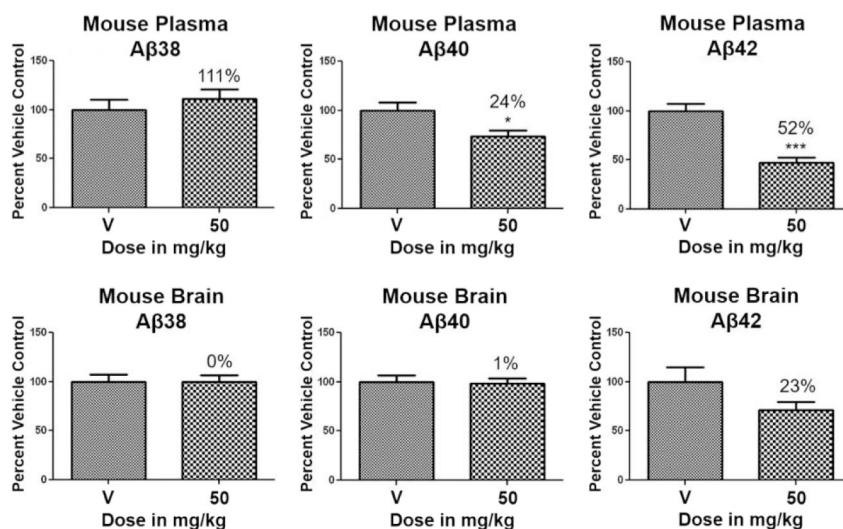
Figure 7.

Levels of Aβ38, Aβ40, and Aβ42 in plasma and brain following daily oral administration of either vehicle or compound **64** to female 5–6 month-old Tg2576 mice ($n = 12$/dose) were measured following a 14-day treatment course. Percent reduction is indicated for the study. Aβ38, Aβ40, and Aβ42 peptide levels were determined using Meso Scale Sector 6000 Multiplex assays. Statistical analysis was performed using Graphpad Prism software and results are expressed as mean ± SEM, and ANOVA was used to detect a significant effect. *: $p < 0.05$. **: $p < 0.005$. ***: $p < 0.0005$.
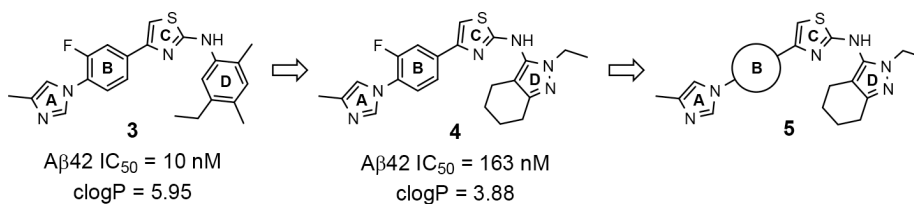
Scheme 1.
GSM B-ring optimization. Aminothiazole **3** (NGP-555) represents the initial lead compound for efforts to discover a potent GSM with improved ADMET properties. Tetrahydroindazole D-ring analog **4** was developed with the aim of improving critical properties of compound **3**, including solubility. The rings are labeled A-D for clarity.
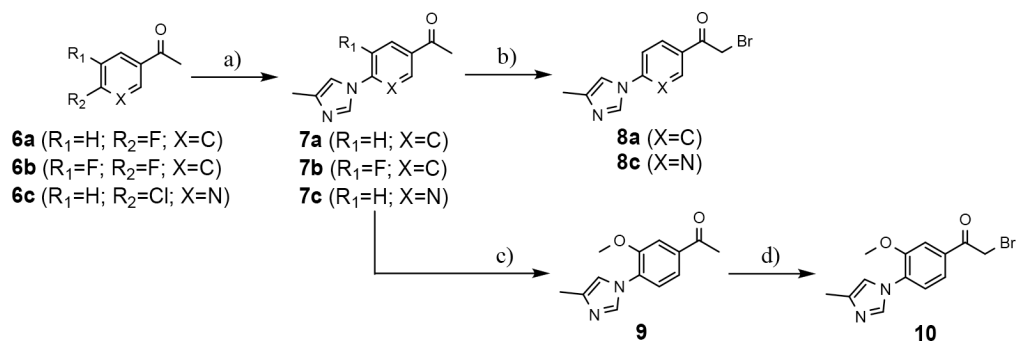
Scheme 2.
Synthesis of phenyl-, methoxyphenyl-, and pyridyl B-ring-containing analogs. Reagents and conditions: a) 4-methylimidazole, K_2CO_3, DMSO, 55 °C, 16 h, 44–67%; b) Br_2, 33% HBr in AcOH, DCM, r.t., 1.5 h, 75–80%; c) NaOMe, DMF, 0 °C to 50 °C, 1 h, 27%; d) Br_2, 33% HBr in AcOH, r.t., 0.75 h, 100%.
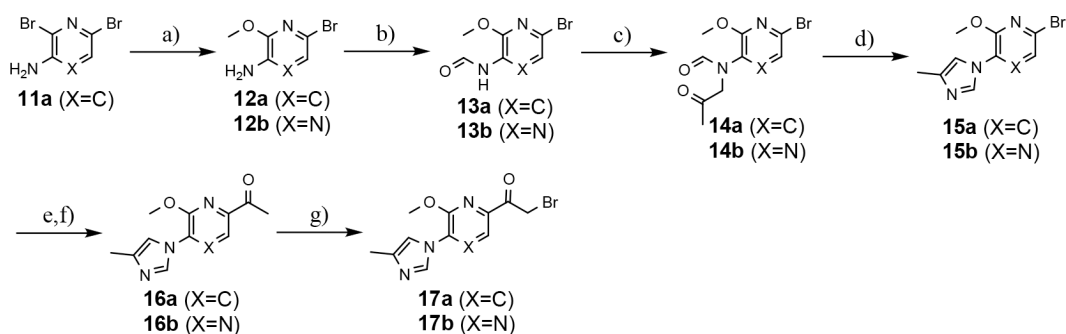
Scheme 3.
Synthesis of methoxypyridine and methoxypyrazine B-ring-containing analogs. Reagents and conditions: a) NaOMe, 1,4-dioxane, reflux, 18 h, 98%; b) Ac$_2$O, formic acid, THF, 0 °C to r.t., 2 h, 95–100%; c) CH$_3$COCH$_2$Cl, K$_2$CO$_3$, KI, DMF, r.t., 4–18 h, 91–93%; d) NH$_4$OAc, acetic acid, 120 °C, 10 h, 85%; e) X=C n-ethylvinylether, Pd(dppf)Cl$_2$, TEA, ethylene glycol, 100 °C, 4 h, 73% or X=N tributyl(1-ethoxyvinyl) tin, Pd(PPh$_3$)$_2$Cl$_2$, dioxane, 100 °C, 18 h, 85%; f) 2N HCl, acetone, r.t., 0.5–18h, 89–96%; g) Br$_2$, 33% HBr in acetic acid, EtOAc, CHCl$_3$, r.t., 0.5–5 h, 85–90%.
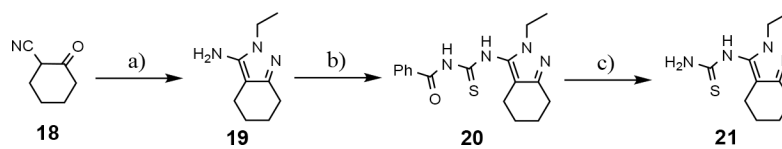
Scheme 4.
Reagents and conditions: a) ethylhydrazine oxalate, EtOH, reflux, 18 h, 88%; b) benzoyl isothiocyanate, 60 °C, 3.5 h, 91%; c) K_2CO_3, MeOH, THF, r.t., 18 h, 92%.
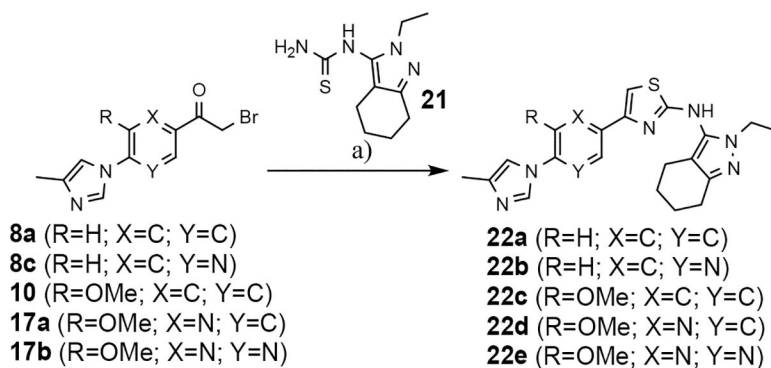
Scheme 5.
Reagents and conditions for substrates **8a**, **8c**, and **10**: a) EtOH, DIPEA, 55 °C, 24 h, 18–33%. Reagents and conditions for substrates **17a** and **17b**: a) EtOH, reflux, 18 h, 40–42%.
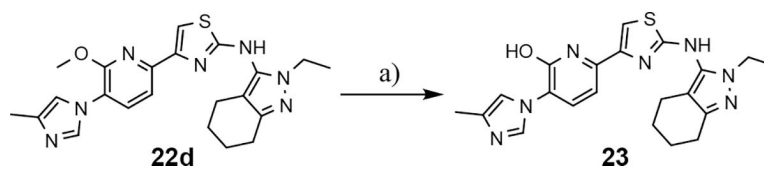
Scheme 6.
Reagents and conditions: a) 33% HBr in AcOH, 50 °C, 1.5 h, 92%.
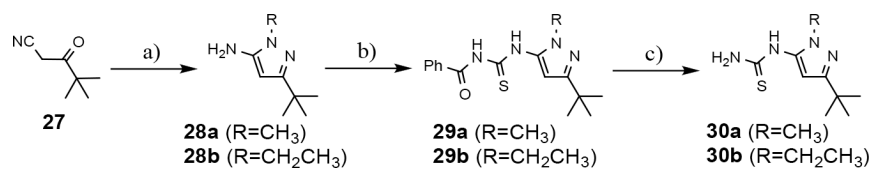
Scheme 7.
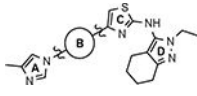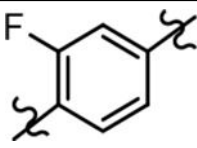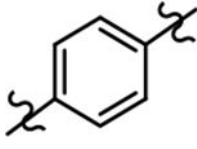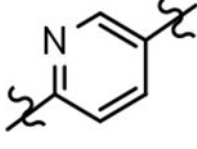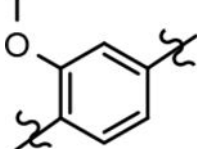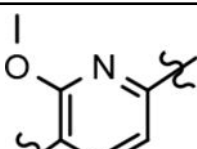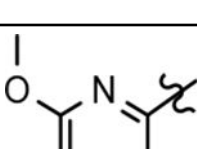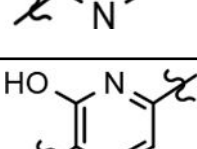
Reagents and conditions: a) ethylhydrazine oxalate or methylhydrazine, EtOH, reflux, 18 h, 61–66%; b) benzoyl isothiocyanate, acetone, reflux, 3.5 h, 88–96%; c) K_2CO_3, MeOH, THF, r.t., 18 h, 81–92%.
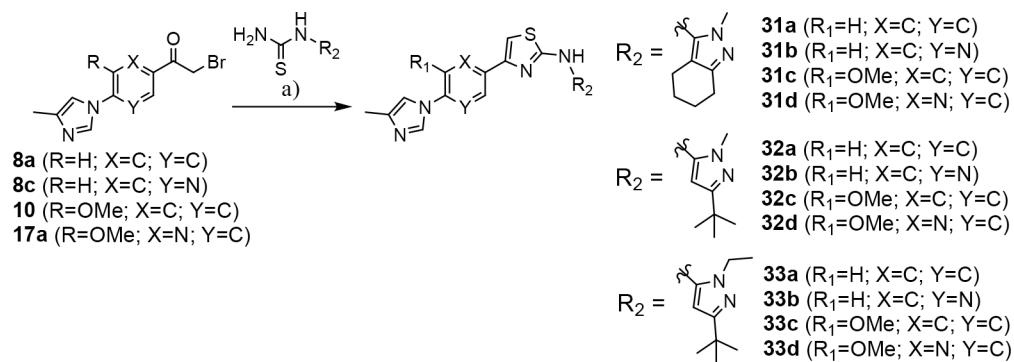
Scheme 8.
Reagents and conditions: a) EtOH, reflux, 18 h, 33–51%.

Table 1.

B-ring analogs of GSM **4**.

Cmpd	B-ring	Aβ42 IC$_{50}$[a]	clogP[b]	Kin. Aq. Sol.[c]
4		163 ± 10	3.88	nt[d]
22a		660 ± 131	3.74	nt[d]
22b		>1000	3.13	nt[d]
22c		171 ± 67	3.49	4.6
22d		60 ± 15	3.28	4.5*
22e		89 ± 38	2.66	<1.6
23		468 ± 165	3.25	nt[d]

[a]IC$_{50}$ represents the concentration in nM of compound required for reducing Aβ42 levels by 50%. The IC$_{50}$ values are the mean ± standard deviation of at least 2 determinations.

[b]Calculated partition coefficient of the simulated ratio of the compound's concentration in octanol to the compound's concentration in water using ChemAxon fragment based approach.

[c]Kinetic aqueous solubility measured at pH 7.4 by UV/Vis absorbance in PBS buffer (μM).

[d]nt = not tested - compound did not meet minimum activity threshold.
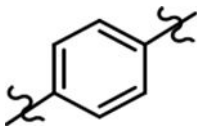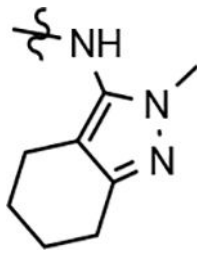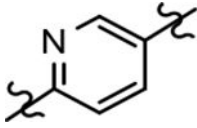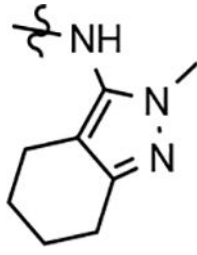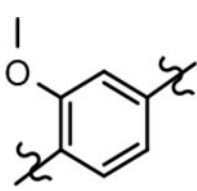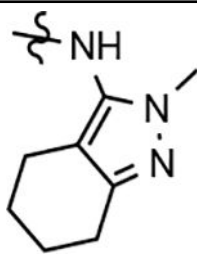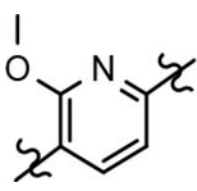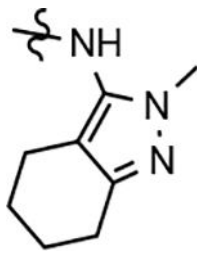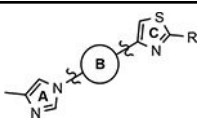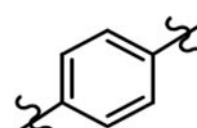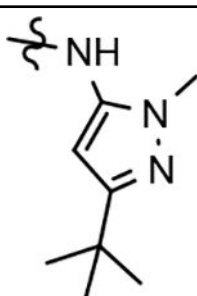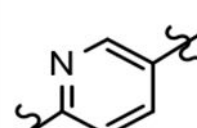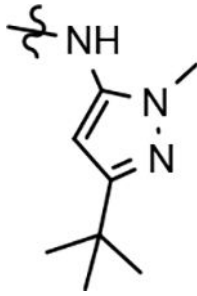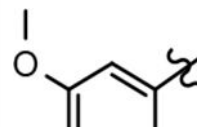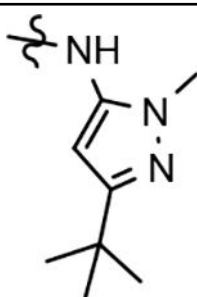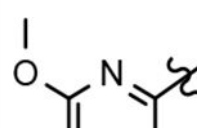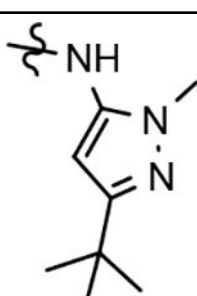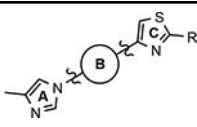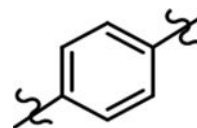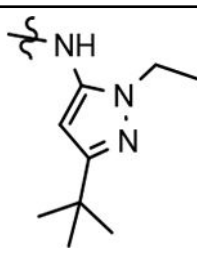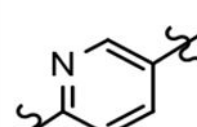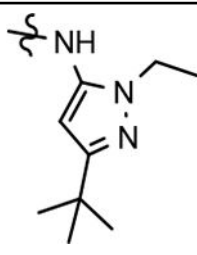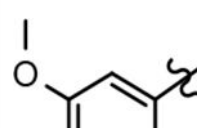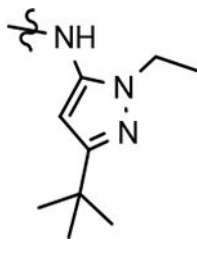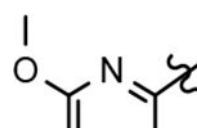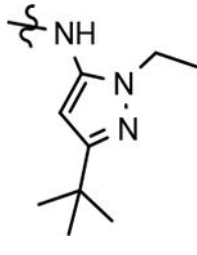
Table 2.

B-ring analogs of tetrahydroindazole-derived GSM **24** and tert-butylpyrazole-derived GSMs **25** and **26**.

Cmpd	B-ring	R	Aβ42 IC$_{50}$[a]	clogP[b]	Kin. Aq. Sol.[c]	Metabolic Stability[d]		
						H	R	M
31a			453	3.40	4.7	55	56	84
31b			>1000	2.79	nt[e]	nt[e]	nt[e]	nt[e]
31c			148	3.15	nt[e]	nt[e]	nt[e]	nt[e]
31d			105	2.93	15	36	60	34

Cmpd	B-ring	R	Aβ42 IC$_{50}$[a]	clogP[b]	Kin. Aq. Sol.[c]	Metabolic Stability[d]		
						H	R	M
32a			275	4.27	nt[e]	nt[e]	nt[e]	nt[e]
32b			590	3.66	nt[e]	nt[e]	nt[e]	nt[e]
32c			253	4.02	5.5	60	76	92
32d			136	3.80	nt[d]	nt[e]	nt[e]	nt[e]

Cmpd	B-ring	R	Aβ42 IC$_{50}$[a]	clogP[b]	Kin. Aq. Sol.[c]	Metabolic Stability[d]		
						H	R	M
33a			339	4.61	nt[d]	nt[e]	nt[e]	nt[e]
33b			292	4.00	<1.6	43	60	87
33c			96	4.36	nt[d]	nt[e]	nt[e]	nt[e]
33d			114	4.14	15	38	89	67

[a] IC$_{50}$ represents the concentration in nM of compound required for reducing Aβ42 levels by 50%. The IC$_{50}$ values are the mean ± standard deviation of at least 2 determinations.

[b] Calculated partition coefficient of the simulated ratio of the compound's concentration in octanol to the compound's concentration in water using ChemAxon fragment based approach.

[c] Kinetic solubility measured at pH 7.4 by UV/Vis absorbance in PBS buffer (μM).

[d] % Remaining after 30 minutes upon incubation with human (H), rat (R) and mouse (M) liver microsomes (1 mg/mL), at 1 μM test compound concentration.
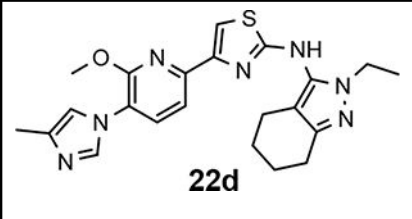
[e] nt = not tested - compound did not meet minimum activity threshold.

Table 3.

In vitro ADMET properties of pyrazole **22d**.

IC$_{50}$ (nM)	60
Kin. sol. pH 7.4 (μM)^{a}	4.5
clog$P$	3.28
hLM (%)^{b}	36
rLM (%)^{b}	71
mLM (%)^{b}	64
CYP450 IC$_{50}$ (μM)^{c}	
3A4	3.7
1A2	>100
2C9	9.0
2C19	5.9
2D6	>100
hERG IC$_{50}$ (μM)^{d}	8.6
% PPB^{e}	99.6

[a] Kinetic solubility measured at pH 7.4 by UV/Vis absorbance in PBS buffer (μM).

[b] % Remaining after 30 minutes upon incubation with human (hLM), rat (rLM) and mouse (mLM) liver microsomes (1 mg/mL), at 1 μM test compound concentration.

[c] Five recombinant CYP isoforms were tested for inhibition by the test compound using fluorescence-based assays.

[d] Patch-Xpress patch-clamp assay; compounds were tested (n = 3) in a five-point concentration-response on HEK-293 cells stably expressing the hERG channel.

[e] % PPB = plasma protein binding.

Table 4.

In vivo pharmacokinetic profile of tetrahydroindazole **22d**.

Mouse Pharmacokinetics of **22d**[a]		
Route	iv	po
Dose (mg/kg)	1	5
C_{max} (ng/mL)	824	705
T_{max} (hrs)	0.083	0.25
$t_{1/2}$ (hrs)	0.5	cnd[b]
AUC_{last} (ng·h/mL)	443	1,089
AUC_{inf} (ng·h/mL)	463	1,243
Cl (mL/hr/kg)	2,159	
Vss (mL/kg)	1,413	
F (%)	100	53.7
Brain/Plasma Ratio (@ 1 hr post dose)	0.4	0.4

[a]Male CD-1 mice; n = 24.

[b]Cannot be determined from data.
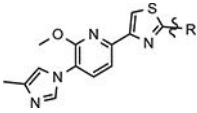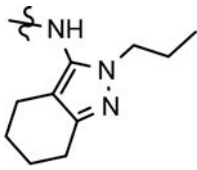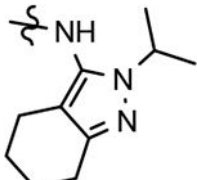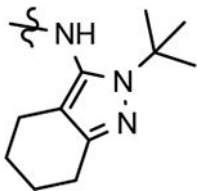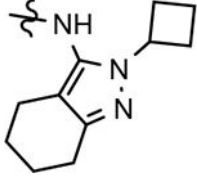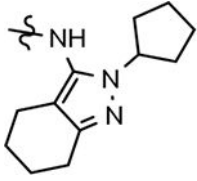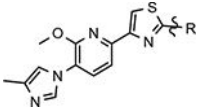
Table 5.
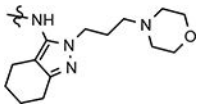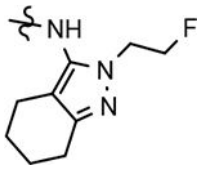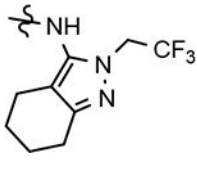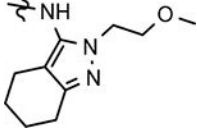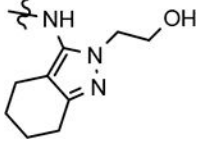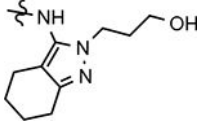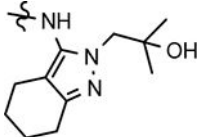
Methoxypyridine-derived D-ring GSM analogs.
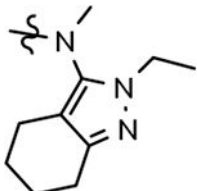
Cmpd	R	Aβ42 IC$_{50}$[a]	Parent Aβ42 IC$_{50}$[b]	clogP[c]	Kin. Aq. Sol.[d]	Metabolic Stability[e]			CYP450 IC$_{50}$ (μM)[f]					hERG[g]	P$_{app}$[h]	Efflux Ratio[i]
						H	R	M	3A4	1A2	2C9	2C19	2D6			
34		48 ± 17	148	3.75	<1.6											
35		46 ± 6	195	3.69	3.3	10	64	45								
36		71 ± 25	216	3.77	34	19	63	23	5.3	9.1	47	12	>100	7.18	14.8	0.9
37		64 ± 26	99	3.73	30	9.5	42	44	0.59	>100	0.66	1.6	>100			
38		83 ± 18	225	4.12	1.8											

Cmpd	R	Aβ42 IC$_{50}$[a]	Parent Aβ42 IC$_{50}$[b]	clogP[c]	Kin. Aq. Sol.[d]	Metabolic Stability[e]			CYP450 IC$_{50}$ (μM)[f]					hERG[g]	P$_{app}$[h]	Efflux Ratio[i]
						H	R	M	3A4	1A2	2C9	2C19	2D6			
39		63 ± 6	280	4.52	<1.6											
40		102 ± 33	289	2.71	19	2.1	42	70								
41		102 ± 40	766	2.77	4.7											
42		>1000	>1000	2.91	92											
43		208 ± 25	475	3.64	46											
44		177 ± 40	>1000	2.57	70	0	22	11								

Cmpd	R	Aβ42 IC_{50}[a]	Parent Aβ42 IC_{50}[b]	clogP[c]	Kin. Aq. Sol.[d]	Metabolic Stability[e]			CYP450 IC_{50} (μM)[f]					hERG[g]	P_{app}[h]	Efflux Ratio[i]
						H	R	M	3A4	1A2	2C9	2C19	2D6			
45		126 ± 23	270	2.62	39	1.9	6.4	0.7								
46		47 ± 4	110	3.09	15	100	100	100	1.0	>100	6.8	4.6	>100	11.4	32.6	1.9
47		57 ± 17	179	3.91	7.4	13	41	39								
48		144 ± 54	272	2.77	20	1.8	45	29								
49		144 ± 55	362	2.19	31	40	78	58	30	>100	>100	76	>100	2.63	18	
50		50 ± 13	229	2.24	23	17	52	32	2.2	>100	>100	31	>100			
51		38 ± 14	55	2.68	22	12	57	78	1.1	>100	9.0	3.9	>100	5.8	17.5	1.6

Cmpd	R	Aβ42 IC$_{50}$[a]	Parent Aβ42 IC$_{50}$[b]	clogP[c]	Kin. Aq. Sol.[d]	Metabolic Stability[e]			CYP450 IC$_{50}$ (μM)[f]					hERG[g]	P$_{app}$[h]	Efflux Ratio[i]
						H	R	M	3A4	1A2	2C9	2C19	2D6			
52		636 ± 44	>1000	3.52	3.4											

[a] IC$_{50}$ represents the concentration in nM of compound required for reducing Aβ42 levels by 50%. The IC$_{50}$ values are the mean ± standard deviation of at least 2 determinations.

[b] IC$_{50}$ represents the concentration in nM of compound required for reducing Aβ42 levels by 50% for the parent 2-fluoro-1,4-phenyl B-ring compound. Connectivity is illustrated by compound **4** in Table 1. The IC$_{50}$ values are the mean of at least 2 determinations.

[c] Calculated partition coefficient of the simulated ratio of the compound's concentration in octanol to the compound's concentration in water using ChemAxon fragment based approach.

[d] Kinetic solubility measured at pH 7.4 by UV/Vis absorbance in PBS buffer (μM).

[e] % Remaining after 30 minutes upon incubation with human (hLM), rat (rLM) and mouse (mLM) liver microsomes (1 mg/mL), at 1 μM test compound concentration.

[f] Five recombinant CYP isoforms were tested for inhibition by the test compound using fluorescence-based assays.

[g] Patch-Xpress patch-clamp assay; compounds were tested (n = 3) in a five-point concentration-response on HEK-293 cells stably expressing the hERG channel.

[h] Apparent permeability (A-B; × 10^{-6} cm/s) determined in MDR1-MDCK cell monolayers.

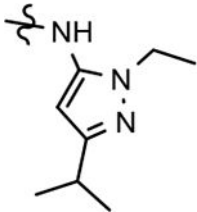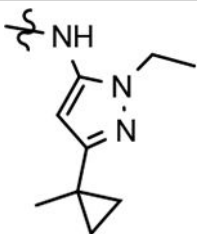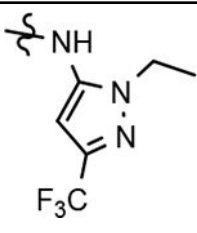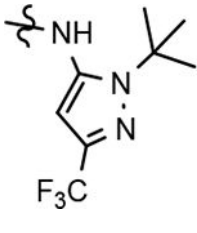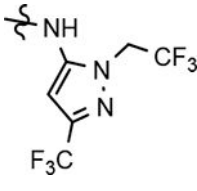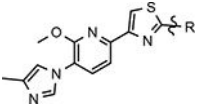[i] Calculated efflux ratio determined using MDR1-MDCK cell monolayers (B-A/A-B).
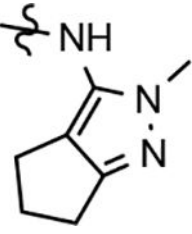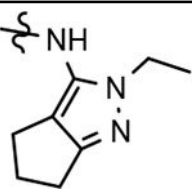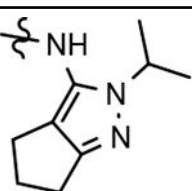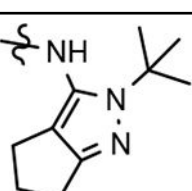
Table 6.

Methoxypyridine-derived D-ring GSM analogs.
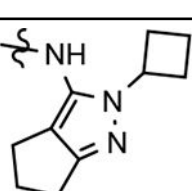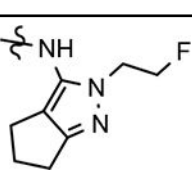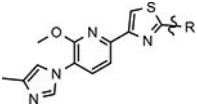
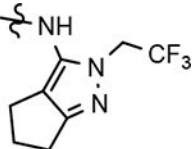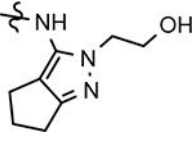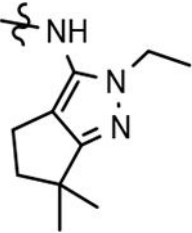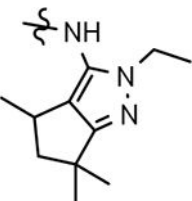| Cmpd	R	$A\beta42$ IC_{50}[a]	Parent $A\beta42$ IC_{50}[b]	clogP[c]	Kin. Aq. Sol.[d]	Metabolic Stability[e]			CYP450 IC_{50} (μM)[f]					hERG[g]	P_{app}[h]	Efflux Ratio[i]
						H	R	M	3A4	1A2	2C9	2C19	2D6			
53		100 ± 4	86	4.61	2.1											
54		64 ± 3	87	4.56	23	21	75	40	2.3	>100	14	14	>100			
55		40 ± 7	85	4.64	<1.6											
56		73 ± 11	NA	3.96	3.3	49	86	67	0.04	64	4.1	3.3	>100			
57		73 ± 20	87	4.78	1.7	47	90	93	1.0	18	20	9.0	>100			
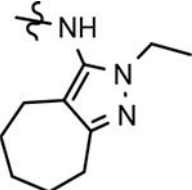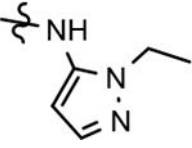
Cmpd	R	Aβ42 IC$_{50}$[a]	Parent Aβ42 IC$_{50}$[b]	clogP[c]	Kin. Aq. Sol.[d]	Metabolic Stability[e]			CYP450 IC$_{50}$ (μM)[f]					hERG[g]	P$_{app}$[h]	Efflux Ratio[i]
						H	R	M	3A4	1A2	2C9	2C19	2D6			
58		184 ± 75	394	3.48												
59		32 ± 12	67	3.64	6.7	67	73	81	4.1*	>100	>100	>100	>100	12.3	18.5	1.3
60		58 ± 20	98	3.40	15	84	96	71	5.3	9.1	47	12	>100	18.9	23.3	1.0
61		126 ± 16	121	3.89	<1.6											
62		199 ± 28	771	4.03	2.0											

Cmpd	R	Aβ42 IC$_{50}$[a]	Parent Aβ42 IC$_{50}$[b]	clogP[c]	Kin. Aq. Sol.[d]	Metabolic Stability[e]			CYP450 IC$_{50}$ (µM)[f]					hERG[g]	P$_{app}$[h]	Efflux Ratio[i]
						H	R	M	3A4	1A2	2C9	2C19	2D6			
63		80 ± 34	>1000	2.54	44	76	71	75*	4.5	>100	>100	37	>100	0.92	22.3	1.9
64		33 ± 10	41	2.88	7.8	51	67	54	20*	>100	>100	>100	>100	1.19	29.6	0.8
65		90 ± 21	66	3.29	5.7	23	56	34								
66		62 ± 1	175	3.37	3.9	21	55	20								
67		21 ± 3	92	3.33	2.7	3	37	26								
68		64 ± 14		2.70	23	58	68	60	10.5	>100	>100	35	>100	2.88		

Core structure (shown at top of table).

Cmpd	R	Aβ42 IC$_{50}$[a]	Parent Aβ42 IC$_{50}$[b]	clogP[c]	Kin. Aq. Sol.[d]	Metabolic Stability[e]			CYP450 IC$_{50}$ (μM)[f]					hERG[g]	P$_{app}$[h]	Efflux Ratio[i]
						H	R	M	3A4	1A2	2C9	2C19	2D6			
69	(structure: NH-pyrazole, N-CH$_2$CF$_3$, fused cyclopentane)	36 ± 12	94	3.51	22	66	72	46	1.4	27	11	7.1	>100	0.92	17.6	0.9
70	(structure: NH-pyrazole, N-CH$_2$CH$_2$OH, fused cyclopentane)	75 ± 11	>1000	1.80	29	42	86	73	<0.05	>100	50	9.2	>100			
71	(structure: NH-pyrazole, N-ethyl, fused cyclopentane with gem-dimethyl)	109 ±13	62	4.11	8.8	31	61	49	0.75	>100	48	15	>100			
72	(structure: NH-pyrazole, N-ethyl, fused cyclopentane with methyl and gem-dimethyl)	72 ± 28	49	4.44	9.2	12	38	21	1.5	>100	35	33	>100			
73	(structure: NH-pyrazole, N-ethyl, fused cycloheptane)	32 ± 12	114	3.67	4.3	0.1	41	15	11	>100	37	85	>100			
74	(structure: NH-pyrazole, N-ethyl)	>1000	>1000	2.12												

[a] IC$_{50}$ represents the concentration in nM of compound required for reducing Aβ42 levels by 50%. The IC$_{50}$ values are the mean ± standard deviation of at least 2 determinations.

[b]IC$_{50}$ represents the concentration in nM of compound required for reducing Aβ42 levels by 50% for the parent 2-fluoro-1,4-phenyl B-ring compound. Connectivity is illustrated by compound **4**in Table 1. The IC$_{50}$ values are the mean of at least 2 determinations.

[c]Calculated partition coefficient of the simulated ratio of the compound's concentration in octanol to the compound's concentration in water using ChemAxon fragment based approach.

[d]Kinetic solubility measured at pH 7.4 by UV/Vis absorbance in PBS buffer (μM).

[e]% Remaining after 30 minutes upon incubation with human (hLM), rat (rLM) and mouse (mLM) liver microsomes (1 mg/mL), at 1 μM test compound concentration.

[f]Five recombinant CYP isoforms were tested for inhibition by the test compound using fluorescence-based assays.

[g]Patch-Xpress patch-clamp assay; compounds were tested (n = 3) in a five-point concentration-response on HEK-293 cells stably expressing the hERG channel.

[h]Apparent permeability (A-B; $\times 10^{-6}$ cm/s) determined in MDR1-MDCK cell monolayers.

[i]Calculated efflux ratio determined using MDR1-MDCK cell monolayers (B-A/A-B).

Table 7.

Pharmacokinetic parameters of test article following single iv and po administration to male CD-1 mice.

Cmpd	Route	Dose (mg/kg)	C_{max} (ng/mL)	T_{max} (hrs)	$t_{1/2}$ (hrs)	AUC_{last} (ng·h/mL)	AUC_{inf} (ng·h/mL)	Cl (mL/hr /kg)	Vss (mL/kg)	F (%)	Brain/ Plasma Ratio (1 hr post dose)
						Mouse Pharmacokinetics					
46	iv	1	309	0.083	0.65	283	288	3,468	2,826		0.81
	po	5	167	1.0	2.6	639	669			46.4	0.68
59	iv	1	384	0.083	3.84	1,247	1,378	725	3,609		0.62
	po	5	592	2.0	cnd[a]	3,976	cnd[a]			63.8	0.57
60	iv	1	359	0.083	1.6	605	623	1,606	3,640		0.73
	po	5	470	1.0	cnd[a]	1,727	2,369			76.0	0.62
63	iv	1	478	0.083	1.9	723		1,308	3,180		0.21
	po	5	580	1.0	1.6	2,700				74.6	0.22
64	iv	1	549	0.083	0.7	376	383	2,608	2,234		0.37
	po	5	377	0.25	5.3	1,205	1,257			66.0	0.40

[a]Cannot be determined from data

Table 8.

Drug levels in plasma and brain of female J20 mice ($n = 5$/dose) following a 3-day treatment course of vehicle, tetrahydroindazole **46**, or cyclopentapyrazole **64**.

Mouse Brain and Plasma Drug Levels[a]				
Cmpd	**Dose (mg/kg)**	**Plasma Drug Level (ng/mL)**	**Brain Drug Level (ng/g)**	**Brain/Plasma Ratio**
Vehicle	0	0	0	NA
46	25	72	39	0.53
	50	639	282	0.42
	100	183	105	0.57
64	25	86	31	0.37
	50	223	83	0.38
	100	726	337	0.46

Tissue samples were collected 4 hrs post final dose administration on Day 3. NA: not applicable.

[a] All samples were analyzed by LC-MS/MS. Compound **46** had a plasma lower limit of quantitation (LLOQ) of 1 ng/mL and brain LLOQ of 5 ng/g. Compound **64** had a plasma lower limit of quantitation (LLOQ) of 1 ng/mL and brain LLOQ of 5 ng/g.

Table 9.

Drug levels in plasma and brain of female Tg2576 mice (n = 12/dose) following a 14-day treatment course of cyclopentapyrazole **64**.

Mouse Brain and Plasma Drug Levels[a]				
Cmpd	**Dose (mg/kg)**	**Plasma Drug Level (ng/mL)**	**Brain Drug Level (ng/g)**	**Brain/Plasma Ratio**
Vehicle	0	0	0	NA
64	50	1,131	425	0.374

Tissues samples were collected 4 hrs post final dose administration on Day 14. NA: not applicable.

[a]All samples were analyzed by LC-MS/MS. Compound **64** had a plasma lower limit of quantitation (LLOQ) of 1 ng/mL and brain LLOQ of 5 ng/g.